ISBN 978-82-326-1304-5 (printed version)
ISBN 978-82-326-1305-2 (electronic version)
ISSN 1503-8181

Doctoral theses at NTNU, 2015:324

Karla Hornbostel

The role of concrete resistivity in chloride-induced macro-cell corrosion

NTNU
Norwegian University of
Science and Technology

NTNU
Norwegian University of
Science and Technology

Faculty of Engineering
Science and Technology
Department of StructuralEngineering

Doctoral theses at NTNU, 2015:324

NTNU

Karla Hornbostel

The role of concrete resistivity in chloride-induced macro-cell

Thesis for the degree of Philosophiae Doctor

Trondheim, August 2015

Norwegian University of Science and Technology Faculty of Engineering
Science and Technology
Department of StructuralEngineering

NTNU
Norwegian University of
Science and Technology

NTNU
Norwegian University of Science and Technology

Thesis for the degree of Philosophiae Doctor

Faculty of Engineering
Science and Technology
Department of StructuralEngineering

ISBN 978-82-326-1304-5 (printed version)
ISBN 978-82-326-1305-2 (electronic version)
ISSN 1503-8181

Doctoral theses at NTNU, 2015:324

Printed by Skipnes Kommunikasjon as

Preface

The doctoral thesis is submitted to the Norwegian University of Science and Technology (NTNU) for the degree *Philosophiae Doctor* (PhD). The research was carried out at the Department of Structural Engineering, Faculty of Engineering Science and Technology at NTNU in Trondheim, Norway. Main supervisor was Professor Dr Mette Rica Geiker (NTNU, Norway), co-supervisors were Dr Claus Kenneth Larsen (NTNU and Norwegian Public Roads Administration (NPRA), Norway), Professor Dr Bernhard Elsener (Eidgenössische Technische Hochschule Zürich (ETH Zürich), Switzerland and University of Cagliari, Italy), and Dr Ueli Michael Angst (ETH Zürich and Swiss Society for Corrosion Protection, Switzerland).

The PhD project started in December 2009 and the thesis was submitted in August 2015. The PhD position included one year of duty work as scientific assistant at the Department of Structural Engineering, NTNU. During the project period, the candidate had two maternity leaves of in total 19 months.

The project was initiated and founded through the Concrete Innovation Centre (COIN, www.coinweb.no), a centre for research-based innovation, which was established in 2006 by the Research Council of Norway for an eight year period. In addition, the project was supported by the NPRA.

The thesis consists of an extended summary, five appended papers (four of them accepted or submitted to international scientific journals, one published in an international conference proceeding) and an appendix.

The author, Karla Hornbostel, declares that the thesis and the work presented in it are her own. The thesis contains no material that has previously been submitted for a degree at this university or any other institution.

Karla Hornbostel
Trondheim, 31 August 2015

Acknowledgements

I would like to acknowledge the financial support of COIN, the NPRA and NTNU, and to thank them for the opportunity to do this PhD. I would also like to express my thanks to Professor Emeritus Øystein Vennesland for helping initiating this PhD project.

My sincere thanks to all my supervisors for supporting me on this journey, for our valuable discussions, for our intense meetings, and for pushing me forward with encouragement and patience. You have made this project enjoyable and extraordinarily instructive for me. I feel honoured by your interest. Thank you very much Ueli M. Angst, Bernhard Elsener, Claus K. Larsen and Mette R. Geiker.

There are many people at NTNU and the Department of Structural Engineering who have helped me during my PhD time. Thanks go to all the people in the administration and in the laboratory. My special thanks to Ove Loraas and Steiner Seehuus in the concrete laboratory, for supporting my experiments with valuable ideas and strong arms. Thanks also to the students Maria Belen Pina Fernandez, Kristine Andersen, Kristian Sætre, Miguel Boix Roca, Denisa Orsakova and Ann-Marie Thoresen for their help in the laboratory. Appreciated was also the help of Ulla Hjorth Jakobsen (Danish Technological Institute), Anne-Kristin Mjøen (SINTEF Building and Infrastructure), and Trine-Lise Lorentsen (NTNU) with microstructural analyses, chloride profiles, and 3D analyses. For supporting me by proofreading parts of the thesis and appended papers, my thanks to Lawrence White (Language Support Centre, Denmark) and Carolyn Rosten.

To all my colleagues in the concrete group, a warm thanks – for keeping alive a good working atmosphere and for your companionship. For sharing the same worries and concerns; it is a pleasure to work with you.

For their encouragement in life and for loving me regardless, my deep thanks to my parents, Steffi and Detlef Hornbostel, and sister, Kerstin Hornbostel. Many thanks also to my parents-in-law, Ulrike and Rudolf Zeevaert, for their helpful and supportive care during these last years; you made things easier for me. My friends in Trondheim are thanked for offering me valuable chats, good advice and allied support, which carried me through tough times. Last, but certainly not least, grateful thanks to my husband, Jens, for his support and patience, for clearing my way, and for distracting me at the right moments. He and our two children, Lotta and Mattis, helped to hold my focus on the most important things in life.

Abstract

Norwegian concrete structures are exposed to salt contamination from both sea water and de-icing salts. Chlorides penetrate the concrete cover and initiate corrosion of the reinforcement. The deterioration process can propagate at high rates and endanger serviceability and structural safety. Concrete resistivity is usually assumed to correlate closely with the corrosion process, and its measurement is in principle simple and cost-efficient, and widely recommended to support service life assessment. However, the extent to which concrete resistivity measurements can provide us with detailed information about the corrosion process needs critical examination.

The main objective of this PhD project was to study the applicability of concrete resistivity measurement for predicting the rate of reinforcement corrosion induced by chlorides. A review of the literature led to the conclusion that a general correlation could be found between increasing concrete resistivity and decreasing corrosion rate, but a large scatter was observed within and between the studies reviewed. Various possible reasons for the discrepancies were identified: researchers used dissimilar procedures for determining both concrete resistivity and corrosion rate, and concrete composition was recognised as affecting the overall tendency. Interestingly, the literature contained very limited discussion on the mechanisms involved in providing the correlation assumed between concrete resistivity and corrosion rate.

On the basis of the literature review, it seemed appropriate to investigate the relationship between concrete resistivity and corrosion rate further using specially designed laboratory experiments. In total, three experimental studies were conducted using mortar to investigate the subject. The first study focused on the limitations of measuring galvanic currents in macro-cells. It was confirmed that galvanic current measurements provide an indication of the actual corrosion current, and thereby rate, only if the actively corroding segment is sufficiently small.

The second experimental study investigated the limitations of bulk resistivity measurements for predicting the ohmic resistance in a macro-cell between small anodes and a large cathode network. It was found that for small anodes the ohmic resistance between the anode and the cathode is not directly correlated with the bulk resistivity. Local inhomogeneities strongly influence the measurements. The ratio between bulk resistivity and the resistance between a specific anode and the cathode was not constant over time and varied in particular with changes in the moisture conditions.

The third experimental study examined the influence of mortar resistivity on the rate-limiting steps of chloride-induced corrosion. It was shown that for small anodes the local conditions around the anode are more decisive for the anodic and ohmic partial processes than the bulk resistivity. The cathodic partial process was found to be practically independent of the mortar resistivity. For the setup and materials investigated, it was not possible to identify any one rate-limiting step as dominant. The

controlling rate-limiting step varied for the different materials investigated. For mortar prepared with fly ash, and therefore possessing high mortar resistivity, the concept of anodic-resistance control suggested in the literature was found to fit well. Cathodic control was identified for mortars with a comparatively low bulk resistivity (prepared only with Portland cement). Furthermore, it was confirmed that the generally assumed inverse correlation between corrosion rate and concrete resistivity depends very much on the material composition.

In conclusion, it was found that there can be no direct relationship between concrete resistivity and the corrosion rate. The dependency on material composition and in particular the fact that concrete resistivity is not directly correlated with the underlying partial processes that determine the corrosion rate must be considered as decisive on this question. It must therefore be assumed that the direct relationships between concrete resistivity and corrosion rate introduced in the literature, and any models and general threshold values based upon them, are not generally applicable.

Table of contents

List of appended papers

The thesis includes the following appended papers, which are referred to by their Roman numbers.

I **Relationship between concrete resistivity and corrosion rate – A literature review**
Cement and Concrete Composites, Volume 39, 60 – 72 (2013)
Hornbostel, Karla; Larsen, Claus K.; Geiker, Mette R.

II **Application of segmented rebars for studying corrosion of steel in concrete**
Proceedings Eurocorr 2013, digital, Portugal 2013.
Hornbostel, Karla; Geiker, Mette R.; Larsen, Claus K.

III **On the limitations of predicting the ohmic resistance in a macro-cell in mortar from bulk resistivity measurements**
Cement and Concrete Research, Volume 76, 147 – 158 (2015)
Hornbostel, Karla; Angst, Ueli M.; Elsener, Bernhard; Larsen, Claus K. and Geiker, Mette R.

IV **Influence of mortar resistivity on the rate-limiting step of chloride-induced macro-cell corrosion of reinforcing steel**
Submitted to Corrosion Science (2015)
Hornbostel, Karla; Angst, Ueli M.; Elsener, Bernhard; Larsen, Claus K. and Geiker, Mette R.

V **Limitations of the use of concrete resistivity as an indicator for the rate of chloride-induced macro-cell corrosion**
Submitted to Structural Concrete (2015)
Hornbostel, Karla; Elsener, Bernhard; Larsen, Claus K.; Angst, Ueli M. and Geiker, Mette R.

Declaration of authorship

Karla Hornbostel planned and conducted most of the experiments, evaluated the results, and wrote the major part of the appended papers. The co-authors contributed in planning the experiments, discussing and evaluating the results, and by assisting in writing the papers. Parts of the experimental work presented in Paper III were conducted within a master project (student: Kristine Andersen). Corroded steel pieces (Appendix D.2, Papers IV and V) were scanned by CASCADE CONTROL AB. The scans were analysed by Trine-Lise Lorentsen. For Papers III, IV and V, as well as the thesis itself, language support was provided by the LANGUAGE SUPPORT CENTRE Denmark (Lawrence White).

Other publications

In addition to the appended papers, the author of this thesis has contributed to the following publications, which are not a part of the thesis.

Books

Workshop Proceedings: "Understanding the Fundamental Properties of Concrete" Celebrating Professor Erik J. Sellevold on his 75th birthday.
Trondheim, Norway, 25-26 April 2013, ISBN 82-7482-101-7.
Edt. Mindess, Sidney; Hornbostel, Karla

Proceedings of ICDC 2012, International Congress on Durability of Concrete
Trondheim, Norway, 18-21 June 2012, ISBN 978-82-8208-031-6.
Edt. Justnes, Harald; Jacobsen, Stefan; Cepuritis, Rolands; Hornbostel, Karla; Peng, Ya

Part of books/conference proceedings

Prediction of reinforcement corrosion in concrete structures.
Proceedings of the Concrete Innovation Conference CIC, Oslo, Norway, June 2014 (digital).
Geiker, Mette Rica; De Weerdt, Klaartje; Hornbostel, Karla; Kioumarsi, Mohammad Mahdi; Hendriks, Max; Larsen, Claus Kenneth; Angst, Ueli

Relationship between concrete resistivity and corrosion rate – a literature review.
Proceedings of ICDC 2012, International Congress on Durability of Concrete, Trondheim, Norway 18-21 June 2012 (digital).
Hornbostel, Karla; Larsen, Claus Kenneth; Geiker, Mette Rica

The Electrical Resistivity of Concrete as Service Life Parameter.
Proceedings of XXI Nordic Concrete Research Symposium, Finland, 2011, pages 123-126.
Hornbostel, Karla; Larsen, Claus Kenneth; Geiker, Mette Rica

Articles in Popular Science Magazines/ Trade Magazines

Betongens elektriske motstand og korrosjon
Byggeindustrien 2015 (12) page 86
Hornbostel, Karla; Geiker, Mette Rica; Larsen, Claus Kenneth

List of symbols and abbreviations

Latin letters

A	Area	[m^2]
E	Electrochemical potential	[V]
E^o	Standard electrode potential	[V]
E^{rev}	Reversible potential	[V]
E_a	Anode potential	[V]
E_a^{rev}	Reversible anode potential	[V]
E_c	Cathode potential	[V]
E_c^{rev}	Reversible cathode potential	[V]
E_{corr}	Corrosion potential	[V]
I	Current	[A]
I_{corr}	Corrosion current	[A]
I_{galv}	Galvanic current	[A]
I_{lim}	Limited corrosion current	[A]
I^o	Exchange current	[A]
i_{corr}	Corrosion current density, corrosion rate	[A/m^2]
i_{lim}	Limited corrosion rate	[A/m^2]
k	Cell constant	[m]
l	Length	[m]
m	Mass loss	[$g/m^2 \cdot year$]
M	Molar mass	[g/mol]
Q	Electrical charge passed	[Cs]
R	Electrical (ohmic) resistance	[Ω]
R_{cell}	Cell resistance, resistance between anode and cathode	[Ω]
R_p	Polarisation resistance	[Ω]
$R_{p.a}$	Polarisation resistance of the anode	[Ω]
$R_{spreading}$	Spreading resistance	[Ω]
T	Temperature	[K] or [°C]
U	Voltage	[V]
z	Valence number	[/]

Greek letters

β_a	Anodic TAFEL slope	[V/dec]

β_c	Cathodic TAFEL slope	[V/dec]
σ	Conductivity	[S]
ρ	Resistivity	[Ωm]
ρ_{bulk}	Resistivity of the bulk material	[Ωm]
ΔU	Voltage drop	[V]

Abbreviations and constants

AC	Alternating current
C/A	Cathode-to-anode area ratio
CE	Counter electrode
DC	Direct current
EIS	Electrical Impedance Spectroscopy
ERE 20	Reference Electrode from FORCE TECHNOLOGY
F	Faraday constant ($9.648 \cdot 10^4$ C/mol)
FA	Fly ash
IR drop	Voltage drop between anode and cathode
LPR	Linear polarisation resistance
PC	Portland cement
R	Gas constant (8.314 J/(K·mol))
RE	Reference electrode
RH	Relative humidity
SCE	Saturated calomel electrode (+244 mV vs. Stand hydrogen electrode)
SCM	Supplementary cementitious materials
w/b	Water-to-binder ratio
WE	Working electrode

Part I – Extended Summary

1 Introduction

Reinforced concrete surrounds us in our everyday life. It is important for social and industrial buildings and essential for infrastructure structures. There are numerous examples of the application of reinforced concrete ranging from small-scale, such as foundations and barriers, to large structures like bridges, tunnels, dams and offshore platforms. Its variability in both shape and properties allows the use of reinforced concrete in a variety of forms and environments.

Reinforced concrete is considered a durable building material with a lifespan over several decades. However, some existing reinforced concrete structures are reaching the end of their calculated lifetime or show distinct signs of deterioration, such as spalling and cracking. To avoid failure of these structures, it is essential to gain profound knowledge about the deterioration processes of reinforced concrete, not only to assess existing structures, but also to be able to make reliable predictions for new structures. Research on the topic has been going on for more than 100 years, with increased activity in the last 50 years (Page and Treadaway 1982). Nevertheless, some of the fundamental mechanisms and testing procedures are still under discussion. General understandings from the traditional material, 'Portland cement', need to be questioned for the new materials that are steadily entering the market to reduce CO_2-emissions from cement production.

It is necessary to distinguish between deterioration processes affecting the concrete and those processes attacking the reinforcement (Bertolini et al. 2013). The corrosion of reinforcement steel in concrete has been identified as the most common cause of failure and 'arguably the largest single infrastructure problem facing industrialised countries'[1].

The reinforcement in concrete is protected by a thin film of iron oxides and iron hydroxides (the passive layer) that forms spontaneously on the steel surface due to the highly alkaline pore solution of the concrete material. The high alkalinity arises from sodium and potassium oxides being present in the clinker minerals of the cement or other constituent materials, when passing into solution, hydroxyl ions are formed. Mainly, Portlandite $Ca(OH)_2$ formed during cement hydration provides the alkali reserve in concrete (Broomfield 1997).

Two causes of reinforcement corrosion are recognised. One arises from the reaction between CO_2 from the air and calcium-containing phases in concrete leading to the carbonation of the concrete cover. The reaction causes a decrease in pH from initial values between 12 and 14 to near neutrality. The passive layer on the reinforcement is no longer stable in these conditions (depassivation), and corrosion can initiate. Commonly, the whole passive layer in contact with carbonated concrete is dissolved leading to a general type of corrosion. The cause and extent of corrosion depends on the

[1] Broomfield (1997) – Page 1.

environmental conditions in which the concrete is located. Carbonation-induced corrosion is common in urban environments with a high concentration of carbon dioxide in the atmosphere and the rate of carbonation of the concrete cover is favoured at relative humidity (RH) between 60% and 70%. With increasing wetting periods, the carbonation rate decreases (Broomfield 1997, Bertolini et al. 2013).

Chlorides penetrate the concrete cover if the structure is in contact with water containing chloride, such as sea-water or surface water polluted with de-icing salts. Before the topic of chloride-induced reinforcement corrosion was generally recognised, chloride-containing mixing water, aggregates, cements and admixture (e.g. accelerators (Myrdal 2007)) were occasionally used. Today, the maximum amount of chloride in the concrete mix is limited and defined in standards, e.g. (EN206-1 2000). Corrosion of the steel reinforcement initiates when a certain amount of chloride is present at the surface of the reinforcement (Angst et al. 2009). This leads to a local breakdown of the passive layer, iron dissolution takes place in a limited area (pits), while most of the steel surface remains passive. The local corrosion rates can be considerably higher than for corrosion initiated by carbonation.

The research for this thesis focused on chloride-induced steel corrosion in concrete that is considered the main risk for Norwegian infrastructural structures. Norway's long coast line and its harsh winters, which make the extensive use of de-icing salts necessary, mean that more than 18 000 bridges and some 1 000 tunnels (NPRA 2015) are exposed to severe salt contamination. For the owners of these structures, the mechanisms and assessment criteria for chloride-induced reinforcement corrosion is of special interest.

The process of chloride-induced reinforcement corrosion can be divided between the initiation and the propagation periods (Figure 1). The initiation period describes the time chlorides need to penetrate the concrete cover. The depassivation of the steel surface ends this period and marks the start of active corrosion propagation.

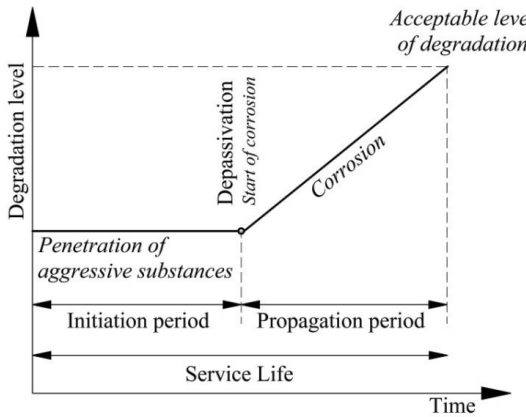

Figure 1 – Process of reinforcement corrosion, model according to Tuutti (Tuutti 1982) .

The penetration of chlorides into concrete is often described as a diffusion phenomenon characterised by the effective diffusion coefficient *D*. The latter primarily depends on the pore structure of the concrete, which is a result of not only the water-to-cement ratio, cement type, cement content and curing conditions, but also the exposure conditions, chloride binding and the surface concentration of chlorides (Larsen 1998, Luping et al. 2012). The amount of chloride needed to initiate corrosion on the reinforcement surface is referred to as the critical chloride content or threshold value. It depends on a variety of parameters, such as the electrochemical potential of the steel, the pH and interfacial conditions between the concrete and steel (Angst et al. 2009). Corrosion propagates at a rate dependent on both the material and exposure conditions, such as the degree of saturation, temperature, pore solution composition, as well as oxygen and water availability (Hope et al. 1986, López and González 1993, Bertolini and Polder 1997, Andrade et al. 1998). Corrosion rates of up to 1 mm/year are reported for chloride-induced corrosion (Bertolini et al. 2013).

Several inspection methods can be used to assess concrete durability in both the initiation and the propagation periods; some of them are destructive, others non-destructive (Broomfield 1997, Bertolini et al. 2013). With regard to periodical field surveys and monitoring, non-destructive methods are to be preferred. In addition to well-known electrochemical inspection methods like half-cell potential mapping (Elsener et al. 2003) and polarisation resistance measurements (Andrade et al. 2004), determination of the electrical resistivity of concrete is often used (Polder et al. 2000), with measurement techniques adapted from the field of geophysics (Wenner 1915, Lataste 2010). Resistivity measurement is a favoured method as it is easy to use, relatively quick and cheap (Polder 2001, Lataste 2010).

Electrical resistivity is a quantity that describes the charge transport ability of a material; it is independent of geometry. In concrete, it characterises the flow of ions in the cement paste matrix which depends both on material properties (e.g. porosity, pore solution composition) and exposure conditions (degree or pore saturation, temperature). The pore solution composition and pore network connectivity are closely related to concrete resistivity (Bürchler et al. 1996, Hunkeler 1996). The degree of saturation has been identified as the main factor influencing concrete resistivity (Gjørv et al. 1977). Since the electrochemical process of steel corrosion in concrete requires the transport of ions through the concrete, it is widely held that concrete resistivity influences the corrosion process.

Numerous publications report decreasing corrosion rates with increasing concrete resistivity, found in a variety of different contexts. Occasionally, the trend observed is used to define threshold values or create prediction models for the corrosion rate (Polder et al. 2000, Broomfield and Millard 2002, Andrade et al. 2004, Smith et al. 2004, Andrade and d'Andrea 2008, Ahmad 2014). The selection of modern binders, blended cements with fly ash, silica fume, slag, and others is often justified with reference to their commonly high resistivity compared to traditional materials and the consequently

expected lower corrosion rate of embedded steel (Cabrera and Ghoddoussi 1994, Smith et al. 2004, Gastaldini et al. 2009).

However, whether this overall trend, though well-established, can be exploited as a reliable and trustworthy fundament for prediction of corrosion propagation and material choice needs critical scrutiny. The main research question for this thesis was to study to what extent concrete resistivity can be used as a direct indication of the corrosion rate.

1.1 Objectives, research approach and organisation of the thesis

1.1.1 Objectives

The PhD project aimed at improving the basis for assessment of the service life of reinforced concrete structures. It focused on the propagation of chloride-induced reinforcement corrosion. The aim of the study was **to investigate to what extent concrete resistivity can be used to predict the corrosion rate of chloride-induced corrosion.**

The following objectives were defined:

1. To identify the lack of knowledge in the current discussion about the relationship between corrosion rate and concrete resistivity.
2. To study the rate-limiting processes of chloride-induced macro-cell corrosion.
3. To discuss the applicability of concrete resistivity as an indicator of the rate of chloride-induced corrosion.

1.1.2 Research approach and limitations

The study focused on chloride-induced reinforcement corrosion and the relationship between the corrosion rate and the concrete resistivity during the propagation period. As background for the PhD study and further experimental investigations a state-of-the-art literature review was provided to meet the first objective. Based on the literature review it was considered adequate to undertake experiments with mortar specimens and accelerated corrosion initiation. Segmented rebars with electrically isolated segments were the preferred experimental setup. The materials used in the experimental studies were representative for materials commonly used in Norway. The second and third objectives are discussed on the basis of the results of the experimental studies. It was not intended to create or provide input data for service life models. Carbonation-induced corrosion (uniform corrosion) was not studied in this PhD project.

1.1.3 Organisation

The thesis consists of three parts. Part I gives an extended summary of the theoretical background for the research and the experiments undertaken. The three experimental programmes (Experimental Studies I – III) conducted are briefly described, and the main results are given, the main findings and conclusions are summarised, and proposals are made for future research. Part II of the thesis consists of the appended papers, which contain detailed descriptions of the work and findings of the PhD project and are to be considered the main part of the thesis. Part III contains appendices presenting results of experimental work not published in the appended papers and more detailed information on the materials used.

2 Theoretical background

2.1 Electrical resistivity in concrete

The electrical resistivity (ρ) of a material quantifies how strongly it opposes the flow of electric current. It can be expressed as the product of the electrical resistance (R), which in turn is the ratio of voltage (U) to current (I), and a cell constant (often referred to as k and valid for homogenous conditions where k = constant (Lataste 2010)). Resistivity is expressed in the SI-unit [Ωm].

$$\rho = \left(\frac{U}{I}\right) \cdot k = R \cdot k \qquad \text{Eq. 1}$$

The cell constant can be calculated if the volume penetrated by the current field has a constant area and length.

$$k = \frac{A}{l} \qquad \text{Eq. 2}$$

If the geometry of the electrical field is unknown, the cell constant can be determined either by numerical modelling or by calibration using materials (e.g. solutions) with known resistivity.

The range over which the electrical resistivity of materials spans is one of the greatest of any physical property. Concrete resistivity ranges from 10^6 Ωm for oven-dried to 10 Ωm for saturated concrete (Whiting and Nagi 2003).

Concrete is an inhomogeneous material and is considered biphasic from an electrical point of view, with non-conductive aggregates embedded in a more or less conductive cement paste (Hunkeler 1996, Lataste 2010). Cement paste consists of porous hydration products, mainly calcium silicate hydrates (C-S-H) and calcium hydrates (CH) (Bensted and Barnes 2009). Depending on the degree of saturation, the pore solution is adsorbed and/or condensates on the pore walls or fills the pores. The composition of the pore solution is dominated by the positively charged ions, sodium (Na^+), potassium (K^+) and calcium (Ca^{2+}), and the anions sulphate (SO_4^{2-}) and hydroxyl (OH^-) (Bürchler 1996). The latter can be found in high concentrations, corresponding to a high alkalinity of the pore solution (pH of up to 13.5) (Bertolini et al. 2013).

Ion transport in solution depends on the strength of the electrical field and the charge of the ions, also referred as ion mobility (u) (Bertolini et al. 2013). Table 1 gives an overview of the mobility of ions commonly found in the pore solution of cement paste as well as the chloride ion. The conductivity σ (inverse of resistivity) of the bulk solution can be calculated from the mobility and concentration of all ions in the solution

(Hunkeler 1996). Hydroxide ions have a major impact on resistivity due to their high mobility and high concentration in the pore solution.

Table 1 – Ion mobility in water at 298 K (Atkins and de Paula 2006).

Ion	Valence	Mobility 10^{-8} $m^2/(s\ V)$
Hydroxide ion (OH^-)	-1	20.64
Sulphate (SO_4^{2-})	-2	8.29
Chloride ion (Cl^-)	-1	7.91
Potassium ion (K^+)	+1	7.62
Calcium ion (Ca^{2+})	+2	6.17
Sodium ion (Na^+)	+1	5.19

The effect of chloride ions in the pore solution on concrete resistivity is still under discussion. There seems to be a dependency on the alkalinity of the pore solution; with increasing alkali content, the effect of chloride concentration on the resistivity strongly decreases (Hunkeler 1996). It is also suggested that the cation associated with the chloride ion has an influence on the effect of chlorides on pore solution conductivity (Bertolini and Polder 1997).

The resistivity of cement paste is 2-3 orders of magnitude higher than the resistivity of the pore solution (Bürchler 1996). Ions move not by the shortest distance between the electrodes applied, but have to take tortuous paths through the pore system. They can only move in pores filled or partly-filled with pore solution that interconnect with each other. Cement paste consists of different pores with dimensions between 2 nm (gel pores) and 4 – 1 000 nm (capillary pores) (Bertolini et al. 2013). Depending on the degree of saturation, these pores are covered by one or more layers of adsorbed water. When the RH increases (>40–45%), they will also be filled by capillary condensation. It has been found that only the capillary condensed water can be assumed to be conductive; the adsorbed water in the gel pores appears to be nonconductive although the concentration of ions is high (Hunkeler 1996). Air and macro pores in the range of several μm up to mm do not normally fill with water. They show no capillary suction effects and only fill under water pressure. Consequently, in the cement paste, it is the capillary pore system which contributes to the overall conductivity.

Research over recent decades has clearly shown that the degree of saturation of the pore system has the most significant influence on concrete resistivity (examples are given in Figure 2). The correlation between the degree of saturation and concrete resistivity depends on the concrete composition, age (degree of hydration), and temperature.

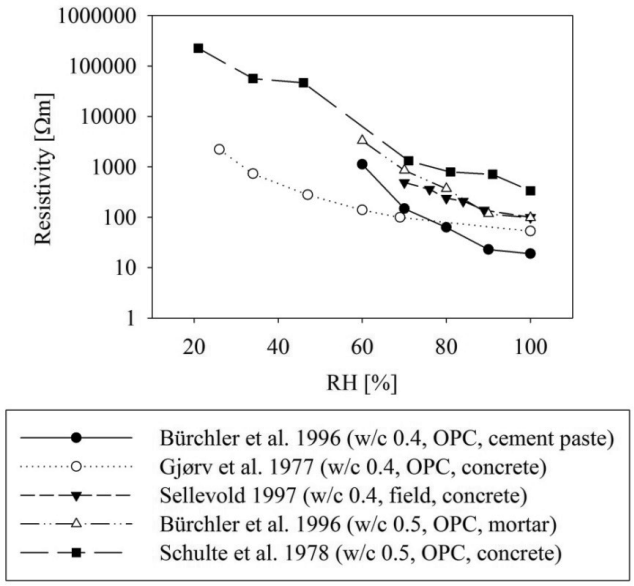

Figure 2 – Influence of moisture content on resistivity (Gjørv et al. 1977, Schulte et al. 1978, Bürchler et al. 1996, Sellevold 1997).

The temperature dependency of concrete resistivity is related to the properties of the pore solution and ion-solid interactions (absorption behaviour), and has been a matter of discussion for several decades (Raupach 1992, Bürchler 1996, Bertolini and Polder 1997, Whiting and Nagi 2003, Østvik 2005, Larsen et al. 2006). It seems to depend on the degree of pore saturation and the concrete composition (Elkey and Sellevold 1995, Polder et al. 2000). As a rule of thumb, the change in resistivity for samples with moisture contents above 70% lies at about 3% per 1°C and for samples with a moisture content below 30% at about 5% per 1°C; this is, however, a very rough estimation (Elkey and Sellevold 1995). Improved approaches can be found in the literature (Monfore 1968, Woelfl and Lauer 1979, Castellote et al. 2002, Whiting and Nagi 2003, Østvik 2005, Michel et al. 2013a).

2.1.1 Measurement of concrete resistivity

No standardised method for measuring concrete resistance appears available. However, attempts have been made to give general guidelines and recommendations (DuraCrete 1997, Polder et al. 2000, Spragg et al. 2013). In principle, two or four metal electrodes are placed at a certain distance from each other on the surface of a concrete sample or are embedded in the fresh mix. The electrical resistance can be measured using either DC (Direct Current) or AC (Alternating Current). By multiplying the electrical resistance by a geometrical factor, the resistivity can be derived (cf. Eq. 1).

Current and frequency

The electrical resistance of a concrete sample can be determined either by AC or DC measurements. DC measurements are not usually recommended because the electrodes are polarised during the measurement (Raupach 1992). Using AC, on the other hand, prevents the occurrence of chemical reactions at or the polarisation of, the electrodes (Gautefall and Venneslad 1994). Nevertheless, to avoid capacity effects on the electrode-concrete interface, a high measurement frequency is recommended, with values between 50 Hz and 1 000 Hz considered suitable (DuraCrete 1997, Polder et al. 2000). The measurement frequency can influence the readings for ohmic resistance. Detailed investigations have shown that the optimal measurement frequency depends on the moisture state and temperature of the sample (Østvik et al. 2006). For wet concrete, frequencies between 100 Hz and 10 000 Hz seem to be suitable. At very low temperatures, a measurement frequency above 1 000 Hz should be avoided. The recommendation is somewhat different for dry concrete, however, with frequencies between 500 Hz and 1 000 Hz showing acceptable fluctuation (Østvik 2005, Østvik et al. 2006).

Electrodes and electrode contact

Electrodes of different metals can either be placed on the concrete surface or be embedded in the concrete. Plates on the outside are often used when the bulk resistance of a standardised concrete cube or cylinder is to be determined in the laboratory (DuraCrete 1997, Spragg et al. 2013). On site, two or four electrodes are placed on the concrete surface. When the electrodes are embedded, wires or bars are often used, also parallel metal mesh are suited (Østvik 2005).

If the electrodes are placed on the concrete surface, special attention has to be paid to the contact between the concrete and the electrodes. The use of wet cloth or sponges placed between the electrode and the concrete is recommended. Saturated calcium hydroxide or sodium chloride solutions can be used to wet the contact material (Newlands et al. 2008), tap water is also suited. Pressure on the electrodes generally improves the results; a contact pressure of 6 kPa has been recommended (Newlands et al. 2008). The extent of squeezing prior to applying the contact material can also have an influence.

To ensure good contact when measuring on site, it is occasionally recommended to insert the electrodes into predrilled holes filled with conductive solutions (Bungey et al. 2006). However, this is only suitable for single measurements. Where large areas are to be monitored, non-destructive methods are to be preferred.

Measurement setup

The most common methods used to measure resistance are summarised in the following subsections. A number of additional methods can be found, such as the use of direct

radar waves (Sbartai et al. 2007). Listing all the methods available is beyond the scope of this section.

Two-electrode systems

The most commonly used method to determine concrete resistivity in the laboratory is a two-electrode setup. This means that the electrical resistance is measured between two parallel electrodes on the concrete surface (Figure 3 a)) or cast in the fresh material (Figure 3 b)). Two-electrode setups are also used in the field, e.g. in the form of multiring electrodes (Figure 3 c)). A special arrangement is the 'disc method', whereby a small metal disc is placed on the concrete surface and the resistance to a comparatively large counter electrode is measured (Figure 3 d)) (Feliu et al. 1996).

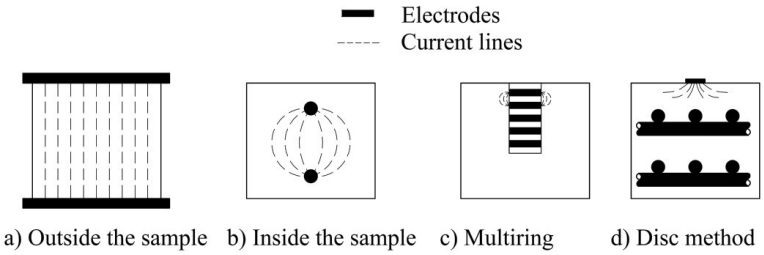

Figure 3 – Two-electrode setups.

The electrodes can be steel plates, rods, wires or the reinforcement itself. With the two-electrode arrangement, insufficient electrode-concrete contact leads to serious measurement errors (Polder et al. 2000).

Multiring electrodes are a series of two-electrode arrangements next to each other (Figure 3 c)) (Schießl and Raupach 1992). They are used to follow the moisture distribution or carbonation front in the cover concrete by monitoring resistivity changes. The commercially available sensor consists of about eight stainless steel rings with a diameter of 20 mm and a thickness of about 5 mm (DuraCrete 1997, Sensortec 2015). They are separated by PE insulation rings. An AC resistance measurement is performed between neighbouring steel rings. The sensor is embedded in the fresh concrete or a repair mortar at a depth of at least 2.5 mm from the concrete surface.

Four-electrode systems

The four-electrode setup is the most common method used for field measurements. A current is sent between the two outer electrodes, while the two inner electrodes measure the potential drop, which determines the resistance (Figure 4).

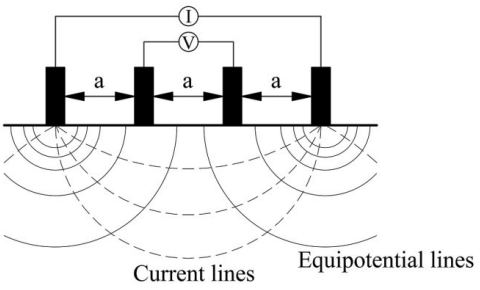

Figure 4 – Four-electrode setup.

The method is also called WENNER-technique, named after its inventor *Frank Wenner*, who introduced the setup in 1915 for soil resistance measurements (Wenner 1915). The technique normally consists of steel rods placed on the concrete surface or embedded in pre-drilled holes. There can be found several commercially available hand-held devices. Although a good contact also has to be established for the four-electrode setup between the concrete surface and the electrode, the method is less susceptible to contact problems than the two-electrode technique. The resistivity can be calculated with the following equation, provided that the electrodes are separated by an equal distance (a) and are placed on the surface:

$$\rho = 2\pi \cdot a \cdot R \qquad \text{Eq. 3}$$

There are several parameters which have to be taken into account when measuring the resistance of a sample with the four-electrode method; in particular, the distance (a) between the electrodes and the position of the equipment on the concrete surface are important. Difficulties can be encountered when measurements are made too close to edges, in line with underlying reinforcement, or when the distance between electrodes is smaller than the size of inhomogeneities in the concrete (aggregates, air voids, etc.). Recommendations on electrode spacing and positioning can be found in the literature (Millard 1991, Gowers and Millard 1999, Polder et al. 2000, Broomfield and Millard 2002, Bungey et al. 2006, Sengul and Gjørv 2008, Sengul and Gjørv 2009, Angst and Elsener 2014).

Good agreement has been observed when comparing the two-electrode setup using parallel steel plates on the outside of the concrete with the WENNER technique (McCarter and Barclay 1993, Sengul and Gjørv 2008, Deutscher Ausschuss für Stahlbeton 2012). The comparability of other methods is less well documented.

Validity

Concrete is an inhomogeneous material, which is partly a result of its composite nature, but also due to insufficient compaction or curing differences over the cross section. It is therefore not surprising that resistivity readings can vary over a concrete structure. A

variation coefficient of about 10-20% must be considered as normal in the laboratory, and up to 30% can be observed on site (Polder et al. 2000).

When making resistivity measurements, comparing the observed values with reference values obtained for similar conditions can help exclude major measurement mistakes. Reference values are given in Table 2 (Polder et al. 2000).

Table 2 – Reference values for concrete resistivity [Ωm] at 20°C (Polder et al. 2000).

Environment	Concrete prepared with PC	Concrete prepared with SCM
Very wet	50 – 200	300 – 1000
Outside, exposed	100 – 400	500 – 2000
Outside, sheltered	200 – 500	1000 – 4000
Indoor	3000 and higher	4000 – 10 000 and higher

2.2 Chloride-induced reinforcement corrosion

The passive layer breaks down locally (pitting) when a sufficient amount of chloride has penetrated the concrete cover, (cf. Section 1). In the presence of water and oxygen, corrosion occurs with the two half-cell reactions; anodic (oxidation) and cathodic (reduction) (Figure 5). During the anodic reaction iron ions dissolve in the electrolytic solution, and electrons are released in the metallic phase. The electrons are consumed in a cathodic reaction. In concrete under common environmental conditions, oxygen reduction takes place which produces alkalinity and thus strengthens the passive layer. However, other half-cell reactions, such as hydrogen evolution, may occur under special conditions. To equilibrate the anodic and cathodic reactions, an ionic current flows between them through the concrete matrix (ohmic partial process). Chloride-induced corrosion is characterised as macro-cell corrosion because anodic and cathodic regions are spatially separated from another. (Pease 2010, Bertolini et al. 2013)

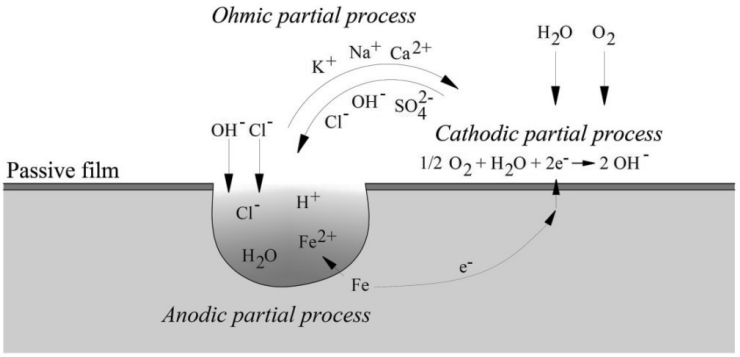

Figure 5 – Schematic illustration of chloride-induced macro-cell corrosion with the related partial processes, after (Angst 2011).

Thermodynamics

The laws of thermodynamics provide information about the likelihood of a reaction occurring spontaneously. The tendency of a metal to dissolve in a specific condition can be assessed by comparing its electrochemical potential with its reversible potential (E^{rev}). The reversible potential can be calculated based on the standard electrode potential (E^o), which can be found tabulated for a large number of reduction reactions (Hamann et al. 1998). The reversible potential is calculated by the Nernst equation (Hamann et al. 1998) taking into account the metal ion concentration ($a_{M^{z+}}$), the valence of the metal ion (z), and the temperature (T).

$$E^{rev} = E^0 + \frac{R \cdot T}{z \cdot F} \ln a_{M^{z+}} \qquad \text{Eq. 4}$$

where R is the gas constant and F is the Faraday constant.

Electrode potentials can only be measured in terms of difference from other half-cell reactions. For this purpose, reference electrodes (RE) with well-defined potentials are used. The half-cell reaction of platinised platinum in an acid solution equilibrated with hydrogen gas at 1 atm is declared to be 0 V (SHE).

Using the Nernst equation (cf. Eq. 4) and considering feasible reduction reactions, thermodynamically stable corrosion products can be illustrated over a range of pH values (Pease 2010). This approach was first applied by *Marcel Pourbaix* and these diagrams are known as POURBAIX diagrams (Pourbaix 1974). They allow the assessment of the possible corrosion reactions of a metal in solutions with different pH. The POURBAIX diagram for iron in water is shown in Figure 6; this is commonly also applied for the corrosion behaviour of carbon steel in concrete (Angst 2011). In the diagram, various thermodynamic states are illustrated: active iron dissolution/corrosion (white area), the formation of passive layers (light grey area), and the thermodynamically stable/immune state (dark grey area) where corrosion cannot take place. The hydrogen evolution and oxygen reduction reactions are represented by dashed lines in Figure 6. Between these lines, water is stable (in the form of H^+ and OH^-).

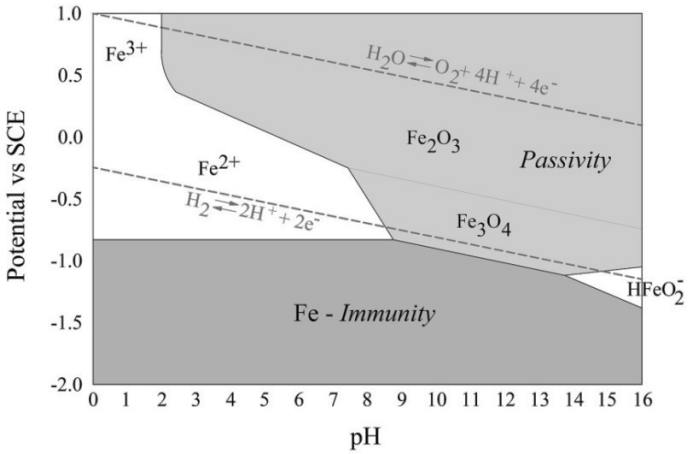

Figure 6 – Pourbaix diagram for iron in water (Temperature 25°C, iron concentration 10^{-6}mol/l) from (Pourbaix 1974), approximate reproduction.

The POURBAIX diagram shows that steel is passive under most environmental conditions without external polarisation and without Cl^-, as long as high alkalinity is maintained in the concrete pore solution.

Kinetics

While thermodynamics describes the likelihood of a corrosion reaction occurring, kinetics provides information about the rate at which the reaction proceeds.

The rate of corrosion is defined as the amount of metal (m in [g/m^2·year]) removed from the metal surface over a time period ($t_1 - t_2$). It can be calculated using Faraday's law of electrolysis (Hamann et al. 1998):

$$m = \frac{M}{F \cdot z} \int_{t_1}^{t_2} I(t)\, dt \qquad \text{Eq. 5}$$

where I is the current flowing in the corrosion cell and M is the molar mass of the metal. In electrochemical investigations, it is more common to describe the corrosion rate in the form of current density in [mA/m^2] or [µA/cm^2]. The corrosion current I_{corr} can be measured e.g. by electrochemical techniques. The corrosion rate of metal dissolution at the anode is determined by dividing the corrosion current by the corroding/anodic area:

$$i_{corr} = \frac{I_{corr}}{A} \qquad \text{Eq. 6}$$

Levels of corrosion rates published in the literature for the assessment of steel corrosion in concrete are given in Table 3.

Table 3 – Assessment of corrosion rate of steel in concrete (cf. (Broomfield 1997, González et al. 2004, Bungey et al. 2006, Bertolini et al. 2013)).

corrosion activity	corrosion rate [µA/cm^2]
passive	< 0.1
low	0.1 – 0.5
moderate	0.5 – 1
high	1 – 9
very high	> 9

The rate of the corrosion process of steel in concrete is governed by the rate of the anodic and cathodic reaction as well as the transport rate of ionic current in the concrete (ohmic partial process) (cf. Figure 5). The transport of electrons through the metallic phase is assumed to be considerably faster than the other partial processes; it does not contribute to slowing the corrosion process and is commonly neglected. The remaining three processes are complementary to another, which means that they have to occur at the same rate (Bertolini et al. 2013).

$$I_{corr} = I_{cathodic} = I_{anodic} = I_{ohmic} \qquad \text{Eq. 7}$$

Accordingly, the corrosion rate is governed by the slowest of the three partial processes; the result is referred to as anodic, cathodic or ohmic control. One of the partial processes can dominate slowing the corrosion rate in certain conditions. In water-saturated concrete where the supply of oxygen is restricted, the slow rate of the cathodic

partial process will prevent corrosion propagation. In very dry conditions, the concrete resistivity is high, which constrains current transport between anode and cathode. If chloride content is low and pH is high, the anodic reaction will be slow and no significant corrosion current will flow. In between these extremes, it is likely that a mixed control determines the overall corrosion rate.

The charge transfer reaction rate of the anodic and cathodic reactions can, under certain conditions, be measured experimentally. They are commonly illustrated in EVANS diagrams, named after *Ulick R. Evans*, who developed the idea of presenting polarisation curves in the form *E* vs log *I*, which allows the description and explanation of many corrosion related issues (Evans 1960). Figure 7 shows a simplified EVANS diagram for the process of chloride-induced (macro-cell) corrosion of steel in concrete.

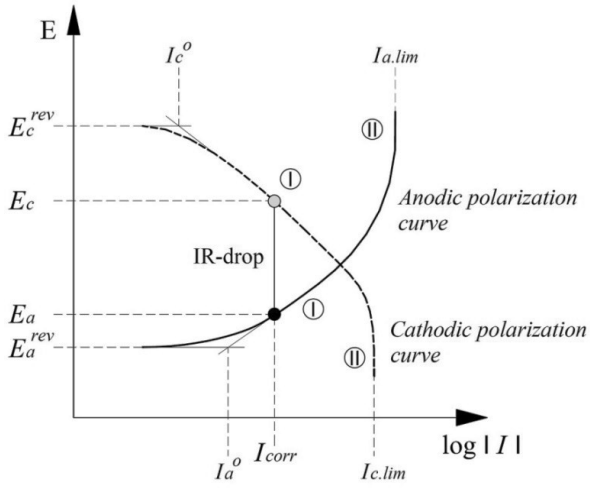

Figure 7 – Evans diagram for active corrosion.

According to thermodynamics, steel will corrode if the potential of the metal increases above E_a^{rev}. The rate will depend on the potential difference (E_a - E_a^{rev}) given by the anodic polarisation curve. The same can be derived for the cathodic reaction (cathodic polarisation curve).

The progression of the anodic and cathode polarisation curves gives information about the limiting factors determining the reaction rate. It can be distinguished between activation (I) and diffusion (II) control with a transition region between them (cf. Figure 7) (Nisancioglu 2015). In conditions where the resistance of the electrochemical reaction at the metal-electrolyte interface to convert species involved in the corrosion reaction predominates, the reaction rate is activation controlled (curve part (I) in Figure 7). A necessary precondition is the availability of all reactants at the interface. The curve progression can be approximated by a TAFEL-equation (Copson 1963).

$$E - E^{rev} = \beta \log\left|\frac{I}{I^o}\right| \qquad \text{Eq. 8}$$

The slope of the curve is termed the TAFEL constant (β), and I^o defines the exchange current (current in the absence of electrolysis). For the curves illustrated in Figure 7, the TAFEL equation can only be applied when the potential difference $E - E^{rev}$ is sufficiently high.

Various TAFEL constants have been reported for the anodic and cathodic reactions of steel in concrete. For the anodic reaction, values between 67 and 1050 mV/decade have been found (67-80 mV (Jäggi 2001), 73-136 mV (Garcés et al. 2005), 450-1050 mV (Angst et al. 2011a), 90-800 mV (Beck 2010)). For the cathodic reaction, TAFEL constant values between 97 and 239 mV/dec have been reported (97-194 mV (Raupach 1992), 170-220 mV (Angst et al. 2011a), 130-220 (Beck 2010), 222-239 (Jäggi 2001)).

In cases where the supply of reactants is slower than the rate of their reaction, the process becomes diffusion-controlled. The availability of substances is independent of the electrochemical process and therefore independent of the potential (vertical line or steep slope, part (II) in Figure 7). The corrosion current is limited (I_{lim}). Diffusion control might be expected for the cathodic reaction, in cases of limited oxygen supply. However, it has been found that it is solely in cases of long-term water saturation that the diffusion of oxygen to the electrode is a limiting factor for the cathodic reaction in concrete (Page and Treadaway 1982, Raupach 1992).

For macro-cell (chloride-induced) corrosion, the anode and cathode are spatially separated from one another (cf. Figure 5). This requires a current to be transported through the concrete (electrolyte) between them. Concrete has a certain electrical resistance, which results in a potential drop between anode and cathode, illustrated as IR drop in Figure 7. Consequently, the potentials at the anode (E_a) and cathode (E_c) are different. The IR drop depends on the strength of the current field and the electrical resistance between anode and cathode.

2.2.1 Measurement of corrosion rate

Usually, the instantaneous corrosion current I_{corr} is determined by measuring the linear polarisation resistance (R_p). The concept is based on the assumption that the *E-I* relationship is linear within a small potential range around E_{corr} (Figure 8) (Elsener 2005). A mathematical description for calculating the corrosion current from the polarisation resistance R_p was suggested by *Stern* and *Geary* in 1957 based upon the TAFEL slopes β_a and β_c (Stern and Geary 1957). The equation was later summarised as:

$$I_{corr} = \frac{\beta_a \cdot \beta_c}{2.3(\beta_a + \beta_c)} \cdot \frac{1}{R_p} = \frac{B}{R_p} \qquad \text{Eq. 9}$$

A calibration factor *B* was introduced to allow for a calculation of the corrosion current even when anodic and cathodic polarisation curves (e.g. TAFEL constants) are not available. From experiments in solution, the values *B* = 26 mV for active ongoing corrosion and *B* = 52 mV for passive conditions were derived (Andrade and González 1978). These values are frequently also used for corrosion current calculations in concrete. The uncertainties related to the calibration factor *B* are assumed to lead to an error for the corrosion current calculations within a factor of 2 (Raupach 1992, Bertolini et al. 1998, Elsener 2002, Jäggi et al. 2007, Nygaard et al. 2009).

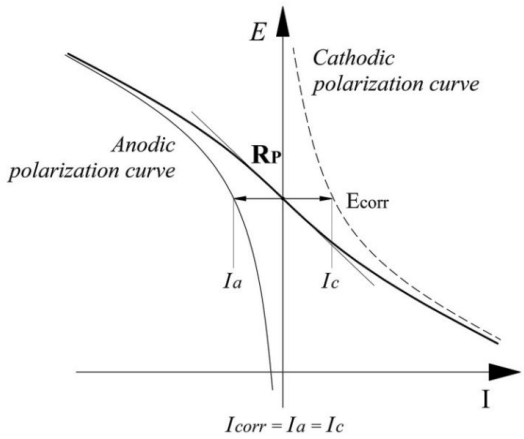

Figure 8 – Concept of the polarisation resistance, after (Elsener 2005).

It has recently been shown that the *Stern-Geary* equation (Eq.9) is not applicable for localised corrosion because the equation is based on the mixed-potential theory valid only for uniform corrosion (Angst and Büchler 2014). The following paragraphs present the techniques most commonly used for determining the corrosion current, all of them based on the polarisation resistance and the *Stern-Geary* equation. It is not claimed that they are generally applicable, and as result of the above-mentioned research (Angst and Büchler 2014), none of them can be recommended for use in connection with chloride-induced (macro-cell) corrosion.

Techniques used to determine the polarisation resistance

The polarisation resistance is measured with a three-electrode setup including the embedded steel (working electrode (WE)), a counter (CE) and a reference electrode (RE). Counter and reference electrodes can be either located on the concrete surface or embedded in the concrete. There are several techniques available.

Potentiostatic, potentiodynamic and galvanostatic techniques

With help of the counter electrode, the reinforcement can be polarised, and the change in potential is measured with the reference electrode. The static techniques are aimed at

measuring either the current response to a constant potential or the potential response to a constant current. In dynamic measurements, slow potential sweeps around E_{corr} are applied and the current response is monitored. There are various factors that influence the measurements, such as the waiting or delay time used from introducing the potential or current until the response is measured, and the rate at which the potential sweeps are applied. Information about these influences can be found in the literature (Andrade and Alonso 1996, Andrade et al. 2004, Elsener 2005, Nygaard 2008, Nygaard and Geiker 2012). Moreover, there are several challenges which have to be overcome when using the techniques in the field. In particular, the fact that the counter electrode is considerably smaller than the reinforcement steel network makes controlling and knowing the polarised surface area and thus the interpretation of the measurements difficult (Kranc and Sagüés 1993, Nygaard et al. 2009, Andrade et al. 2012).

In most such techniques, the measured polarisation resistance R_p contains the ohmic drop between the electrodes in the three-electrode arrangement (R_Ω). For electrolytes with a high electrical resistivity, as is the case for concrete, it is particularly important to correct the measured R_p for the ohmic drop; otherwise, the corrosion current will be underestimated. There are various ways of compensating for the ohmic drop. Some of them are available in automatic IR compensation features included in the common measurement procedures of potentiostats and other commercial devices. An overview of common methods of compensating for IR drop can be found in (Oelssner et al. 2006).

Electrical impedance spectroscopy

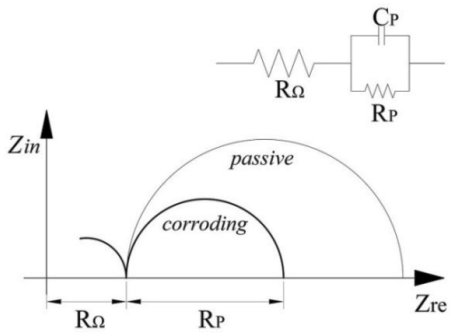

Figure 9 – Theoretical sketch of EIS results – Nyquist plot.

The IR drop and the polarisation resistance can be measured with electrical impedance spectroscopy (EIS). During EIS, an AC signal of small amplitude with changing frequencies is applied to the working electrode and the current response is measured. The impedance of the corroding system is studied in different frequency ranges. The data is analysed in BODE and/or NYQUIST plots and interpreted using appropriate equivalent circuit diagrams (Hope et al. 1986). A simplified approach is given in Figure 9; the ohmic and polarisation resistance can be obtained when analysing EIS data in this way.

Corrosion rate for localised corrosion attacks

To determine the corrosion rate of iron dissolution, the corrosion current has to be related to the corroding (anodic) area (cf. Eq. 5). In concrete structures or specimens, the corroding area can only be measured through inspections. As a simplification and to avoid opening and destroying parts of the structure or samples, the corrosion current is frequently divided by the whole area assumed polarised during the measurements.

In a localised corrosion attack, however, the corroded area might be significantly smaller than the area polarised during the measurements (Figure 10). This can cause a considerable underestimation of the actual corrosion rate. This is a known source of error with LPR measurements, and the application of a somewhat arbitrary 'pitting factor' is recommended; values between 4 and 15 have been proposed (González et al. 1995, Andrade and Alonso 1996, Elsener 1998).

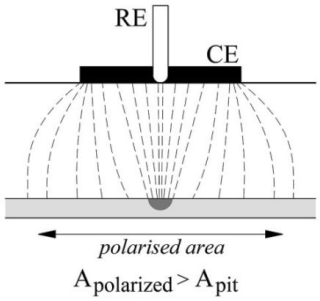

Figure 10 – Current distribution for LPR measurement for local corrosion pits.

Moreover, the determination of the ohmic drop is also related to uncertainties when localised corrosion is involved. The usual methods for measuring the ohmic drop are based either on AC, with various (preferably high) frequencies, or by interrupting a DC for a short time («1s). In both cases, the current is distributed comparatively uniformly over the polarised rebar area and consequently does not account for the actual ohmic drop arising from a non-uniform current distribution, such as must be expected in localised attacks (Elsener 2002) (cf. Figure 10). As a consequence, the IR drop measured by AC or short-time DC techniques does not reflect the actual ohmic resistance met during DC measurement, which can lead to an erroneous calculation of the corrosion current. The extent of this error depends on the distribution of anodic and cathodic areas in the polarised steel area. It has been found that an error of about two may be expected, comparable with the uncertainties related to the calibration factor *B* (Elsener 1998).

2.3 Relationship between corrosion rate and concrete resistivity

The transport of ionic current within the macro-cell between anode and cathodes and the transport process of ions through the pore structure from the surface to the reinforcement are inherent parts of the corrosion process. A relationship between corrosion rate and concrete resistivity can therefore be expected. And indeed, an inverse correlation between them is commonly observed.

The relationship between corrosion rate and concrete resistivity was studied in a literature survey. The results of this study are presented in **Paper I**. The main conclusion of the investigation was that although a tendency can be found that the corrosion rate decreases with increasing concrete resistivity, the scatter observed is high within and between the reviewed publications (Figure 11). Various reasons for the discrepancies were identified, but none of them could be recognised as the dominating cause. It was suggested that variation may arise from inaccuracies in determining the corrosion rate and/or the concrete resistivity and concrete composition. Very little discussion was found in the literature on mechanisms that might potentially provide a direct correlation between concrete resistivity and corrosion rate.

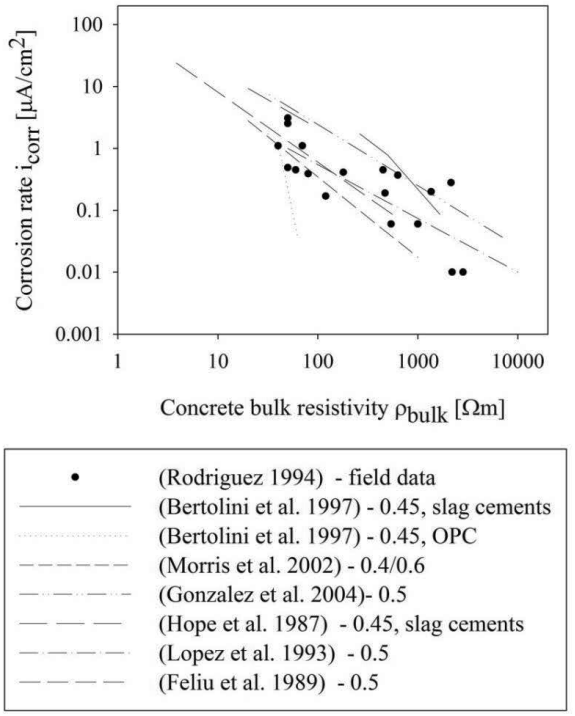

Figure 11 – Trend lines and data published in the literature on the relationship between corrosion rate and concrete resistivity for chloride-induced corrosion. The first value after the references indicates the water/binder ratio; the cement type used (if known) is given as well (cf. **Paper I**).

3 Summary of work

Three experimental studies were conducted to investigate the main objective of the PhD project (cf. Section 1.1.1). The studies are named according to the objective of the experiment, but for reasons of simplification, the terminology, 'Experimental Studies I-III' is also introduced.

Experimental Study I – Measuring galvanic currents in simulated macro-cells

Experimental Study I explored the possibilities of using galvanic current measurements to characterise the corrosion current. Various segment sizes were tested. The limitations of the pitting factor concept common in (electrochemical) methods of determining the corrosion rate for localised attack were also studied.

Experimental Study II – Resistance between small anodes and a large cathode network

In Experimental Study II, the resistance between small anodes and a large cathode network was measured and compared to the bulk resistivity. The study identified limitations of mortar resistivity measurements as a means of characterising the ohmic resistance within a macro-cell.

Experimental Study III – Rate-limiting step of chloride-induced macro-cell corrosion

Experimental Study III examined the influence of mortar resistivity on the rate-limiting step of chloride-induced macro-cell corrosion. The extent to which mortar resistivity can be related to the partial process was discussed.

The materials used in the experiments are described in detail in **Appendix A**. Results not published in the appended papers are given in **Appendices B-D**. An overview of the papers and appendices related to the experimental work is given below.

Table 4 – Experiments and related papers and appendices

	Topic	Paper/ Appendix
Experimental Study I	Galvanic current measurements	Paper II Appendix B
Experimental Study II	Resistance between small anodes and a large cathode network	Paper III Appendix C
Experimental Study III	Rate-limiting step of chloride-induced reinforcement corrosion	Papers IV + V Appendix D

3.1 Experimental Study I – Measuring galvanic currents in simulated macro-cells

The non-destructive determination of the instantaneous corrosion rate of steel embedded in concrete or mortar is subject to a variety of potential errors (cf. Section 2.2.1). For chloride-induced corrosion in particular, several uncertainties arise from the local character of the attack (cf. Section 2.2.1). Using segmented rebars and measuring the galvanic current between actively corroding and passive segments is an alternative method appropriate for laboratory investigations to avoid some of these potential errors.

Segmented rebars have occasionally been used in experiments (Nöggerath 1990, Raupach 1992, Bertolini et al. 1998, Elsener 2002, Jäggi et al. 2007, Nygaard et al. 2009). The current flowing between the segments is measured with zero-resistance ammeters (ZRAs). Shunts with known ohmic resistance can also be used. The accuracy of the device should be in the range of less than 1 µA because the current between anode and cathode segments (galvanic current I_{galv}) can be very low. Galvanic current measurements are much more robust than electrochemical measurements. However, the anode segment will hardly ever have a uniform corrosion attack. In most cases, a certain amount of cathode (passive areas) on the anode segment will lead to current flow on the segment itself, referred to as micro-cell corrosion or self-corrosion (Andrade et al. 2008, Beck 2010). In case of large amounts of micro-cell corrosion, the corrosion rate can also be considerably underestimated in experiments using segmented rebars and relying on galvanic current measurements.

With regard to experiments executed in solution, it has been found that for a cathode-to-anode area ratio (C/A ratio) of 10 (exposed area of the anode segment 50 mm^2), the amount of self-corrosion is limited to 25% (Andrade et al. 2008). A detailed study of the extent of self-corrosion on anode segments embedded in a variety of different concrete mixes was undertaken by *Matthias Beck* (Beck 2010). He found that specimens with high galvanic currents between anode and cathode showed lower self-corrosion fractions than macro-cells with low galvanic currents (constant exposed area of the anode segment 314 mm^2). *Beck* also found a dependence of self-corrosion on the w/b ratio, chloride content, temperature and degree of saturation. He identified self-corrosion fractions between 4% and 75% for the various conditions tested (Beck 2010, Deutscher Ausschuss für Stahlbeton 2012).

To explore the possibility of using segmented rebars for determining the corrosion rate, a setup was designed with differing segment sizes. The amount of self-corrosion depending on the segment size was studied (**Paper II**). The setup also made it possible to study the concept of 'pitting factor' taking into account the corroding area and IR drop correction (**Appendix B**).

3.1.1 Experimental setup

Segmented rebars consisting of one mild steel segment (anode segment, ribbed, Ø 10 mm) and two stainless steel segments (cathode segments, unribbed, Ø 10 mm), were embedded adjacent to one another in chloride-contaminated mortar (Figure 12).

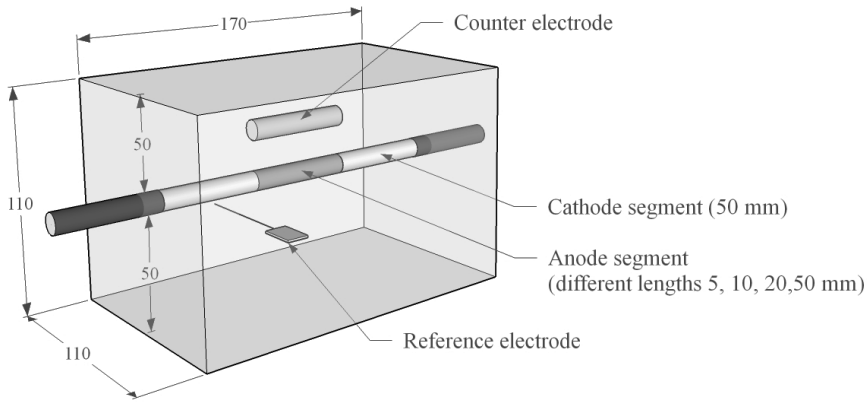

Figure 12 – Experimental setup – Experimental Study I (measures in [mm]).

The length of the anode segment was varied between 5 mm (exposed area 157 mm^2), 10 mm (314 mm^2), 20 mm (628 mm^2) and 50 mm (1570 mm^2). The cathode segments had a constant length of 50 mm each (1570 mm^2). Anode and cathode segments were electrically isolated from one another with silicon.

Each segmented bar was placed in an individual mould along with a reference electrode and a counter electrode (cf. Figure 12). An activated titanium mesh was used as reference electrode [4], and the counter electrode was a 45 mm long stainless steel tube.

To shorten the initiation period and enhance corrosion, a chloride-contaminated mortar was used (2.5% Cl^- by cement weight, composition and material see **Appendix A**). After removing the formwork, the specimens were stored for 5 days in a laboratory environment to ensure a sufficient surface dryness to apply an epoxy coating. Epoxy was painted on all vertical sides of the specimens; the top and bottom sides were not painted. Subsequently, the specimens were kept in a relative humidity of approximately 95-98% and a temperature of 20-22 °C for the whole testing period.

More details on the setup and methods of investigation can be found in **Paper II** and **Appendix B**.

3.1.2 Summary of results

The results of Experimental Study I are presented in **Paper II** and **Appendix B** and are summarised in the following:

- It was confirmed that the ratio between the corrosion current determined with LPR measurements and the galvanic current measured between anode and cathode segments strongly depends on the size of the anode segment. Moreover, even small anode segments (exposed area 157 mm^2, C/A ratio = 20) were subject to a large amount of self-corrosion (>50%).

- For the geometry tested here, pitting factors up to ~36 were recognised. The pitting factor is strongly related to the C/A ratio (Figure 13). On the basis of the results, the application of a random pitting factor to take account of localised corrosion cannot be recommended when the actual corroding area is unknown, as in non-destructive corrosion current measurements (such as LPR).

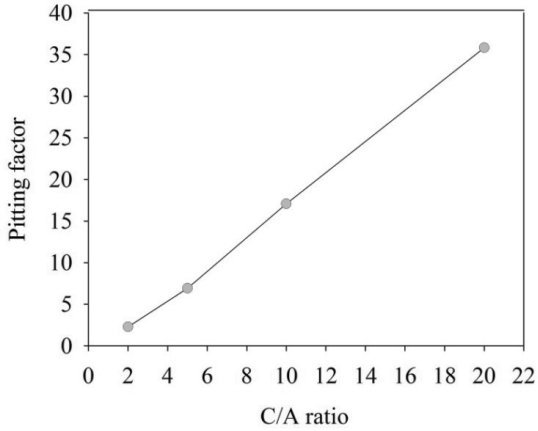

Figure 13 – Dependence of the pitting factor on the C/A ratio; each point indicates a different anode size – cf. **Appendix B.1**.

3.2 Experimental Study II – Resistance between small anodes and a large cathode

Experimental Study II investigated the influence of inhomogeneities on the resistance between small anodes and a large cathode network (termed cell resistance R_{cell} in the context of Experimental Study II).

Chloride-induced corrosion develops as a localised type of corrosion with small anodic areas spatially separated from a much larger cathode (cf. Section 2.2). During the corrosion process, current flows through the concrete material between the anodic and cathodic areas. The current concentrates at the pit opening (anode), resulting in a 'potential drop' right in front of the anode. This is known from other fields as spreading resistance, $R_{spreading}$. In homogenous materials, the spreading resistance can be calculated based on the bulk resistivity of the surrounding material and the geometry of the small electrode. Various approaches and formulations can be found in the literature (Nanis and Kesselman 1971, Denhoff 2006). Concrete, however, is an inhomogeneous material not only due to its composite nature, but also due to differences in casting, compaction, curing, exposure, etc. Inhomogeneities will have considerable influence on the cell resistance of small anodes. Because the cell resistance has a direct influence on the corrosion process (ohmic partial process, cf. Figure 5), its characteristics are of particular interest.

The main objective of the experimental study was to investigate the influence of various parameters on the cell resistance. Mortar specimens equipped for the purpose were designed, which consisted of simulated macro-cells with small anode segments (circular discs Ø 6.0 mm – exposed area 28.3 mm^2). This was considered a realistic pit size, especially in the early stages after corrosion initiation (cf. Table 5).

Table 5 – Pit surface areas reported in the literature (maximum values are presented).

	Pit area [mm^2]	Exposure period	Exposure
(Apostolopoulos et al. 2013)	max = 29.8	1 year	Salt spraying
(Angst et al. 2011a)	max = 0.035[*1]	20 – 40 days	Wetting/Drying
(Pacheco-Farías 2015)	max = 9[*2]	36 weeks	Wetting/Drying

[*1] theoretical estimations
[*2] cracked concrete

Two mortar mixes were used to evaluate the effect of low and high resistivity (quality) mortars on the cell resistance. It is known that bleeding zones below the embedded steel bars in relation to the casting direction exhibit a different (coarser) microstructure than the bulk material or the material above the reinforcement (Al Khalaf and Page 1979, Soylev and François 2003, Bensted and Barnes 2009, Angst 2011). For this reason, anode segments were positioned facing the bottom, top or sides in relation to the casting direction.

Chlorides were mixed in some of the mortars to investigate the effect of corrosion products on the cell resistance. The electrical resistivity of corrosion products is seldom stated in the literature, but investigations on the corrosion of electrical contacts reported a contact resistivity of up to 10^3 Ωm when the metal is heavily corroded (Slade 2013). This is comparable to the bulk resistivity of high resistivity concretes (cf. Table 2) and indicates that the resistivity of corrosion products may influence the cell resistance.

3.2.1 Experimental setup

A detailed description of the experimental setup can be found in **Paper III**. Additional information about the materials used as well as the mortar composition and properties is given in **Appendix A**. The initial idea of the setup is based on experiments using instrumented rebars with small pins undertaken at the Technical University of Denmark (DTU) (Pease et al. 2011, Michel et al. 2013b).

Experimental Study II consisted of four mortar specimens. Each of them was equipped with two instrumented stainless steel tubes and a segmented centre tube of stainless steel (Figure 14). Five anode segments (Ø 6 mm, exposed area 28.3 mm^2, carbon steel) were mounted in different positions on each tube. The cathode-to-anode area ratio could be varied between 11 and 575 (with several values in between).

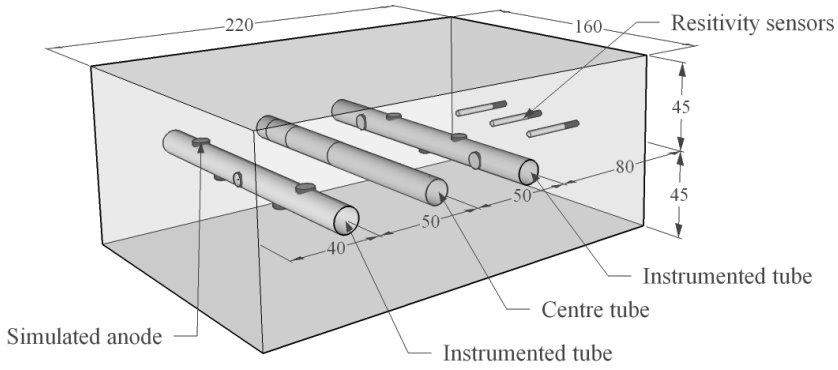

Figure 14 – Experimental setup – Experimental Study II (measures in [mm]).

Three resistivity sensors (built of small stainless steel tubes Ø 2.5 mm) were embedded in each specimen. With the help of the sensors, the bulk resistivity could be measured.

For each of the four specimens, a different mortar mix was prepared (high and low resistivity mortars, with and without chlorides mixed in). See **Appendix A** for the composition and properties.

All the instrumented mortar specimens were wrapped in plastic foil after demoulding, 24 hours after casting. They were kept in sealed conditions for the first 10 months after

casting. Then they were unwrapped and an epoxy coating was applied on all vertical sides to ensure one-dimensional moisture profiles while the samples were exposed to tap water. Approximately one year after casting, the specimens were pressure-saturated. More detailed information on the exposure conditions can be found in **Paper III**.

Electrical resistance measurements of the bulk material and the cell resistance were carried out during the study. Measurements were made using electrical impedance spectroscopy (EIS) and with a hand-held LCR meter (additional explanations on the resistance measurements can be found in **Appendix C**).

A supplementary study was carried out with a comparable setup using water as the electrolyte to simulate homogenous conditions for the test setup. Information on this additional experiment is also provided in **Paper III**.

3.2.2 Summary of results

The results of Experimental Study II are presented in **Paper III** and **Appendix C** and are summarised in the following:

- The cell resistance (resistance between anode and cathode) is independent of the cathode-to-anode ratio when the latter exceeds a value of 40. For the geometrical conditions tested in the study, no pronounced influence of cathode distance on the cell resistance (maximum distance 100 mm) was found.

- Local inhomogeneities (inherent to concrete (here: mortar), such as aggregates and air voids) in front of small anodes influenced the cell resistance. This led to a considerable scatter between cell resistances for anodes of the same size and embedded in the same material (with a factor of up to ten). The position of the anode in relation to the casting direction influenced the cell resistance in low-resistivity (low quality) mortar, but had little influence in high-resistivity (high quality) mortars.

- The ratio between bulk resistivity and cell resistance (cell constant, cf. Eq.1 and Figure 15) for one and the same anode was not constant over time and depended on moisture conditions. It was concluded that cell resistance is not directly correlated with bulk resistivity.

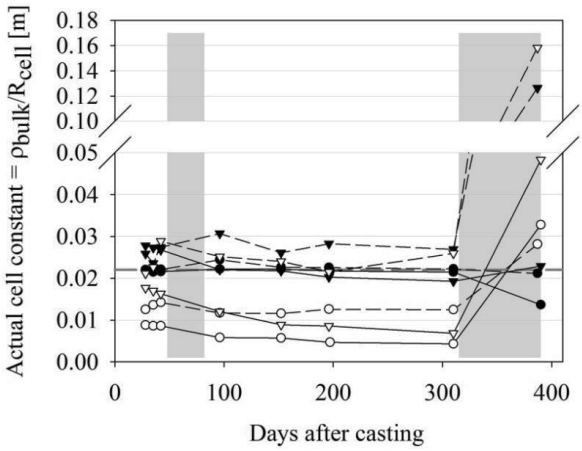

Figure 15 – Actual cell constants determined during Experimental Study II. The theoretical value for homogenous material conditions is indicated as a dashed grey line. Grey areas mark times of different exposure than sealed storage; the specimens were pressure-saturated approximately 380 days after casting (cf. **Paper III**).

3.3 Experimental Study III – Rate-limiting step of chloride-induced macro-cell corrosion

The third Experimental Study was intended to investigate the influence of mortar resistivity on the corrosion process. The three main partial processes (anodic, cathodic and ohmic, cf. Figure 5) that contribute to the overall corrosion propagation were studied with regard to their potential correlation with the mortar resistivity.

In the literature, the anodic partial process was found to depend on the moisture state as well as the mortar composition and chloride content (Warkus 2014). A potential correlation between the anodic partial process and the bulk resistivity is discussed in (Angst et al. 2011a), where a relationship is suggested because both are related to the flow of ionic charge.

For the cathodic polarisation behaviour, a rather poor correlation with the moisture content is documented (Raupach 1992). Whereas temperature influences the cathodic reaction markedly (Brem et al. 2002). The extent to which the cathodic partial process can be related to mortar resistivity is therefore somewhat unclear.

It might be expected that the ohmic partial process could be reflected in mortar resistivity because it accounts for current transport through the mortar matrix. However, the findings presented in Experimental Study II indicate that there is no direct correlation between bulk resistivity and the ohmic resistance between small anodes and a large cathode network.

In Experimental Study III, macro-cell corrosion was simulated using an experimental setup comparable to the one in Experimental Study II. Small anode segments were electrically separated from a large cathode network. Galvanic current and resistance measurements could be undertaken between the anode and cathode. It was also possible to study the polarisation behaviour of the anode and cathode in isolation. The setup enabled the investigation of the three partial processes, separate from one another and in comparison with the mortar bulk resistivity.

3.3.1 Experimental setup

The experimental setup is described in detail in **Paper IV**. A sketch of the setup is shown in Figure 16. The concept of the setup is comparable to that of Experimental Study II. Anode segments with an exposed area of 28.3 cm^2 were also chosen for this study (carbon steel, Ø 6 mm).

The anode segments were mounted on a stainless steel tube (instrumented tube, termed C1). All the anode segments were placed on the lower side of the tube in relation to the casting direction, because the highest corrosion activity was expected in this area (Soylev and François 2003). Four anode segments were placed in each specimen,

mainly to increase the probability of corrosion onset at one of them. After corrosion initiation, macro-cell corrosion was simulated with just one of the four anode segments; the other anode segments were isolated. The macro-cell cathode was represented by a network of stainless steel bars (C1-1 to C2-2) with different cover depths and distances from the anode segment. The C/A ratio for all cathodes connected was 685.

All stainless tubes and bars intended to work as cathode were preheated to increase the cathodic capacity of the exposed surface. Details are given in **Appendix D.1**.

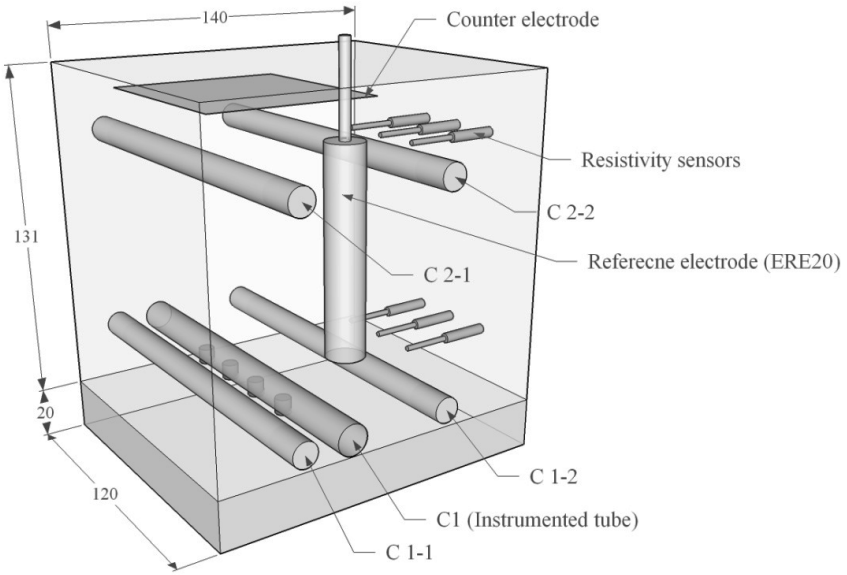

Figure 16 – Experimental setup – Experimental Study III (measures in [mm]).

The anode and cathode segments were electrically isolated from one another and connected manually for most of the testing period. They were disconnected occasionally so that measurements could be undertaken for the anode and cathode separately.

Electrochemical measurements were undertaken with an embedded reference electrode (ERE20 FORCE TECHNOLOGY) and an embedded counter electrode (stainless steel mesh) (cf. Figure 16).

The same mortar recipes as studied in Experimental Study II were used in Experimental Study III (**Appendix A**), except that no chlorides were added to the mix. Corrosion was initiated by exposing the specimens to a chloride solution (3 mol/l NaCl). To speed up chloride ingress, the cover depth of the anodes (originally 30 mm to ensure a realistic cover depth under casting) was reduced to 10 mm (Nygaard and Geiker 2005, Angst et al. 2011b). Subsequently, the specimens were gently dried in an oven (30 °C – low RH) before chloride exposure (following the procedure reported in (Nygaard and Geiker

2005)). The specimens were exposed to a variety of different RH and temperatures. The primary aim of the different kinds of exposure was to achieve a broad range of different mortar resistivities. It was not within the scope of the experiment to study the influence of different temperature or moisture conditions on the corrosion process itself. Details on the exposure can be found in **Paper IV**.

3.3.2 Summary of results

The results of Experimental Study III are presented in **Paper IV**, **Paper V** and **Appendix D**, and are summarised in the following:

- It was found that the process of chloride-induced macro-cell corrosion (for the geometry and materials studied) is controlled by a combination of the anodic, cathodic and ohmic partial processes.

- The ohmic and anodic partial processes are governed by the local conditions in close proximity to the anode (for small anodes). No direct relationship was observed between these partial processes and the bulk resistivity.

- It was observed that the cathodic reaction kinetics are not related to the mortar bulk resistivity.

- For small anodes, the corrosion kinetics at the anode are directly influenced by local inhomogeneities in the vicinity of the anode (mass transfer limitation). The concept of anodic-resistance control (meaning the combined effect of the anodic charge transfer reaction and the ohmic resistance associated with the anode) was found to be appropriate, especially for the corrosion process in mortars prepared with fly ash.

These findings indicate that there cannot be one direct relationship between mortar resistivity and the corrosion rate. This is due to the fact that mortar resistivity is not directly correlated to the underlying partial processes that determine the corrosion rate.

- The empirical relationship between corrosion rate and mortar resistivity is material-dependent (Figure 17). It was found that although mortar prepared with fly ash exhibited one order of magnitude higher bulk resistivity than mortars made of plain Portland cement, the corrosion rates differed less.

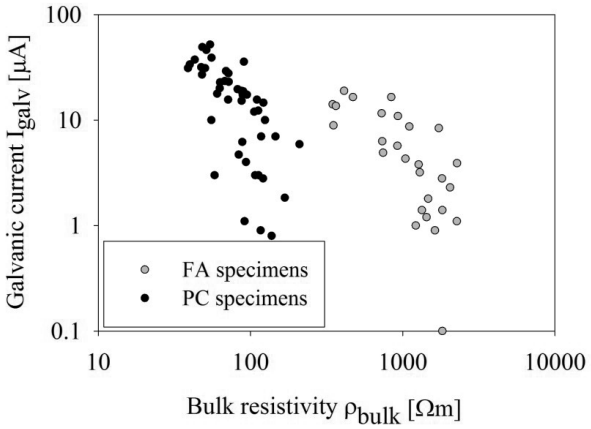

Figure 17 – Comparison between the bulk resistivity and the galvanic current (cf. **Paper IV**).

4 Main findings and conclusions

The following chapter summarises and discusses the main findings of the PhD project and gives the conclusions. The main objective of the project was to investigate the possibilities of using measurement of concrete resistivity to predict the rate of chloride-induced corrosion. Based on findings from an extended literature review an experimental investigation was undertaken. The main focus in the choice of materials and exposures was to offer a broad range of variation in mortar resistivity and promote active corrosion. The mortar resistivity was varied by using various mortar mixes and a range of different exposures (in terms of both temperature and moisture conditions). It was not within the scope of the study to investigate the influence of given exposure conditions (e.g. temperature, moisture state) nor material composition on the corrosion process or mortar resistivity. The investigations were undertaken for chloride-induced macro-cell corrosion of steel reinforcement in mortar, conclusions are limited to the geometrical dimensions defined when designing the experimental setup (in terms of both anode size and cathode-to-anode ratio).

Objective 1: To identify the lack of knowledge in the current discussion about the relationship between corrosion rate and concrete resistivity

The literature on the correlation between corrosion rate and concrete resistivity was reviewed and discussed in **Paper I**. A general tendency has been reported that corrosion rate decreases with increasing concrete resistivity, but the scatter within and between the studies reviewed was high. The relationship was investigated in a variety of studies using different setups, materials and conditions. The methods used to measure corrosion rate and concrete resistivity varied. The principal approaches to handling and comparing data were also found to be inconsistent. These differences in the principal approaches to investigating the relationship between corrosion rate and concrete resistivity may partly explain the scatter observed. However, comparisons between the various investigations also showed that the relationship depends on the corrosion mechanism (localised or uniform), and that the concrete composition, and especially the use of supplementary cementitious materials, seems to alter the overall trend.

It was shown in the review (**Paper I**) that the overall scatter of the reported data covers the whole range of expected corrosion rates from low to high for a given bulk resistivity. All the studies on the relationship between corrosion rate and concrete resistivity were purely empirical. It was especially clear with regard to chloride-induced corrosion that no attempts were made to explain the principal mechanisms that might create the assumed correlation. Yet without improved understanding of the corrosion process and the partial processes that affect the corrosion rate and its correlation with concrete resistivity, one cannot adequately explain, nor make general use of any potential relationship between corrosion rate and concrete resistivity.

Conclusion

The lack of knowledge in the current discussion about the relationship between corrosion rate and concrete resistivity is rooted in the absence of fundamental understanding of the assumed mechanistic connection between them. The current state of the art does not permit the assessment of corrosion rates based on resistivity measurements.

Objective 2: To study the rate-limiting processes for chloride-induced macro-cell corrosion

An experimental setup was designed using instrumented steel tubes where steel surfaces acting as anodes and cathodes were electrically separated. Such a setup allows galvanic current and resistance measurements between the simulated anodes and cathodes. It also enables the study of anodic and cathodic reaction kinetics in isolation from each other. The setup was considered well suited for the investigation of the corrosion process and the influence of concrete resistivity on the partial processes.

Galvanic current measurements between anode and cathode segments are assumed to be more robust than common electrochemical methods, but galvanic current measurements can considerably underestimate the actual corrosion current depending on the extent of self-corrosion on the anode segment. A suitable segment size, preferably as small as possible but still realistic, must be chosen to avoid an underestimation of the actual corrosion current (**Paper II**). For most of the experimental work, anodes in the form of discs with a diameter of 6 mm were used (**Paper III**, **Paper IV** and **Paper V**). The simulated anodes were intended to present a single pit, which would develop on the reinforcement during the early propagation stage of chloride-induced corrosion.

The partial processes (anodic, cathodic and ohmic) were studied separately with regard to their correlation with mortar bulk resistivity. Information was obtained by measuring the ohmic resistance between small anodes and a cathode network. It was shown that the ohmic partial process is strongly dependent on the local conditions around the anode (**Paper III**). In particular, inherent inhomogeneities in the mortar (such as aggregates and air voids) in the immediate vicinity of the anodes influence the resistance (current flow) between the anode and the cathode. Inhomogeneities arising from e.g. bleed water zones can also affect the ohmic resistance between the anode and the cathode. Consequently, it could be shown that for small anodes (comparable in size with inherent inhomogeneities such as aggregates and air voids) the ohmic partial process is not directly related to the bulk resistivity. For the dimensions and materials (mortars) tested, a variation in the ohmic resistance between the simulated anode and cathode for a given bulk resistivity of up to one order of magnitude was found. Such variation must be expected in concrete for pit sizes of several centimetres as typically aggregates up to 32 mm are used.

On the basis of anodic polarisation curve measurements, it was found that the anodic partial process can be characterised by a polarisation resistance (a linear correlation between potential and current changes). The polarisation resistance of the anode was found to be closely correlated with the local conditions around the anode, which suggests mass transfer control of the anodic partial process (**Paper IV**). This can be described by the concept of anodic-resistance control, introduced in the literature. No direct correlation between the bulk resistivity and the anodic polarisation resistance was found, even though a trend can be observed that increasing mortar resistivity also increases the anodic polarisation resistance (**Paper IV**).

The cathodic polarisation behaviour was found to be adequately described by a TAFEL equation. The TAFEL constant and exchange current density showed no correlation with the bulk resistivity (**Paper IV**). No influence of mortar resistivity on the corrosion rate can be expected in cases where the corrosion process is controlled by the cathodic partial process. This is in agreement with limitations related to the empirical relationship between corrosion rate and concrete resistivity proposed in the literature, where it is stated that such a relationship is not valid in the case of saturated concrete or above an atmospheric relative humidity of approximately 95% (**Paper I**). In these cases, cathodic control of the corrosion process is to be expected.

It was found that, for the macro-cell geometry and materials tested none of the partial processes was dominant in controlling the overall rate of the corrosion process. It was observed that all three partial processes have a certain influence. For mortars with a comparatively low bulk resistivity, 40-60% of the corrosion process was found to be controlled by the cathodic partial process. For high resistivity mortar, 60-80% of the corrosion process was under anodic-resistance control (**Paper IV**).

Comparisons between the galvanic current and the bulk resistivity on the one hand, and the ohmic resistance associated with the anode on the other, showed clearly that for small anodes the corrosion process is more influenced by the local conditions around the anodes than by the bulk resistivity.

Consequently, no unique correlation between the corrosion rate and the mortar bulk resistivity could be documented because mortar resistivity is not directly related to the partial processes underlying the corrosion process. The scatter obtained for comparisons between corrosion rate and concrete resistivity can thus be explained.

Conclusion

The cathodic partial process cannot be related to bulk resistivity at all, and the anodic and ohmic partial processes are not directly correlating with the bulk resistivity (for the anode size tested). In addition, a mixed control of all three partial processes was identified for the conditions tested in this research. On the basis of these findings, it can be concluded that there can be no mechanistic relationship between corrosion rate and concrete resistivity.

Objective 3: To discuss the applicability of concrete resistivity as an indicator of the rate of chloride-induced corrosion for service life assessment.

The previous section explained that the relationship between corrosion rate and concrete resistivity can only be of an empirical nature and that a scatter must be expected because concrete resistivity cannot be directly correlated with the partial processes underlying corrosion propagation.

Nevertheless, the corrosion rate determined for the simulated anodes was compared with the bulk resistivity and with the trend lines from the literature reviewed (**Paper V**). This was done to allow an evaluation of the scatter found in the experimental study presented and to enable comparison with the literature data. It was confirmed that the empirical relationship between corrosion rate and concrete resistivity is material-dependent, which is in agreement with suggestions from the literature (**Paper I**). It was proposed that the material dependency of the empirical relationship can be explained by differences in the pH of the pore solution. Lower pH in the pore solution results in a higher bulk resistivity, but can also favour higher corrosion rates (**Paper V**). The scatter obtained in the dataset for the two materials investigated was high. For a given resistivity, the corrosion rate varied by more than one order of magnitude. This exceeds the scatter observed in other studies in the literature. Moreover, it was found that the instantaneous corrosion rates determined in the study presented (based on galvanic current measurements and a small anode area) were considerably higher than corrosion rates published in the literature. This was ascribed not only to the corrosion conditions established, but also to the method of determining the corrosion rate, which differed from common approaches (mainly due to differences in the anode size used for calculating the corrosion rate).

Inherent concrete inhomogeneities were identified as major causes of the high scatter obtained in the empirical relationship between corrosion rate and bulk resistivity (**Paper III, Paper IV** and **Paper V**). In particular, inhomogeneities in the near vicinity of anodes were shown to have considerable influence on the corrosion process in the early and intermediate stages of corrosion propagation. The author is not aware of any service life models that take into account the inhomogeneity of concrete. The findings of this research suggest that assuming concrete to be homogenous is an oversimplification.

The possibility of using the empirical relationship between corrosion rate and concrete resistivity for service life assessment and service life modelling is briefly summarised in what follows.

Material choice for the planning of new structures

In the literature, the high bulk resistivity of concretes made with supplementary cementitious materials (SCM) such as fly ash, silica fume or slag is often emphasised and related to an assumed improved durability performance. In this research (**Paper V**), as in earlier investigations (**Paper I**), it has been found that although mortars/concrete

prepared with SCM exhibit a higher bulk resistivity (in particular in the long term) than mixes prepared with Portland cement alone, the corrosion rate is not correspondingly lower. So the use of concrete made with SCM to improve durability performance (in the propagation period) cannot be justified on the basis of increased concrete resistivity alone.

Assessment criteria for existing structures

In this research, it has been shown that the measurement of both corrosion rate and concrete resistivity are subject to several challenges. In particular, the determination of the rate for chloride-induced corrosion is very uncertain due to the local nature of attacks. Common methods cannot adequately take this into account (**Paper V** and **Appendix B.1**). Measurements of the bulk resistivity also depend on a variety of parameters (e.g. frequency, **Appendix C.1**). Moreover, it has been shown that local conditions around the anode are more important for the early and intermediate stages of corrosion propagation than bulk resistivity.

Consequently, general threshold values and/or models based on experimental data like those compared in the literature review (**Paper I**) can only be valid and applicable for the conditions and materials they were obtained for. They are also limited to the specific measurement methods used (**Paper V**). It is not recommended to transfer the empirical relationship between corrosion rate and concrete resistivity to other materials or conditions.

Measurement methods of all kinds (electrochemical, destructive, non-destructive, etc.) and assessment criteria for reinforced concrete structures are generally connected with considerable uncertainty. In particular, measurement techniques for determining corrosion current or rate (such as LPR techniques) are associated with general reservations and application challenges. There are currently no methods available that allow a reliable and non-destructive determination of the corrosion rate. In this context, an empirical relationship between corrosion rate and concrete resistivity may still be utilised to identify potential areas in a concrete structure which are subject to a risk of high corrosion rates. This is, however, only possible for one and the same material.

Conclusion

In the absence of other reliable methods for assessing corrosion propagation in existing concrete structures, the empirical relationship between corrosion rate and concrete resistivity may be utilised to a limited extent. However, further applications, in the form of general threshold values or any models based upon them, are not generally applicable. This conclusion can be explained with the dependency of the relationship on material composition and in particular the fact that concrete resistivity is not directly correlated with the underlying partial processes that determine the corrosion rate.

5 Future research

Corrosion propagation in concretes prepared with fly ash and other supplementary cementitious materials

In literature, the extent of corrosion commonly observed for concretes prepared with SCM is lower than for those made of plain PC. This is often explained by an increased bulk resistivity of concretes made with SCM compared to concretes made with PC only. However, it was shown that instantaneous corrosion currents in mortars prepared with fly ash were measured in the same range as for mortars prepared with PC, despite a difference in bulk resistivity of a factor of ten (**Paper V**). Based on the presented findings, the improved durability performance of concrete prepared with fly ash (and presumably other SCM) cannot be explained solely by their higher bulk resistivity. Future research is needed to study the corrosion performance of concretes prepared with SCM once corrosion has started so that an appropriate understanding can be gained.

The influence of inhomogeneities on the corrosion process and for service life modelling

In the research presented, small anodes were investigated representing the early stages of corrosion propagation. It was found that for small anodes the corrosion process is to a great extent influenced by inhomogeneities inherent to concrete (such as aggregates and voids) (**Paper III** and **Paper IV**). As corrosion proceeds, the anodic area will reach and exceed the dimensions of voids and aggregates, the variation caused by these inherent inhomogeneities will decrease and eventually vanish. However, the resistance related to the anode will also depend on other parameters, such as the deposit of corrosion products or the expansion of corrosion products causing cracks and degradations around the anode, which will introduce other inhomogeneities during the long-term of corrosion propagation. To what extent these inhomogeneities influence the corrosion process needs further investigation.

To simplify models, homogenous material conditions are commonly assumed. The findings of this research indicate that inhomogeneities have an influence on the corrosion process and that certain assumptions (e.g. anodic-resistance control) can only be explained by taking them into account. Moreover, disregarding their influence introduces a considerable scatter in results. Further research is needed to allow for an adequate description of the influence of inhomogeneities on the corrosion process and to verify the extent to which they have to be considered in service life models.

Interaction between anodes

Localised corrosion was studied in this project by simulating one pit in a well aerated, passive cathode network. However, usually several pits are identified on the steel surface; mutual interaction between them has to be expected. Using a setup comparable

to the one developed in Experimental Studies II and III or similar approaches (perhaps models) offers the possibility of studying the effect of several pits and their mutual interaction. Detailed investigation of the corrosion process for several neighbouring pits and the extent to which corrosion propagation is influenced by their interactions is highly relevant and needed.

Rate-limiting step of chloride-induced corrosion

Small-scale laboratory specimens can only provide a limited steel surface area which is considerably smaller than the steel surface in large-scale structures. The implications of the limited cathode area on the determination of the rate-limiting step were discussed in this project (**Paper IV**). The ohmic resistance associated with a remote cathode was ascribed to the ohmic partial process, consequently it was suggested that in large-scale structures the corrosion process can only be under anodic or resistance control, because in principle an infinitely large cathode area is available for the cathodic reaction. The approach needs further verification, and its implications for the extrapolation of findings from small laboratory-scale specimens to large structures must be studied.

References

Ahmad, S. (2014). An experimental study on correlation between concrete resistivity and reinforcement corrosion rate. Anti-Corrosion Methods and Materials 61(3): 158-165.

Al Khalaf, M. N. and C. L. Page (1979). Steel/mortar interfaces: Microstructural features and mode of failure. Cement and Concrete Research 9(2): 197-207.

Andrade, C. and C. Alonso (1996). Corrosion rate monitoring in the laboratory and on-site. Construction and Building Materials 10(5): 315-328.

Andrade, C., C. Alonso, J. Gulikers, R. B. Polder, R. Cigna, Ø. Vennesland, M. Salta, A. Raharinaivo and B. Elsener (2004). Rilem TC 154-EMC: Electrochemical techniques for measuring metallic corrosion - Test methods for on-site corrosion rate measurement of steel reinforcement in concrete by means of the polarization resistance method. Materials and Structures 37(273): 623-643.

Andrade, C., C. Alonso and J. Sarría (1998). Influence of relative humidity and temperature on-site corrosion rates. Materiales de Construcción 48(251): 5-17.

Andrade, C. and R. d'Andrea (2008). Electrical resistivity as microstructural parameter for the calculation of reinforcement service life. First International Conference on Microstructure Related Durability of Cementitious Composites. W. Sun, K. v. Breugel, C. Miao, G. Ye and H. Chen. Nanjing, China, RILEM Publications.

Andrade, C., P. Garcés and I. Martinez (2008). Galvanic currents and corrosion rates of reinforcements measured in cells simulating different pitting areas caused by chloride attack in sodium hydroxide. Corrosion Science 50(10): 2959-2964.

Andrade, C. and J. A. González (1978). Quantitative measurements of corrosion rate of reinforcing steels embedded in concrete using polarization resistance measurements. Materials and Corrosion-Werkstoffe und Korrosion 29: 515-519.

Andrade, C., J. Sanchez, J. Fullea, N. Rebolledo and F. Tavares (2012). On-site corrosion rate measurements: 3D simulation and representative values. Materials and Corrosion-Werkstoffe und Korrosion 63(12): 1154-1164.

Angst, U. (2011). Chloride induced reinforcement corrosion in concrete - Concept of critical chloride content - methods and mechanisms, Doctoral Thesis, Norwegian University of Science and Technology.

Angst, U. and M. Büchler (2014). On the applicability of the Stern-Geary relationship to determine instantaneous corrosion rates in macro-cell corrosion. Materials and Corrosion-Werkstoffe und Korrosion doi: 10.1002/maco.201407997.

Angst, U., B. Elsener, C. K. Larsen and Ø. Vennesland (2009). Critical chloride content in reinforced concrete - A review. Cement and Concrete Research 39(12): 1122-1138.

Angst, U., B. Elsener, C. K. Larsen and Ø. Vennesland (2011a). Chloride induced reinforcement corrosion: Rate limiting step of early pitting corrosion. Electrochimica Acta 56(17): 5877-5889.

Angst, U. M. and B. Elsener (2014). On the Applicability of the Wenner Method for Resistivity Measurements of Concrete. ACI Materials Journal 111(6): 661-672.

Angst, U. M., B. Elsener, C. K. Larsen and O. Vennesland (2011b). Chloride induced reinforcement corrosion: Electrochemical monitoring of initiation stage and chloride threshold values. Corrosion Science 53(4): 1451-1464.

Apostolopoulos, C. A., S. Demis and V. G. Papadakis (2013). Chloride-induced corrosion of steel reinforcement - Mechanical performance and pit depth analysis. Construction and Building Materials 38: 139-146.

Atkins, P. and J. de Paula (2006). Atkins' Physical Chemistry [8th ed.], Oxford Univ. Press.

Beck, M. F. (2010). Zur Entwicklung der Eigenkorrosion von Stahl in Beton (in German), Doctoral Thesis, RWTH Aachen.

Bensted, J. and P. Barnes (2009). Structure and Performance of Cements [2nd ed.], Taylor & Francis.

Bertolini, L., B. Elsener, P. Pedeferri, E. Redaelli and R. B. Polder (2013). Corrosion of Steel in Concrete: Prevention, Diagnosis, Repair (2nd Edition), Wiley-VCH Verlag GmbH & Co.

Bertolini, L., M. Gastaldi, M. P. Pedeferri, P. Pedeferri and T. Pastore (1998). Effects of galvanic coupling between carbon steel and stainless steel reinforcement in concrete. International Conference on Corrosion and Rehabilitation of Reinforced Concrete Structures. Orlando, USA.

Bertolini, L. and R. B. Polder (1997). Concrete resistivity and reinforcement corrosion rate as a function of temperature and humidity of the environment, TNO Building and Construction Research.

Brem, M., S. Jäggi, B. Elsener and H. Böhni (2002). Numerical and Experimental Modeling of Localized Corrosion - Part I: Numerical Method and Input Parameters. Electrochemical Society Proceedings 24: 502-510.

Broomfield, J. and S. Millard (2002). Measuring concrete resistivity to assess corrosion rates. Concrete 36(2): 37-39.

Broomfield, J. P. (1997). Corrosion of steel in concrete: understanding, investigation, and repair. London and New York, E & FN Spon.

Bungey, J. H., S. G. Millard and M. G. Grantham (2006). Testing of concrete in structures, Taylor & Francis.

Bürchler, D. (1996). Der elektrische Widerstand von zementösen Werkstoffen: Modell, Einflussgrössen und Bedeutung für die Dauerhaftigkeit von Stahlbeton (in German), Doctoral Thesis, Eidgenössische Technische Hochschule, Zürich.

Bürchler, D., B. Elsener and H. Böhni (1996). Electrical resistivity and dielectric properties of hardened cement paste and mortar. Fourth Int. Symp. on Corrosion of Reinforcement in Concrete Construction. Society of Chemical Industry. C. L. Page, P. B. Bamforth and J. W. Figg. Cambridge, UK, Royal Society of Chemistry: 283-293.

Cabrera, J. G. and P. Ghoddoussi (1994). The Influence of Fly Ash on the Resistivity and Rate of Corrosion of Reinforced Concrete. Durability of concrete third Int. Conference. V. M. Malhotra. Nice, France: 229-244.

Castellote, M., C. Andrade and M. C. Alonso (2002). Standardization, to a reference of 25 degrees C, of electrical resistivity for mortars and concretes in saturated or isolated conditions. ACI Materials Journal 99(2): 119-128.

Copson, H. R. (1963). The electrochemical nature of corrosion. Corrosion resistance of metals and alloys. F. L. LaQue and H. R. Copson. New York, Reinhold Publishing Corporation: 83-105.

Denhoff, M. W. (2006). An accurate calculation of spreading resistance. Journal of Physics D-Applied Physics 39(9): 1761-1765.

Deutscher Ausschuss für Stahlbeton (2012). Dauerhaftigkeitsbemessung von Stahlbetonbauteilen auf Bewehrungskorrosion. Berlin, Beuth.

DuraCrete (1997). Compliance Tests State-of-the-Art The European Union - Brite EuRam III (Project BE95-1347).

Edwards, D. D., J. H. Hwang, S. J. Ford and T. O. Mason (1997). Experimental limitations in impedance spectroscopy .5. Apparatus contributions and corrections. Solid State Ionics 99(1-2): 85-93.

Elkey, W. and E. J. Sellevold (1995). Electrical resistivity of concrete - Publication no. 80, Directorate of Public Poads Norway.

Elsener, B. (1998). Corrosion rate of steel in concrete - From laboratory to reinforced concrete structures. Corrosion of Reinforcement in Concrete: Monitoring, Prevention and Rehabilitation. J. Mietz, B. Elsener and R. Polder, Maney Publishing: 92-103.

Elsener, B. (2002). Macrocell corrosion of steel in concrete - implications for corrosion monitoring. Cement & Concrete Composites 24(1): 65-72.

Elsener, B. (2005). Corrosion rate of steel in concrete - Measurements beyond the Tafel law. Corrosion Science 47(12): 3019-3033.

Elsener, B., C. Andrade, J. Gulikers, R. B. Polder and M. Raupach (2003). Half-cell potential measurements - Potential mapping on reinforced concrete structures. Materials and Structures 36(261): 461-471.

EN206-1 (2000). European Standard EN 206-1 "Concrete - Part 1: Specification, performance, production and conformity", European Committee for Standardization.

Evans, U. R. (1960). The corrosion and oxidation of metals: Scientific principles and practical applications. London, Edward Arnold Ltd.

Feliu, S., C. Andrade, J. A. González and C. Alonso (1996). A new method for in-situ measurement of electrical resistivity of reinforced concrete. Materials and Structures 29(190): 362-365.

Ford, S. J., J. D. Shane and T. O. Mason (1998). Assignment of features in impedance spectra of the cement-paste/steel system. Cement and Concrete Research 28(12): 1737-1751.

Garcés, P., M. C. Andrade, A. Saez and M. C. Alonso (2005). Corrosion of reinforcing steel in neutral and acid solutions simulating the electrolytic environments in the micropores of concrete in the propagation period. Corrosion Science 47(2): 289-306.

Gastaldini, A. L. G., G. C. Isaia, T. F. Hoppe, F. Missau and A. P. Saciloto (2009). Influence of the use of rice husk ash on the electrical resistivity of concrete: A technical and economic feasibility study. Construction and Building Materials 23(11): 3411-3419.

Gautefall, O. and Ø. Venneslad (1994). Field measurements of moisture in concrete: principles and methods. Trondheim, SINTEF Structures and Concrete

Gjørv, O. E., Ø. Vennesland and A. H. S. El-Busaidy (1977). Electrical Resistivity of Concrete in the Oceans. 9th Annual Offshore Technology Conference. Houston, Texas: 581-588.

González, J. A., C. Andrade, C. Alonso and S. Feliu (1995). Comparison of Rates of General Corrosion and Maximum Fitting Penetration on Concrete Embedded Steel Reinforcement. Cement and Concrete Research 25(2): 257-264.

González, J. A., J. M. Miranda and S. Feliu (2004). Considerations on reproducibility of potential and corrosion rate measurements in reinforced concrete. Corrosion Science 46(10): 2467-2485.

Gowers, K. R. and S. G. Millard (1999). Measurement of Concrete Resistivity for Assessment of Corrosion Severity of Steel Using Wenner Technique. ACI Materials Journal 96(5): 536-541.

Hamann, C. H., A. Hamnett and W. Vielstich (1998). Electrochemistry. Weinheim, Wiley-VCH.

Hope, B. B., J. A. Page and A. K. C. Ip (1986). Corrosion Rates of Steel in Concrete. Cement and Concrete Research 16(5): 771-781.

Hunkeler, F. (1996). The resistivity of pore water solution - A decisive parameter of rebar corrosion and repair methods. Construction and Building Materials 10(5): 381-389.

Jäggi, S. (2001). Experimentelle und numerische Modellierung der lokalen Korrosion von Stahl in Beton unter besonderer Berücksichtigung der Temperaturabhängigkeit (in German), Doctoral Thesis ETH.

Jäggi, S., H. Böhni and B. Elsener (2007). Macrocell corrosion of steel in concrete - experiments and numerical modelling. In Corrosion of reinforcement in concrete - mechanisms, monitoring, inhibitors and rehabilitation techniques. M. Raupach, B. Elsener, R. B. Polder and J. Mietz, Woodhead Publishing Limited / CRC Press: 75-88.

Jakobsen, U. H. (2015). SEM -EDX analysis of paste around anodes (internal report). Order No.: 632017, Danish Technological Institute.

Kranc, S. C. and A. A. Sagüés (1993). Polarization Current Distribution and Electrochemical Impedance Response of Reinforced-Concrete When Using Guard Ring Electrodes. Electrochimica Acta 38(14): 2055-2061.

Larsen, C. K. (1998). Chloride binding in concrete, Doctural thesis, Norwegian University of Science and Technology.

Larsen, C. K., E. J. Sellevold, J. M. Østvik and Ø. Vennesland (2006). Electrical resistivity of concrete part II: Influence of moisture content and temperature. 2nd International Symposium on Advances in Concrete through Science and Engineering Quebec City, Canada.

Lataste, J.-F. (2010). Electrical resistivity for the evaluation of reinforced concrete structures. Non-Destructive Evaluation of Reinforced Concrete Structures, Vol. 2: Non-Destructive Testing Methods, Elsevier: 243-275.

López, W. and J. A. González (1993). Influence of the Degree of Pore Saturation on the Resistivity of Concrete and the Corrosion Rate of Steel Reinforcement. Cement and Concrete Research 23((2)): 368-376.

Luping, T., L.-O. Nilsson and P. A. M. Basheer (2012). Resistance of Concrete to Chloride Ingress testing and modelling. London, Spon.

McCarter, W. J. and S. Barclay (1993). A Comparison of 2 Methods for Resistivity Measurements on Repair Mortar for Cathodic Protection Systems. Cement and Concrete Research 23(5): 1178-1184.

Michel, A., P. V. Nygaard and M. R. Geiker (2013a). Experimental investigation on the short-term impact of temperature and moisture on reinforcement corrosion. Corrosion Science 72: 26-34.

Michel, A., A. O. S. Solgaard, B. J. Pease, M. R. Geiker, H. Stang and J. F. Olesen (2013b). Experimental investigation of the relation between damage at the concrete-steel interface and initiation of reinforcement corrosion in plain and fibre reinforced concrete. Corrosion Science 77: 308-321.

Millard, S. G. (1991). Insitu Measurement of Concrete Resistivity. UK Corrosion '91. Manchester.

Monfore, G. E. (1968). Electrical Resistivity of Concrete. Journal of the Portland Cement Association Research and Development Laboratories 10(2): 35-48.

Myrdal, R. (2007). Accelerating admixtures for concrete A State of the Art SINTEF Report. Trondheim, Norway, SINTEF Building and Infrastructure.

Nanis, L. and W. Kesselman (1971). Engineering Applications of Current and Potential Distributions in Disk Electrode Systems. Journal of the Electrochemical Society 118(3): 454-461.

Newlands, M. D., M. R. Jones, S. Kandasami and T. A. Harrison (2008). Sensitivity of electrode contact solutions and contact pressure in assessing electrical resistivity of concrete. Materials and Structures 41(4): 621-632.

Nisancioglu, K. (2015). Corrosion and Corrosion Protection. Lecture Notes Part I: Basic Principles. Department of Materials Science and Engineering, NTNU.

Nöggerath, J. (1990). Makroelementkorrosion von Stahl in Beton - Wirkungsweise und Einflussgrößen (in German), Doctoral Thesis, ETH Zurich.

Norcem (2015). Produktinformasjon Norcem Anlegg (in Norwegian) available at: http://www.norcem.no/no/norcem_anlegg (retrieved 24/08/2014).

NPRA. (2015). http://www.vegvesen.no (retrieved 15/08/2015).

Nygaard, P. V. (2008). Non-destructive electrochemical monitoring of reinforcement corrosion, Doctoral Thesis, Department of Civil Engineering, Technical University of Denmark.

Nygaard, P. V. and M. R. Geiker (2005). A method for measuring the chloride threshold level required to initiate reinforcement corrosion in concrete. Materials and Structures 38: 489-494.

Nygaard, P. V. and M. R. Geiker (2012). Measuring the corrosion rate of steel in concrete - effect of measurement technique, polarisation time and current. Materials and Corrosion-Werkstoffe und Korrosion 63(3): 200-214.

Nygaard, P. V., M. R. Geiker and B. Elsener (2009). Corrosion rate of steel in concrete: evaluation of confinement techniques for on-site corrosion rate measurements. Materials and Structures 42(8): 1059-1076.

Oelssner, W., F. Berthold and U. Guth (2006). The iR drop - well-known but often underestimated in electrochemical polarization measurements and corrosion testing. Materials and Corrosion-Werkstoffe und Korrosion 57(6): 455-466.

Østvik, J. M. (2005). Thermal Aspects of Corrosion of Steel in Concrete: effect of low temperature on the resistivity and the cathodic reaction rate, Doctoral Thesis, Norwegian University of Science and Technology.

Østvik, J. M., C. K. Larsen, Ø. Vennesland, E. J. Sellevold and M. C. Andrade (2006). Electrical resistivity of concrete Part I: Frequency dependence at various moisture contents and temperatures. 2nd International Symposium on Advances in Concrete through Science and Engineering. Quebec City, Canada.

Pacheco-Farías, J. (2015). Corrosion of steel in cracked concrete: chloride microanalysis and service life predictions, Doctoral Thesis, Technical University Delft.

Page, C. L. and K. W. J. Treadaway (1982). Aspects of the electrochemistry of steel in concrete. Nature 297: 109-114.

Pease, B. (2010). Influence of concrete cracking on ingress and reinforcement corrosion, Doctoral Thesis, Technical University of Denmark.

Pease, B., M. Geiker, H. Stang and J. Weiss (2011). The design of an instrumented rebar for assessment of corrosion in cracked reinforced concrete. Materials and Structures 44(7): 1259-1271.

Pedersen, B. (2011). Manufactured sand in concrete – effect of particle shape on workability. COIN Project report 34. Oslo, SINTEF Building and Infrastructure/ COIN.

Polder, R., C. Andrade, B. Elsener, Ø. Vennesland, J. Gulikers, R. Weidert and M. Raupach (2000). Rilem TC 154-EMC: Electrochemical techniques for measuring metallic corrosion - Test methods for on site measurement of resistivity of concrete. Materials and Structures 33(234): 603-611.

Polder, R. B. (2001). Test methods for on site measurement of resistivity of concrete - a RILEM TC-154 technical recommendation. Construction and Building Materials 15(2-3): 125-131.

Pourbaix, M. (1974). Atlas of electrochemical equilibria in aqueous solutions. Bruxelles, Centre Belge d'Etude de la Corrosion CEBELCOR.

Raupach, M. (1992). Zur chloridinduzierten Makroelementkorrosion von Stahl in Beton (in German). Berlin, Beuth Verlag GmbH.

Sbartai, Z. M., S. Laurens, J. Rhazi, J. P. Balayssac and G. Arliguie (2007). Using radar direct wave for concrete condition assessment: Correlation with electrical resistivity. Journal of Applied Geophysics 62(4): 361-374.

Schießl, P. and M. Raupach (1992). Monitoring System for the Corrosion Risk for Steel in Concrete. Concrete International 14(7): 52-55.

Schulte, C., H. Mader and F. H. Wittmann (1978). Elektrische Leitfähigkeit des zementsteins bei unterschiedlichem Feuchtigkeitsgehalt (in German). Cement and Concrete Research 8(3): 359-367.

Sellevold, E. J. (1997). Resistivity and Humidity Measurements of Repaired and Non-Repaired areas of Gimsøystraumen Bridge. Repair of Concrete Structures - from Theory to Practice in a Marine Environment. A. Blankvoll. Oslo, Norwegian Road Research Laboratory: 283-295.

Sengul, O. and O. E. Gjørv (2008). Electrical Resistivity Measurements for Quality Control During Concrete Construction. ACI Materials Journal 11/12: 541-547.

Sengul, O. and O. E. Gjørv (2009). Effect of Embedded Steel on Electrical Resistivity Measurements on Concrete Structures. ACI Materials Journal 1/2: 11-18.

Sensortec. (2015). http://www.sensortec.de/sensoren-sensors/multiring-elektrode-multiring-electrode.html (retrieved 07/04/2015).

Slade, P. G. (2013). Electrical Contacts: Principles and Applications, Second Edition, CRC Press.

Smith, K. M., A. J. Schokker and P. J. Tikalsky (2004). Performance of supplementary cementitious materials in concrete resistivity and corrosion monitoring evaluations. ACI Materials Journal 101(5): 385-390.

Soylev, T. A. and R. François (2003). Quality of steel-concrete interface and corrosion of reinforcing steel. Cement and Concrete Research 33(9): 1407-1415.

Spragg, R., Y. Bu, K. Snyder, D. Bentz and J. Weiss (2013). Electrical Testing of Cement-Based Materials: Role of Testing Techniques, Sample Conditioning, and Accelerated Curing. Purdue University e-Pubs, West Lafayette, Indiana, USA.

Stern, M. and A. L. Geary (1957). Electrochemical polarization. I. A theoretical analysis of the shape of polarization curves. Journal of the Electrochemical Society 104(1): 56-63.

Tuutti, K. (1982). Corrosion of steel in concrete, Swedish Cement and Concrete Research Institute.

Warkus, J. (2014). Einfluss der Bauteilgeometrie auf die Korrosionsgeschwindigkeit von Stahl in Beton bei Makroelementbildung. Berlin, Deutscher Ausschuss für Stahlbeton, Beuth.

Wenner, F. (1915). A method of measuring earth resistivity. National Bureau of Standards, Bulletin 12 (4), Washington, USA.

Whiting, D. A. and M. A. Nagi (2003). Electrical Resistivity of Concrete - A Literature Review, R&D Serial No. 2457. Skokie, Illinois, USA, Portland Cemente Association.

Woelfl, G. A. and K. Lauer (1979). The electrical resistivity of concrete with emphasis on the use of electrical resistance for measuring moisture content. Cement, Concrete, and Aggregates 1(2): 64-67.

Part II – Appended papers

Paper I

Relationship between concrete resistivity and corrosion rate – A literature review

Cement & Concrete Composites, Volume 39, 60-72 (2013)

Hornbostel, K.; Larsen, C. K. and Geiker, M. R.

Cement & Concrete Composites 39 (2013) 60–72

Contents lists available at SciVerse ScienceDirect

Cement & Concrete Composites

journal homepage: www.elsevier.com/locate/cemconcomp

Relationship between concrete resistivity and corrosion rate – A literature review

Karla Hornbostel [a,*], Claus K. Larsen [a,b], Mette R. Geiker [a]

[a] Norwegian University of Science and Technology, Department of Structural Engineering, Richard Birkelandsvei 1a, 7491 Trondheim, Norway
[b] Norwegian Public Roads Administration, Brynsengfaret 6A, 0667 Oslo, Norway

ARTICLE INFO

Article history:
Received 21 September 2012
Received in revised form 22 March 2013
Accepted 24 March 2013
Available online 4 April 2013

Keywords:
Concrete resistivity
Corrosion rate
Propagation period

ABSTRACT

The process of reinforcement corrosion in concrete is partially controlled by the transport of ions through the concrete microstructure. Ions are charged and the ability of a material to withstand transfer of charge is dependent upon the electrical resistivity. Thus, a connection could be expected between the corrosion process of steel embedded in concrete and the electrical resistivity of concrete. This paper reviews research concerning the relationship between corrosion rate and concrete resistivity. Overall, there exists an inverse proportional correlation between the parameters. However, the dependency varies between studies and one single relationship cannot be established between corrosion rate and resistivity. To address the variation, the article reviews and evaluates the influence of factors including the experimental setup, the concrete mix design and the cause of corrosion.

1. Introduction

Corrosion of steel in concrete has caused numerous costly repairs and a considerable number of structural failures during the last centuries [1]. It is of high interest to evaluate the corrosion process in a sufficient way not only for existing structures but also for the design of new structures. Concrete resistivity is, in this respect, seen as one of the most important parameters that can help to assess corrosion of steel in concrete. Investigations have found correlations between concrete resistivity and both, the initiation and the propagation period [2–22] (Fig. 1).

This paper addresses the relationship between corrosion rate and concrete resistivity (referred to hereafter also as the "C–R relationship"). It is today widely accepted that the corrosion rate decreases with increasing concrete resistivity under common environmental exposure conditions (excluding submerged structures). However, considerable and not fully clarified deviations are found between studies published in the literature.

1.1. Background

The electrical resistivity ρ (Ω m) of a material describes its ability to withstand the transfer of charge. It is the ratio between applied voltage and resulting current multiplied by a cell constant and is thus a geometry independent property [23]. The inverse of resistivity is conductivity σ. The range spanned by resistivity is one of the greatest of any material property. For concrete it varies between $10^6\,\Omega$ m for oven dried samples to $10\,\Omega$ m for saturated concrete [24]. Electrical resistivity in concrete is ascribed to microstructure properties such as porosity and pore solution characteristics. The degree of saturation of the pore structure has been identified as the most important factor influencing concrete resistivity [11,25,26] and temperature also has a considerable impact [27].

In the highly alkaline environment of the concrete pore solution, steel is protected against corrosion by a thin layer of iron-oxides (passive film). However, this passive film is not stable in the presence of a sufficient amount of chlorides or when the concrete surrounding the steel is carbonated. Corrosion can then occur. The propagation of corrosion of steel embedded in concrete is an electrochemical reaction that consists of four separate processes (Fig. 2). Each step represents a resistance against the flow of current in the cell. The resistances are connected in series and consequently the corrosion current will be limited by the highest resistance. The resistance of current flow through the steel will be low with respect to the other three processes. Accordingly, either the cathodic, anodic or concrete resistance limit the corrosion rate, which depends on environmental and/or material properties [6,13,28,29]. Concrete resistivity can have a direct influence on the corrosion process by describing the flow of current between anode and cathode regions (R_{con} in Fig. 2). However, through its ability to describe the moisture stage and the flow of ions such as chlorides through the concrete microstructure, it can also have an indirect correlation to the corrosion process by influ-

* Corresponding author. Tel.: +47 73594537.
E-mail address: Karla.Hornbostel@ntnu.no (K. Hornbostel).

0958-9465/$ - see front matter © 2013 Elsevier Ltd. All rights reserved.
http://dx.doi.org/10.1016/j.cemconcomp.2013.03.019

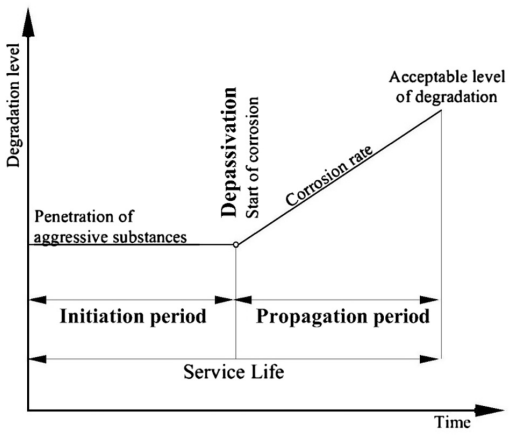

Fig. 1. Definition of the Service Life based on Tuutti's model [22].

encing the anodic and cathodic reaction rates. The corrosion rate is commonly described as current density i_{corr} ($\mu A/cm^2$).

Reinforcement corrosion due to carbonation usually occurs over a large area of reinforcement surface. Cathodic and anodic areas are adjacent and a uniform dissolution of the steel takes place. This mechanism is called microcell [28] or uniform [30] corrosion. Uniform corrosion can also appear if the chloride content along the rebar is very high [1]. Generally however, localized pits develop in the presence of chlorides. The anodic area in the localized pit is much smaller with respect to the cathodic area (the passive rebar surface around the pit) and anodic and cathodic regions are separated in space creating a macrocell. Hence, corrosion in the presence of chlorides is referred to as macrocell corrosion [30].

It is widely accepted that concrete resistivity can easily be measured, especially in the field, compared to other parameters in corrosion science such as the corrosion rate [31]. A relationship between concrete resistivity and corrosion rate would consequently allow the assessment of the corrosion stage in an efficient and reasonably priced way. This can be seen as the main reason for the intensive research over the last decades on the C–R relationship. Assessment criteria to quantify corrosion activity by concrete resistivity measurements can be found in the literature (Table 1). However, a high variation between the threshold values is observed. An upper limit of 1000–2000 Ω m can be identified from the comparison over which the corrosion rate will be low. As a lower limit, concrete with a resistivity under 50 Ω m is likely to allow heavy corrosion. On site, resistivity values between 50 and 1000 Ω m are commonly obtained for concrete made of ordinary Portland cement (OPC), up to 6000 Ω m for blended cements [23]. The upper and lower limits are consequently too rough for the detailed assessment of corrosion activity. To address a more detailed description of the C–R relationship, this report reviews and evaluates literature on experimental investigations, compares their results, and identifies differences between them.

Table 1
Criteria for the assessment of corrosion activity in terms of concrete resistivity (see references).

Refs.	Corrosion intensity in terms of resistivity (Ω m)			Corrosion induced by
	High	Moderate	Low	
[2]	<50	50–120	>120	
[3]	<65	65–85	>85	
[9]	<70	70–300	>300–400	Chlorides
[16]	<100	100–300	>300	
[20]	<200	200–1000	>1000	
[11]	<50	Under discussion	100–730	
[12]	<100	100–1000	>1000–2000	
[15]	<100	100–1000		General
[37]	<50	50–200	>200	
[18]	<80	80–120	>120	

1.2. Objective and methodology

The primary objective of this article is to review existing research on the relationship between corrosion rate and concrete resistivity. The report identifies the applicability and limitation of the C–R relationship and evaluates its suitability for the assessment and prediction of the propagation period. Finally, key points are identified for future research in the area.

An extensive literature search was undertaken. The main reference sources were international studies investigating the relationship experimentally. A review was prepared of the most relevant literature. A comparison was made of the experimental setup (Section 2), the way in which the recorded data was analyzed (Section 3) and the results obtained (Section 4). Several parameters influencing the C–R relationship were identified and compared (Fig. 3). The information observed from the literature search was supplemented by two models which are based on the C–R relationship and which are compared to the experimental data (Section 5). Further selected reports containing information on the C–R relationship complement the literature review. Investigations were considered for both chloride and carbonation-induced corrosion.

Within the individual studies, different terminology has been used to describe the relationship. Some authors compared the corrosion rate with the concrete resistivity, while others preferred concrete conductivity. The differences in the terms used affect the analyses of the relationship. A correlation between concrete resistivity and corrosion rate indicates an inverse proportionality, whereas a relationship between concrete conductivity and corrosion rate gives a direct proportionality.

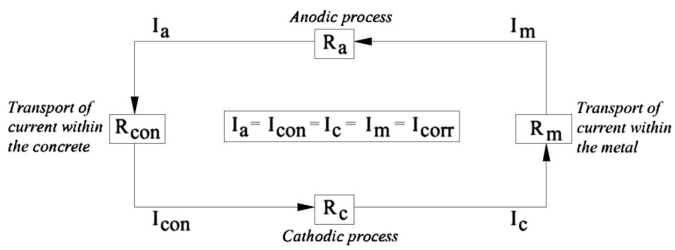

Fig. 2. Electrochemical mechanism of reinforcement corrosion [1].

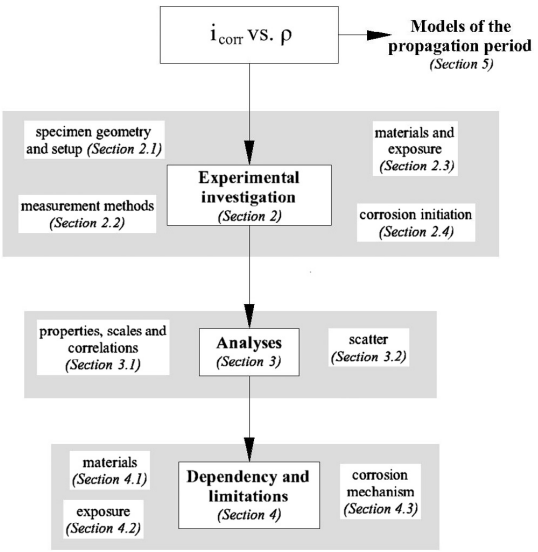

Fig. 3. Outline of the literature review.

Table 2
List of symbols and abbreviations.

	Explanation
C–R relationship	Relationship between corrosion rate and concrete resistivity
Carbo	Corrosion induced by carbonation
Cl	Corrosion induced by chlorides
R	Concrete resistance (Ω)
ρ	Concrete resistivity (Ω m)
σ	Concrete conductivity (1/(Ω m))
i_{corr}	Corrosion rate (μA/cm^2)
R_p	Polarization resistance (Ω)
Log	Logarithmic axis
N	Linear axis
LPR	Linear polarization resistance
WE	Working electrode (corroding steel bar)
CE	Counter electrode
RE	Reference electrode
w/b	Water/binder ratio
c:a:w	Cement:aggregate:water
OPC	Ordinary Portland cement
SC	Slag cement
BFSC	Blast furnace slag cement
FA	Fly ash
/	Not reported

The reviewed data was compared and evaluated in forms of tables and graphs. Tables are ordered by the year of publication. Abbreviations and symbols are defined in Tables 2 and 3. Detailed information on the experimental setups is presented in Tables 4–8. Properties and scales used to analyze the C–R relationship are compared in Table 9. The table includes one additional study besides the ones presented in Tables 4–8. The study contains measurement data from the field [32]. It is the only investigation found in the literature search which is based on field investigations.

The experimental data was fitted to linear trend lines in most reports. The regression lines were compared in the two scales most commonly used in the literature (Figs. 4 and 5). The reproduction of the fitted lines from the references and the transformation between scales was done simply by picking 10 evenly distributed points out of each trend line and connecting them by a straight line. To the extent possible, the regression lines were drawn in the range in which they were found in the reported experiments. The scatter of the observed regression lines is illustrated in Fig. 6. Parts of the reviewed experimental data could not be included in the graphical comparison [7,10]. This data was reported in properties which are dependent on the geometry of the sample and the measurement arrangement. Details on these points were not adequately clarified in the appropriate publications.

2. Comparison of the experimental investigations

Experimental setups to study the C–R relationship must consist of the following:

- Working electrode, preferably construction steel embedded in a mortar or concrete sample to reflect practice-related conditions.
- A technique to measure corrosion rate, either from the surface or as an embedded device.
- A technique to measure concrete resistivity.
- A method to initiate corrosion.

No standardized test method exists to investigate the C–R relationship. Experimental setups were developed individually according to the points listed above and depending on the focus of the work. Most experiments studied not only the C–R relationship but also other corrosion parameters such as electrical potential or chloride diffusion. The following sections compare the experimental setups reported in the literature. The extent to which differences in the setups can influence the C–R relationship will be discussed. A comparison of the experimental setups is given in Tables 4–8.

2.1. Specimen geometry and setup

Commonly, the C–R relationship was studied on samples with dimensions between 10 and 40 cm [4,7,10,13,16] (Table 4). Smaller

Table 3
Explanation to the literature reviewed in Figs. 4 and 5.

Line style	Refs.	w/b	Cement type	Cause of corrosion
———	[13]	0.45	Slag cement (70%)	Carbo
———	[5]	0.5	Different	Carbo
- - - - - - - - - - - - - - - -	[13]	0.45	Slag cement (70%)	Cl
- - - - - - - - - - - - - - - -	[4]	0.45	Slag cement (25% and 50%)	Cl
— · · — · · — · · — · · —	[20]	0.5	/[a]	Cl
	Samples over 10 years old			
— · — · — · — · — · — · —	[6]	0.5	/[a]	Cl
— · — · — · — · — · — · —	[9]	0.5	/[a]	Cl
— · — · — · — · — · — · —	[16]	0.4/0.6	/[a]	Cl
— · — · — · — · — · — · —	[13]	0.45	OPC	Cl

[a] Assumed OPC.

Table 4
Details of the specimen geometry, in terms of specimen size, reinforcement type and number of specimens used in the investigation of the relationship between corrosion rate and concrete resistivity in the studies included in this review (see references).

Refs.	Specimen size		Reinforcement			Total number of specimens
	Type	Size (mm)	Ø (mm)	Exposed area (cm^2)	Cover depth (mm)	
[4]	Slab	114 × 300 × 400	13	102	56	18
[5]	Cube	20 × 55 × 80	/	6	7	/
[6]	Cube	Length 50	1.5	2.4	/	/
[7]	Cube	180 × 180 × 180	/	2	20	7
[9]	Cube	20 × 55 × 80	/	/	/	/
[10]	Cylinder	Ø 70 × 150	12	/	/	/
[13]	Cube	100 × 100 × 300	6	11.4	10, 30	32
[14]	Slab	1180 × 1180 × 216	16	/	25, 51, 76	40
[16]	Cylinder	Ø 150 × 200	10	40	15	16
[20]	Slab	1330 × 1330 × 70	8	/	/	2

Table 5
Details of the measurement methods used to record corrosion rate and concrete resistivity in the investigation of the relationship between corrosion rate and concrete resistivity in the studies included in this review (see references).

Refs.	Corrosion rate			Concrete resistivity			
	Technique	Details	Correction for ohmic drop	Technique	Embedded (WE)	Embedded (Ref. bars)	From the surface
[4]	LPR	Embedded CE RE on the surface	/	2 – Electrodes	×		
[5]	LPR	From surface	Yes	2 – Electrodes		×	
[6]	LPR	From surface	Yes	2 – Electrodes	×		
[7]	LPR	Embedded device	Yes	4 – Electrodes		×	
[9]	LPR	Embedded CE RE on the surface	/	2 – Electrodes	×		
[10]	LPR	From surface	Yes	Ref. sample 2 – electrodes			×
[13]	LPR	Between 3 embedded rebars	No	2 – Electrodes		×	
[14]	LPR	From surface	Yes	Measured with the LPR device			
	Galvanostatic	From surface					
[16]	LPR	/	Yes	2 – Electrodes	×		
[20]	LPR and others	From surface	Yes	/			

Table 6
Details of the materials used in the investigation of the relationship between corrosion rate and concrete resistivity in the studies included in this review (see references).

Refs.	Type	Amount of cement or proportion (*c*:*a*:*w*)	Cement type	*w*/*b*
[4]	Concrete	400 kg/m^3	OPC OPC + 25% slag OPC + 50% slag	0.45
[5]	Mortar	1:3:0.5	OPC sulfate Resistance PC slag cement pozzolanic cement OPC + 30% FA fly ash cement	0.5
[6]	Concrete	1:3:0.5	/	0.5
[7]	Mortar	1:6:0.9/1.1	OPC	0.9, 1.1
[9]	Mortar	1:3:0.5	/	0.5
[10]	Concrete	1:5.85:0.55	OPC OPC + 30% FA	0.55
[13]	Mortar (0–8 mm)	300, 330 kg/m^3	OPC BFSC (70% slag)	0.45, 0.65
[14]	Concrete	337–382 kg/m^3	/	0.41–0.45
[16]	Concrete	300, 400 kg/m^3	/	0.4, 0.6
[20]	Concrete	1:3:0.5	/	0.5

Table 7
Details of the exposure conditions used in the investigation of the relationship between corrosion rate and concrete resistivity in the studies included in this review (see references).

Refs.	Moisture conditions	Temperature	Measurement period
[4]	Changing exposure	Laboratory/105 °C	~1 year
[5]	Changing exposure	Laboratory	500 days
[6]	Wetting/drying cycles	Laboratory	/
[7]	Stored in 38–92% RH changing over time	25 °C	130 days
[9]	Stored in 50% RH	50 °C	500 days
[10]	Immersed in either salt water or tap water	Laboratory	1 year
[13]	Changing exposure	Changing	5 years
[14]	Outdoor exposure	Outside	5 years
[16]	Wetting/drying cycles, seashore	Laboratory, outside	1000 days
[20]	Surface wetting	Laboratory	Several years old specimens 30 days observation

Table 8
Details of the corrosion initiation used in the investigation of the relationship between corrosion rate and concrete resistivity in the studies included in this review (see references).

Refs.	Carbonation	Mixed-in chlorides by cement weight	Wetting/drying cycles
[4]			3.5% NaCl solution
[5]	Accelerated		
[6]		3% $CaCl_2$	
[7]	Accelerated		0.4 or 1% Cl^- solution
[9]		2% NaCl	
[10]		2% Cl^-	5% NaCl solution or pure water
[13]	Accelerated	2% $CaCl_2$	
[14]		0–7.2 kg/m^3 Cl^-	
[16]		0.16–1.65% Cl^-	3.5% Cl^- solution or outside
[20]		3% $CaCl_2$	

Table 9
Details of the analyses and results from the investigation of the relationship between corrosion rate and concrete resistivity in the studies included in this review (see references).

Ref.	Scale	Relation	Dependency	Applicability
[4]	Log (ρ) – Log (i_{corr})	Linear	Not on cement type	/
[5]	Log (R) – Log (i_{corr})	Linear	Not on cement type	Active corrosion
[6]	Log (σ) – Log (R_p)	Linear	/	Active corrosion, RH < 95%
[7]	N (σ) – N (i_{corr})	Linear	/	/
[9]	Log (ρ) – Log (i_{corr})	/	/	/
[10]	Log (R) – Log (i_{corr})	Linear	Cement type	/
[32]	Log (ρ) – Log (i_{corr})	/	/	/
[13]	N (σ) – N (i_{corr})	Linear	Cement type cause of corrosion	Active corrosion
[14]	N (ρ) – N (i_{corr})	Logarithmic	Chloride content, temperature	Active corrosion, not saturated
[16]	Log (ρ) – Log (i_{corr})	Linear	Not on w/c ratio	/
[20]	Log (ρ) – Log (i_{corr})	Linear	/	Active corrosion

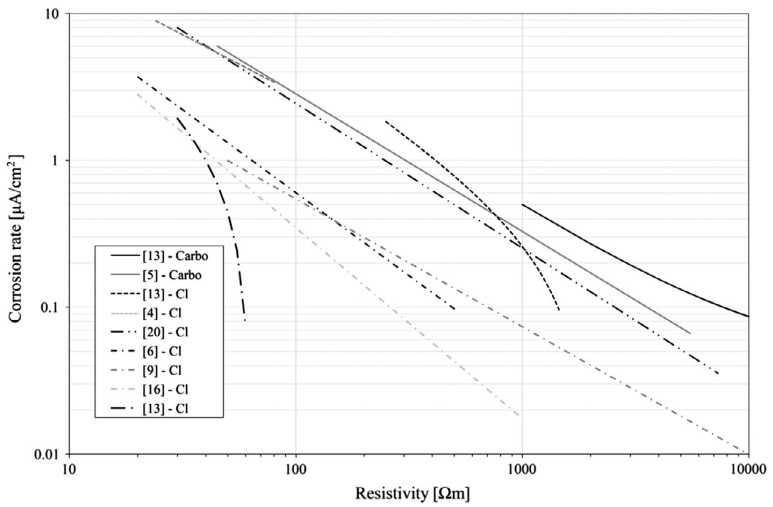

Fig. 4. Comparison of the regression lines for the relationship between corrosion rate and concrete resistivity observed in literature (see references) in the log–log scale, details and abbreviations see Tables 2 and 3.

samples with edge lengths under 10 cm [5,6,9] as well as specimens with dimensions over 1 m [14,20] were more seldom used. The steel diameter varied between 1.5 and 16 mm, according to the sample size. Mostly, no detailed information was provided about the type of the steel embedded, both ribbed and smooth steel was used. In the majority of the studies, several reinforcement bars were placed parallel in cover depths ranging from 7 to 76 mm.

It is seldom discussed to what extent sample size influences experimental investigations of the corrosion process. It seems of minor importance from an electrochemical point of view for localized corrosion, provided that enough cathode area is available [33,34]. For samples with heavily corroding anodes and a comparatively small cathode area, cathodic control might be in force and limit the corrosion rate. No information about the size of the anode and the ratio between anode and cathode is given in the reviewed

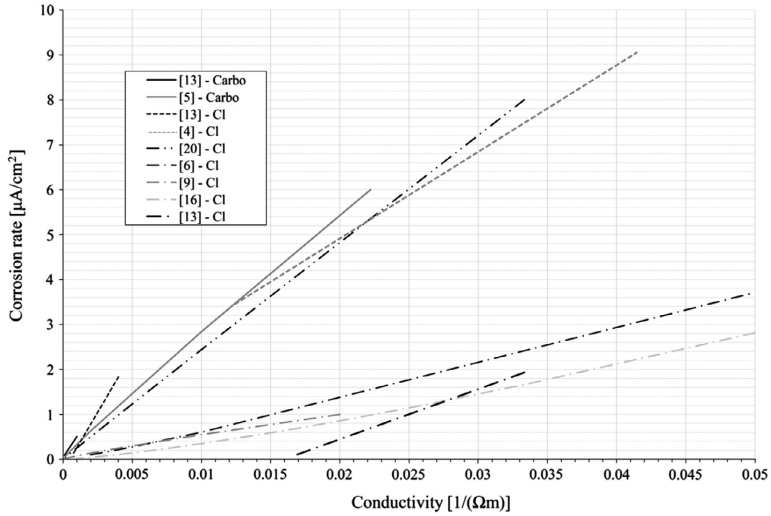

Fig. 5. Comparison of the regression lines for the relationship between corrosion rate and concrete conductivity observed in literature (see references) in the linear–linear scale, details and abbreviations see Tables 2 and 3.

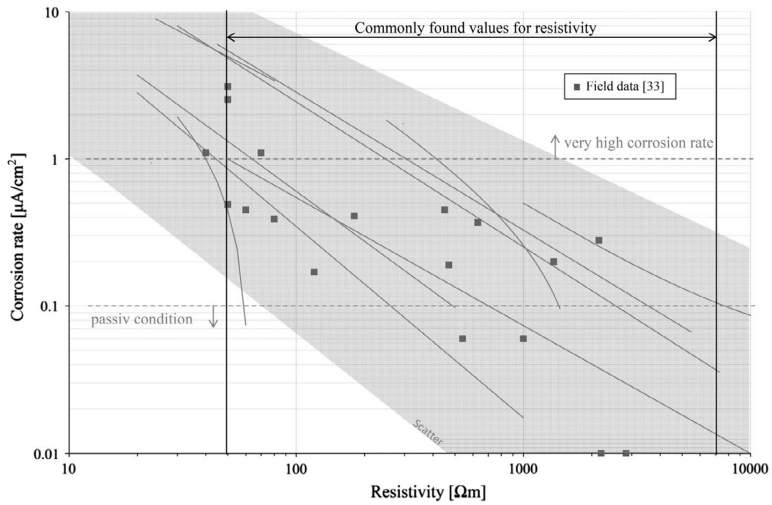

Fig. 6. Scatter within the reviewed studies illustrated as grey cloud around the observed regression lines (details Figs. 4 and 5), compared to field data [32] and framed by upper and lower limits commonly found for corrosion rate and concrete resistivity.

articles. However, when information was provided about the rate limiting step, cathodic control was not observed [5–7]. The influence of the sample's size on the C–R relationship is therefore not considered further in this review.

2.2. Measurement methods

Recommendations for measuring corrosion rate and concrete resistivity have been published [23,35]. However a standardized measuring protocol does not exist for either of them at present.

Recommendations suggest measuring concrete resistance using an alternating current (AC) with a frequency between 50 and 1000 Hz [15]. For low temperatures and high moisture contents, frequencies in a higher range of 100 Hz to 10 kHz have been recommended [36]. Either 2-electrode or 4-electrode (Wenner) techniques are employed to record the resistance (R (Ω)) [23,37,38], which is transformed into resistivity (ρ (Ω m)) by multiplying it with an appropriate geometrical factor (k (m)).

$$\rho = (U/I) \cdot k = R \cdot k \tag{1}$$

where U is the potential (V) and I is the current (A). The k-value is dependent on the volume covered by the measurements.

The resistivity of concrete is influenced by a variety of parameters and is susceptible to moisture changes in particular (Section 1.1). Chloride ions decrease the resistivity [11], whereas

carbonation causes an increase of concrete resistance [39]. Moisture changes, the penetration of chlorides and carbonation takes place mainly in the cover concrete. Accordingly, the concrete resistivity is likely to change over the cover depth and might be considerably different to the resistivity at the depth of the reinforcement. Depending on the expected impact of resistivity on the corrosion process, either the cover resistance or the resistivity at the depth of the reinforcement must be recorded to allow for an accurate comparison with the corrosion rate (Section 1.2). A further problem is that in the case of general corrosion, the resistance of the interfacial transition zone (ITZ) between bulk concrete and steel is of more importance than the bulk resistivity [40]. It is unknown to which extent the resistance of the ITZ can be compared to the bulk resistivity. It is of significance to acknowledge these resistivity differences in the interpretation of the findings. In the reviewed experimental investigations, the concrete resistivity was measured at the level of the reinforcement in most cases (Table 5). The cover resistivity was recorded in part of the studies, where an external LPR device was used to measure the corrosion rate, e.g. [14]. Reference samples to measure resistivity were used in one case [10]. It has to be considered that the concrete resistance measured in parts of the experiment is not accounting for the resistance which influences the corrosion process. The mistake made is dependent on the variation between cover, bulk and local concrete resistivity in the particular experiment, as well as the influence of each on the corrosion process.

Several methods exist to measure corrosion rates in concrete [12]; the most frequently used is the linear polarization resistance (LPR) method, a non-destructive technique. In all reviewed papers, the corrosion rate was determined by LPR, with differences in the arrangement of the measurement setup. The LPR method is based on the observation that the polarization curve near the corrosion potential is linear. A small current is applied from a counter electrode (CE) and the amount required to achieve a defined variation of the potential is recorded. The potential is monitored with a reference electrode (RE). The instantaneous polarization resistance can be calculated from the measurement and transformed into the total corrosion current (I_{corr}) with help of the Stern–Geary equation [41]. The corrosion rate i_{corr} (current density) is obtained by dividing the total corrosion current I_{corr} by the corroding area. Although simple in its theory, the LPR technique meets several challenges in practice [12,42–44].

The amount of corroded surface area is unknown in most measurement situations. It is thus common practice to determine the corrosion rate by dividing the total corrosion current by the area which is affected by the measurement. This calculation may be adequate for uniform corrosion where large parts of the surface area are corroded. However, in the case of localized corrosion only comparatively small pits are affected by corrosion. The local current density inside a pit is significantly higher than the average value for the steel area affected by the measurement. Consequently, the corrosion rate will be underestimated in these cases. The latter must be considered for the reviewed experimental data in the case of localized corrosion as the actual corroding area was unknown in all experiments.

The concrete resistance between the RE and the WE (working electrode, here corroding steel bar) can have a considerable influence on the measured polarization resistance, referred to as ohmic drop. A major error can be made in situations where the concrete resistivity is relatively high. For these cases, the polarization resistance might reflect the concrete resistance rather than the corrosion rate. To avoid this influence, it is commonly suggested to correct LPR measurements for ohmic drop [45]. In parts of the reviewed experiments either no modifications for ohmic drop were done or no information about this was given [4,9,13]. Neglecting the ohmic drop will lead to an underestimation of the corrosion rate. This must be considered as the review moves forward to discuss the results from these studies.

A variety of further parameters not named here can be identified which influence corrosion rate and concrete resistivity measurements, such as confinement techniques, sweep rate, delay time and others [44,46,47]. Only by examining all effects influencing corrosion rate and concrete resistivity measurements can differences observed between studies be explained.

2.3. Materials and exposure conditions

In most experiments, mortar or concrete samples were investigated with a w/b ratio between 0.4 and 0.65 by mass (Table 6). The mixture proportions and cement content varied. Only one work used higher w/b ratios of 0.9 and 1.1, to achieve a fast change of the internal environment when changing the exposure [16]. Such high w/b ratios are not related to current practice. Blended cements such as fly ash or slag cements were used in parts of the studies [4,5,10,13]. No detailed information was given about the cement type in [6,9,16,20]. It is supposed that ordinary Portland cement was used for these cases, as otherwise a comment would have been expected.

The specimens were exposed to different and/or changing exposure conditions over the testing period (Table 7). In most studies, the samples were exposed to a high relative humidity (RH), as it is known that a RH between 90% and 95% favors high corrosion rates [13]. To achieve a wide range of concrete resistivities, the samples were exposed to drier climates occasionally. Samples were exposed to outside conditions, in particular sea climates, in parts of the studies [13,14,16]. The temperature did not vary considerably in most experiments. In general, experiments were undertaken over a period between one and 5 years.

To evaluate the applicability, limitation and scatter of the C–R relationship sufficiently, it is desirable to cover a wide range of values for both parameters. This can be done by changing both materials and exposure conditions. However, to distinguish the effect of material and exposure, it is of importance that both can be explicitly separated from one another. This can be done by using parallel setups of material mixes and exposing them to varying environmental regimes. Both material and exposure were changed in the majority of the reviewed studies; in most cases, the exposure was changed equally for all samples. This allows an evaluation of the influence of material on the C–R relationship, however no information could be observed about the dependency of different exposure regimes/histories on the C–R relationship in these cases. Information about that was solely provided in [6,9,13].

2.4. Corrosion initiation

Chloride-induced corrosion was investigated in the majority of the studies (Table 8). Just one study concentrated solely on carbonation-induced corrosion [5]. A mix of exposure to chlorides and carbonation was considered in two experiments [7,13]. Chloride-induced corrosion was initiated by mixed-in chlorides in most cases. Cyclic exposure to chloride solution was used just partly. Carbonation was accelerated by storage in carbonation cabinets with a high CO_2 concentration and low RH.

The way corrosion is induced is of importance when experimental results should be related to practice. The initiation of corrosion and the exposure conditions in the reported studies differ from one another. Corrosion initiated by mixed-in chlorides was the most frequently used method. This reduces the time to depassivation (Fig. 1), however mixed-in chlorides may also lead to significant changes in the pore structure of the concrete [11] and the corrosion process [48]. Differences between studies with and with-

out mixed-in chlorides by using the same mix design might be explained due to this influence.

2.5. Summary

The experimental setup can have a considerable influence on the C–R relationship observed, as was shown in the previous sections. In particular the measurement methods comprise a variety of parameters influencing the recorded data. The specimen geometry and the general setup have a minor influence on the results in the opinion of the authors. To allow for a sufficient overview of factors affecting the C–R relationship, the material and exposure conditions should carefully be chosen. Practice related results are in any case desirable and the initiation of corrosion must be selected accordingly. This is favorable in particular for experimental results that should be used as input in prediction models. Subjects discussed above must carefully be taken into account when designing and/or evaluating an experimental setup.

A standardized method would be advantageous for testing the C–R relationship. It would then be possible to compare experimental data obtained in different laboratories and conditions. Such a method should assure practice-related materials and exposure conditions. Just one study reporting field data was identified by the authors [32]. An extensive field survey of the C–R relationship is critically needed to identify possible deviations between laboratory studies and reality.

3. Analysis and scatter

An inverse proportional relationship between corrosion rate and concrete resistivity was observed in all experimental investigations. However, variations occur between studies. Differences between the reports concerning analysis of the data will be discussed in following section. The scatter of the relationship will also be addressed.

3.1. Properties, scales and correlations

The propagation of the corrosion process was described by the corrosion rate in all studies with the exception of [6] where the polarization resistance was not transformed into i_{corr} (Table 9). In the publications, either resistivity ρ (resistance R) or conductivity σ was used. Different scales were chosen to illustrate the C–R relationship depending on the chosen properties. A log–log scale was selected in studies where resistance or resistivity was compared with the corrosion rate. This was done for the majority of the studies (Table 9). Linear scaled axes were preferred in cases where conductivity was correlated with corrosion rate. Other axis types are seldom used for these properties [4,6,14]. A linear regression line was fitted to the experimental data in most studies [4–7,10,13,16,20]. This was done in both the log–log and the linear–linear scales.

Data is fitted in a different way dependent on the used scale. The individual data points are weighed differently and consequently, the trend lines differ. A linear regression line fitted to data using linear scales and not passing though the origin is not resulting in a linear line in the log–log scale (trend lines [13] Fig. 4). It can also be observed that trend lines fitted to data in different scales might correlate differently to each other dependent on the scale. As an example, the regression lines of studies [9,16] have approximately the same slope and location illustrated in linear scales (Fig. 5). However, on the log–log scale (Fig. 4) different slopes and positions are identified.

There exists not one clear single linear correlation between corrosion rate and concrete resistivity, as can be seen when comparing the linear trend lines (Figs. 4 and 5). The regression lines differ from one another in both figures. The slopes of regression lines in the linear–linear scale vary considerably (Fig. 5), whereas in the log–log scale trend lines are shifted in parallel (Fig. 4). Different parameters causing this deviation are identified and discussed (Fig. 3).

In the light of the variation between the trend lines, the impact of different scales to analyze the data is small and so this issue will not be stressed any further.

Table 10
Assessment of corrosion conditions [45].

	i_{corr}
Passive condition	<0.1 μA/cm^2
Low – moderate	0.1–0.5 μA/cm^2
Intermediate – high	0.5–1 μA/cm^2
Very high	>1 μA/cm^2

3.2. Scatter

A sufficient amount of data is needed to evaluate the scatter of the trend lines for the C–R relationship. The number of specimens produced for the reviewed experiments differs from 2 to 40 and consequently also the amount of recorded data (Table 4). A scatter of more than one order of magnitude was observed for the corrosion rate for parts of the individual data sets [5–7,16,20,32]. Assessment criteria for corrosion activity distinguish one order of magnitude between very high corrosion activity and passive conditions (Table 10). This should serve as a warning not to rely solely on a given regression line to characterize the C–R relationship.

The general scatter of the data reviewed is illustrated in Fig. 6 as a grey cloud around the regression lines. The borders of resistivity values commonly found in the field [23] are plotted in addition to the classification of the corrosion rate (Fig. 6). In the light of this frame, it becomes apparent that the C–R relationship can be utilized just by understanding the reason for its variation. Otherwise, the clear trend observed for the C–R relationship diminishes to a data cloud.

Field data collected at one building during a period of a half year is plotted as grey squares in Fig. 6 [32]. The scatter of the field data encompasses all trend lines. This demonstrates the difficulties faced when trying to assess the corrosion rate in an accurate way by measuring concrete resistance in the field.

3.3. Summary

The scale in which the experimental data is analyzed influences the regression lines and their comparison. However, this impact on the C–R relationship vanishes in the light of the high scatter observed for the individual data and between the regression lines. To allow for an application of the C–R relationship in practice, it is essential to explain its scatter and variation.

4. Dependency and limitation

The question of which parameters the C–R relationship depends on, is of high interest in the light of the observed variation between the regression lines. To address this variation, this section evaluates the influence of material and exposure on the relationship. The discussion is based on the reported regression lines (Figs. 4 and 5).

4.1. Materials

The dependency of the C–R relationship on concrete properties is explained with contradictory hypotheses in the literature. No changes of the correlation were experienced in some studies [4,16] by changing the w/b ratio from 0.4 to 0.6 or replacing parts of the cement by slag. In other cases, changing w/b ratio and/or cement type influenced the observed trend lines [10,13]. Variations in the slopes of the regression lines were observed for data from carbonated samples prepared with different cement types [5], in particular a difference can be seen between OPC and the other cement types (Table 11). However, in the study it was concluded that the values are in good agreement and that a general relationship between corrosion rate and concrete resistivity can be established [5].

Regression patterns observed for samples made of different cement types are marked with different line types for the case of chloride induced corrosion (Figs. 4 and 5) (Table 3). Based on this, a gap can be observed between trend lines found for OPC (dashed doted lines) and for slag cements (dashed lines), with the exception of one study [20]. Although OPC was used in the latter study [20], the trend line is clearly differing in position from the lines observed for other OPC samples. Variations within the two groups of trend lines can also be observed. This might be explained by differences in the amounts of slag used or different w/b ratios. Another explanation might be variations in the experimental setups, such as the manner in which chlorides were induced or the measurement methods (Section 2). Setting aside these factors, it might be concluded that the C–R relationship is dependent on the cement type in the case of chloride-induced corrosion.

One regression line clearly deviates from the pattern described above (Figs. 4 and 5 trend line for [20]). The samples investigated in this study were more than 10 years old and stored in a dry laboratory climate during these years [20]. It is very likely that large parts of the concrete cover were carbonated when comparing the conditions to similar reports [1]. Carbonation leads to a densification of the concrete pore structure for concrete made of OPC and a decrease of the pH in the pore solution [1]. Also the type of corrosion might be changed which will be discussed as the review moves forward (Section 4.3). Both could be an explanation for the deviation of this regression line. Similar observations were made on samples exposed to accelerated carbonation. The C–R relationship changed noticeably after this treatment [13]. It can thus be concluded that not only the cement type but also carbonation of the concrete cover, might influence the trend lines found for the C–R relationship.

Just two data series could be compared for corrosion due to carbonation (Figs. 4 and 5). The regression line for the mix prepared with slag cement [13] is located somewhat higher than the trend line observed as an average of different cement types [5]. A variation between OPC samples and samples made of other cement types were observed for the latter data series (Table 11), as discussed earlier. Consequently, it might be concluded that the cement type has an influence on the C–R relationship also in the case of carbonate-induced corrosion. It cannot be deduced whether this variation is more or less pronounced than in the case of chloride-induced corrosion, because of the limited amount of data.

4.2. Exposure

The impact of humidity and temperature on the C–R relationship was emphasized in just a few studies (Section 2.3). The influence of exposure was discussed separately for corrosion rate and concrete resistivity in [13]. It was reported that both corrosion rate and concrete resistivity are influenced exponentially by relative humidity and temperature under homogenous material conditions. This suggests that the corrosion rate can be studied by measuring concrete resistivity, once the C–R relationship is established for specific material conditions [13,49–51]. Contradicting this, an a priori relationship between corrosion rate and concrete resistivity was excluded for chloride-induced corrosion in [28]. In this case, it was found that corrosion rate showed a higher dependency on temperature than concrete resistance does. This statement is supported by comparing activation energies found for the corrosion process and concrete resistivity in literature. Commonly the corrosion process shows activation energies around 30–40 kJ/mol (in the range of 85–100% RH and temperatures between 0 and 60 °C) [52]. Resistivity, on the contrary, appears to have a lower temperature dependency with activation energies in the average of 25 kJ/mol (calculated from the constant A in Hinrichson-Rasch Law multiplied with the ideal gas constant) [11].

The complex correlation between climate variables (as temperature and relative humidity) and corrosion rate was also discussed in [53]. It appear from the paper that the complex dependency of corrosion rate on temperature and moisture state could best be correlated to changes in the concrete resistivity [53].

The influence of the degree of moisture saturation of concrete on the C–R relationship was described in [9]. It was stated that the C–R relationship is just applicable for moisture contents below 70% degree of pore saturation under the specific experimental conditions [9]. For concretes with some capillary porosity, this might be in agreement with [6] where it was stated that the C–R relationship is not valid for concrete near water saturation or above an atmospheric relative humidity of approximately 95% [6].

Very little information about the influence of exposure on the C–R relationship can be observed from the graphical comparison. Regression lines found for data from samples with the same mix composition (Table 6) but different exposure conditions (Table 7) show a good correlation, such as data from [9,16]. Based on the data available, it may be concluded that the exposure conditions are of minor importance on the C–R relationship, supporting the findings in [13]. However, there is a need for further research in this area.

4.3. Corrosion mechanism

The anodic, cathodic and concrete resistance will influence the corrosion rate to a varying degree (Fig. 2), depending on environmental and material conditions. Without the presence of chlorides or in non-carbonated concrete, the anodic resistance will be high and prevent corrosion onset. In a submerged structure, oxygen supply is limited and consequently the cathodic reaction will be slow, even though, e.g. a sufficient amount of chloride is present. In contrast, in very dry environments, the high concrete resistance will inhibit the corrosion rate. Between these extremes, the rate limiting step is more undefined. To what extent corrosion rate

Table 11
Slopes of trend lines obtained in [20] – $\lg i_{corr} = \lg i_o + \text{slope} \lg \rho$.

Type of mortar	OPC	Sulfate resistance PC	Slag cement	Pozzolanic cement	OPC + 30% FA	Fly ash cement
Slope	−0.72	−1.11	−1.07	−1.06	−1.08	−1.06

can be correlated to concrete resistance will depend on its influence on the rate limiting step.

Corrosion can be initiated by chlorides or carbonation (Section 1.2). Carbonation will lead to a general type of corrosion with anode and cathode sites immediately adjacent to one another. The current will primarily flow through the interfacial zone between the steel and the bulk concrete [40]. On the contrary, chloride-induced corrosion results in localized pits and, anode and cathode areas are separated in space from one another. The current field which develops between anode and cathode will span through the bulk concrete, but is forced to flow through the pit mouth. Dependent on the pit size, the spreading resistance of this bottleneck to current flow can be very high [33].

For general corrosion due to carbonation, it is proposed that concrete conductivity has an indirect impact on the anodic reaction rate, which limits the corrosion rate. This is termed "anodic resistance control" and is comparable to diffusion or activation polarization under other conditions [7,13]. Contradicting this assumption, theoretical analyses of the corrosion process of general corrosion showed that cathodic activation control might also be considered as a rate limiting step for general corrosion [40]. The resistance of the concrete between anode and cathode areas was not identified to be rate limiting as they are in close proximity of each other and thus the concrete resistance is low. Anodic and cathodic reactions are primarily dependent on the transport through the cover concrete. Consequently, the resistivity of the cover concrete should be compared to the corrosion rate.

For localized corrosion, the mechanism of corrosion control is unclear [13]. Cathodic control was considered as unlikely, particular in the beginning of pit growth [6,33]. An indirect correlation of concrete resistance to the corrosion rate is expected, comparable to what was explained for generalized corrosion. Primarily, the resistance of the bottleneck to ion flow, such as the supply of chlorides into the pit, will inhibit the anodic reaction rate [33]. The extent to which the resistance of the bottleneck can be compared to the bulk resistivity of the concrete is unknown. The influence of the bottleneck will diminish as the pit grows [33]. For later stages, where big pits and high corrosion rates were obtained, it was suggested that rather a mix or pure cathodic control limits the corrosion process [54]. Accordingly, the rate limiting step might change over the course of the corrosion process. This and the unknown relationship between the bottleneck resistance and the bulk concrete resistivity might be a reason that the C–R relationship is less well-defined in the case of chlorides than for carbonation-induced corrosion [13].

Bound chlorides will be released when concrete carbonates. A high amount of chlorides may involve a larger area in the corrosion attack and thus the corrosion rate will be increased [1]. The morphology of pitting corrosion will be less pronounced [1]. This explains the shift of the regression lines observed for carbonated samples prepared with mixed-in chlorides in the direction of higher corrosion rates compared to uncarbonated samples of the same type [13,20] (Figs. 4 and 5). Carbonation seems to have a pronounced effect for samples prepared with OPC; the same is not observed for samples made with slag blended cements [13] (Figs. 4 and 5). An explanation for this might be the difference in the impact of carbonation on OPC and slag concrete. The resistivity of OPC increases due to a combination of reduced pore solution conductivity and porosity. For slag cement, carbonation increases the porosity and thereby contradicts the impact of reduced pore solution conductivity.

Interesting to notice is that in the graphical comparison of the regression lines mainly two areas can be identified where the trend lines gather (Figs. 4 and 5). The first group presents regression lines from carbonated samples and samples made of slag cement. The second group corresponds to trend lines found for samples made with OPC suffering from chloride-induced corrosion. It would be of high interest to study whether these groupings are the result of different corrosion morphology and rate limiting steps or a simple coincidence. Unfortunately, no detailed information about the type of corrosion or rate limiting step was given or obtained in the reviewed literature.

4.4. Summary

Cement type was, in particular, identified to have an influence on the C–R relationship. This seems to be pronounced in the case of chloride-induced corrosion. A distinct difference was observed between regression lines for carbonated and uncarbonated samples prepared with OPC. More research is needed to evaluate the influence of moisture and temperature. They seem to be of minor importance according to the comparison of the trend lines, though doubts were raised concerning the applicability of the C–R relationship in the case of chloride-induced corrosion for temperature changes. It has been emphasized by many authors that the C–R relationship is not valid for the extreme case of concrete near water saturation.

An urgent need for research was identified to be the general understanding of the corrosion process. Without detailed knowledge about the corrosion morphology and the rate limiting step, the exact influence of concrete resistivity on the corrosion process cannot be identified.

5. Models of the propagation period

It is of interest to assess and predict the corrosion process for both existing and new concrete structures. A variety of different forecast models exist helping to estimate the Service Life of structures exposed to severe climates [55,56]. The C–R relationship is a central part of several of these models. Two models have been selected and are compared with the reviewed experimental data.

5.1. Models

A Service Life model derived in parts from the results of the experiments described in [5,32] was reported in [57]. The estimation of the propagation time in the model is based on the C–R relationship. Use is made of an effective resistivity ρ_{ef} that is estimated from the resistivity of saturated concrete, adjusted with factors taking into account concrete age and annual climate changes. The correlation between corrosion rate and concrete resistivity is characterized by a factor K_{corr}:

$$i_{corr} = K_{corr}/\rho_{ef} \quad (2)$$

K_{corr} is the constant for the C–R relationship (3×10^4 μA/cm^2 kΩ cm).

The equation does not consider concrete mix design, the cause of corrosion or exposure conditions [57].

Eq. (2) was supplemented with variables that account for the cause of corrosion in the final DuraCrete report [58]. The following equation is proposed for estimations of the propagation period in the model:

$$i_{corr} = m_o/\rho_c \cdot \alpha^c \cdot F^c_{cl} \cdot \gamma_v \quad (3)$$

m_o is the constant for the C–R relationship (882 μm·Ω m/year), ρ_c the characteristic value of the resistivity, α^c the characteristic value of the pitting factor, F^c_{cl} the characteristic value of the chloride corrosion rate and γ_v is the partial factor for the cost of mitigation of risk relative to the cost of repair.

Most parameters are dependent on the cause of corrosion or the type of corrosion, with the exception of m_o. Details about the char-

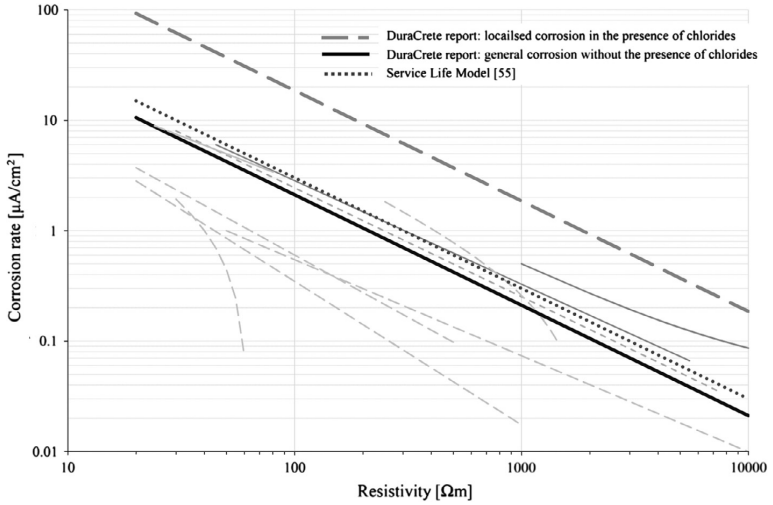

Fig. 7. Comparison between the reviewed Service Life models [57,58] and the regression lines observed in literature (thin dashed lines for chloride induced-corrosion, thin continuous lines for corrosion due to carbonation, details Figs. 4 and 5).

acteristic and statistical quantification of the variables are given in [58,59]. The factors are based on data collected, such as in [13].

5.2. Comparison with experimental investigations

Eqs. (2) and (3) have been compared with the trend lines discussed previously (Fig. 7). The parameters included in the DuraCrete report were chosen for the cases of localized corrosion in the presence of chlorides and for general corrosion without chlorides. The partial factor in Eq. (3) was assumed for a normal relative risk of mitigation costs to repair costs [58].

The computed C–R relationship for corrosion due to carbonation from the DuraCrete report slightly underestimates the corrosion rate compared to the experimental data. However, in the light of the variation observed between the reported trend lines this is seen as a minor deviation. In the case of chloride-induced reinforcement corrosion, the corrosion rate calculated from the DuraCrete report is considerably higher than determined in the experimental investigations (Fig. 7). However, due to the unknown corroding area, it is likely that the corrosion rate was underestimated for localized corrosion in most experiments (Section 2.2). Consequently, the gap observed between the report and the experiments is likely to be smaller and it cannot be assessed whether the report reflects the C–R relationship suitably for localized corrosion. The deviation of the regression lines between the different cement types is not considered in the DuraCrete report, nor is the influence of other parameters such as carbonation of the concrete cover. Additional factors taking into account these influences would be useful.

The model proposed in [57] assumes one single relationship between corrosion rate and concrete resistivity. The presented literature review highlights that this assumption is too simple. Nevertheless, compared with experimental data, Eq. (2) reflects the conditions of carbonated samples and samples made of slag cement suffering from chloride-induced corrosion rather well (Fig. 7). The model should consequently be more specific about its applicability or provide an adjustment of its prediction also for other cases.

The prediction of the models is in good accordance with parts of the experimentally observed regression lines. However, several parameters which might have an influence on the C–R relationship are not considered in the models. None of the models reflected the C–R relationship for chloride-induced corrosion on samples made with OPC as it was observed in the experiments. However, as most of these experiments were undertaken with mixed in chlorides and as the corrosion rate was probably erroneous calculated, it is questionable whether they are representative for practice, see Section 2.4.

It is seen as necessary to refine the equations to be able to predict the C–R relationship sufficiently. In order to enhance and verify the models, more in depth research is needed on factors (such as material, exposure, carbonation of the cover and corrosion mechanism) which have an impact on the C–R relationship and a comparison to practice related data.

6. Summary and conclusions

A clear tendency can be found that with increasing concrete resistivity, the corrosion rate decreases. The relationship can be observed once corrosion has started (active conditions). It will not be valid in the case of saturated concrete, where although the resistivity is low, the corrosion rate will still be small due to a lack of oxygen. Different parameters were identified which might have an influence on the C–R relationship. However, there are still several factors which need intense discussion and investigation. The results of the literature review are summarized in the following.

- Even though a distinct correlation is observed between corrosion rate and concrete resistivity, the scatter observed is high in and between the reviewed investigations (Figs. 4–6). This is reflected also in the ranges suggested for assessment of corrosion activity by means of concrete resistivity (see Table 1).
- The experimental design used to investigate the C–R relationship can have a major impact on the results. Especially, the measurement methods were identified to be susceptible. Corrosion rate measurements should always be corrected for ohmic

drop and for the de facto corroding area, as far as this is possible. The variation between the investigations might partly be explained by differences between the measurement methods.

- The analysis of the experimental data is sensitive to the properties and graphical scales used. It was shown that regression lines found in different scales are not identical. The difference, however, is small compared to the general variation between the trend lines. Nevertheless, it would be desirable for the future to agree upon a concurrent description.
- The scatter of the reported data is relatively high. The probabilistic evaluation of the C–R relationship needs more attention, in particular when it is included in Service Life models.
- The cement type was identified to change the C–R relationship. This was pronounced in the case of corrosion in the presence of chlorides, comparing concretes made of OPC and slag cements. Differences were also observed for carbonated samples prepared with different cement types (chiefly OPC vs. other cement types).
- Carbonation of the concrete cover seems to have an impact on the C–R relationship. Differences were observed between carbonated and non-carbonated samples suffering from chloride-induced corrosion prepared with OPC. The differences for samples made of slag cements were less pronounced. However, more detailed research is needed to strengthen this finding.
- The moisture state and temperature were found to be of minor influence to the C–R relationship, when comparing the same material conditions. However, just a few studies could be used for this comparison and more investigation is needed in this field.
- The cause of corrosion might also be identified to influence the C–R relationship. A gap was observed between samples made of OPC suffering from chloride-induced corrosion and carbonated samples. Unfortunately, no conclusions could be drawn on extent to which the type of corrosion (localized or general) influences the C–R relationship. Different mechanisms underlying these types of corrosion are why a variation of the C–R relationship might be expected. It is highly recommended to study this issue in greater detail.
- The rate limiting step underlying the corrosion process forms the basis of the C–R relationship. To justify and evaluate the applicability of the C–R relationship, it is vital to gain further knowledge about the mechanism which dominates the corrosion process and how it is influenced by the concrete resistance.
- Prediction models risk over-simplifying the complex C–R relationship, owing to the variety of parameters changing and influencing it. Both models discussed here missed detailed differentiation of parameters which have an impact on the C–R relationship.
- Field data was taken into account in just a few studies. It is of high interest to collect further field experience to assess the practicability of the C–R relationship.

It can be concluded that although the concrete resistivity seems promising for the assessment of Service Life of reinforced concrete structures, it is necessary to investigate its relationship to the corrosion rate further.

Acknowledgements

The paper is based on the work performed in COIN – Concrete Innovation Centre (www.coinweb.no) – which is a centre for research-based innovation, initiated by the Research Council of Norway (RCN) in 2006 – and supported by the Norwegian Public Roads Administration (www.vegvesen.no). A special thanks goes to Dr. Carolyn Rosten for her help with the language.

References

[1] Bertolini L, Elsener B, Pedeferri P, Polder R. Corrosion of steel in concrete. Wiley-VCH Verlag GmbH & Co.; 2004.
[2] Cavalier PG, Vassie PR. Investigation and repair of reinforcement corrosion in a bridge deck. PI Civil Eng Pt 1. 1981;70(Aug):461–80.
[3] Hope BB, Ip AKC, Manning DG. Corrosion and electrical-impedance in concrete. Cem Concr Res 1985;15(3):525–34.
[4] Hope BB, Ip AKC. Corrosion of steel in concrete made with slag cement. ACI Mater J 1987;84(6):525–31.
[5] Alonso C, Andrade C, Gonzalez JA. Relation between resistivity and corrosion rate of reinforcements in carbonated mortar made with several cement types. Cem Concr Res 1988;8(5):687–98.
[6] Feliu S, González JA, Feliu SJ, Andrade C. Relationship between conductivity of concrete and corrosion of reinforcing bars. Br Corros J 1989;24(3):195–8.
[7] Glass GK, Page CL, Short NR. Factors affecting the corrosion rate of steel in carbonated mortars. Corros Sci 1991;32(12):1283–94.
[8] Andrade C, Alonso C, Goni S. Possibilities for electrical resistivity to universally characterise mass transport processes in concrete. In: Dhir RK, Jones MR, editors. Concrete 2000 E & FN Spon; 1993.
[9] López W, González JA. Influence of the degree of pore saturation on the resistivity of concrete and the corrosion rate of steel reinforcement. Cem Concr Res 1993;23:368–76.
[10] Cabrera JG, Ghoddoussi P. The Influence of hootsohooh. In: Malhotra VM, editor. Durability of concrete third international conference. Nice, France; 1994.
[11] Elkey W, Sellevold EJ. Electrical resistivity of concrete. Publication No. 80. Oslo: Norwegian Road Research Laboratory; 1995.
[12] Andrade C, Alonso C. Corrosion rate monitoring in the laboratory and on-site. Constr Build Mater 1996;10(5):315–28.
[13] Bertolini L, Polder RB. TNO report – concrete resistivity and reinforcement corrosion rate as a function of temperature and humidity of the environment. TNO Building and Construction Research; 1997.
[14] Liu T, Weyers RW. Modeling the dynamic corrosion process in chloride contaminated concrete structures. Cem Concr Res 1998;28(3):365–79.
[15] Polder RB. Test methods for onsite measurement of resistivity of concrete – a RILEM TC-154 technical recommendation. Constr Build Mater 2001;15(2–3):125–31.
[16] Morris W, Vico A, Vazquez M, de Sanchez SR. Corrosion of reinforcing steel evaluated by means of concrete resistivity measurements. Corros Sci 2002;44(1):81–99.
[17] Shi CJ. Effect of mixing proportions of concrete on its electrical conductivity and the rapid chloride permeability test (ASTM C1202 or ASSHTO T277) results. Cem Concr Res 2004;34(3):537–45.
[18] Smith KM, Schokker AJ, Tikalsky PJ. Performance of supplementary cementitious materials in concrete resistivity and corrosion monitoring evaluations. ACI Mater J 2004;101(5):385–90.
[19] Morris W, Vico A, Vazquez M. Chloride induced corrosion of reinforcing steel evaluated by concrete resistivity measurements. Electrochim Acta 2004;49(25):4447–53.
[20] Gonzalez JA, Miranda JM, Feliu S. Considerations on reproducibility of potential and corrosion rate measurements in reinforced concrete. Corros Sci 2004;46(10):2467–85.
[21] Sengul O, Gjørv OE. Electrical resistivity measurements for quality control during concrete construction. ACI Mater J 2008;105(6):541–7.
[22] Polder RB. Critical chloride content for reinforced concrete and its relationship to concrete resistivity. Mater Corros 2009;60(8):623–30.
[23] Polder R, Andrade C, Elsener B, Vennesland Ø, Gulikers J, Weidert R, et al. Rilem TC 154-EMC: electrochemical techniques for measuring metallic corrosion – test methods for onsite measurement of resistivity of concrete. Mater Struct 2000;33(234):603–11.
[24] Whiting DA, Nagi MA. Electrical resistivity of concrete – a literature review. Skokie (Illinois): Portland Cemente Association; 2003.
[25] Gjørv OE, Vennesland Ø, El-Busaidy AHS. Electrical Resistivity of Concrete in the Oceans. In: 9th Annual offshore technology conference. Houston, Texas; 1977.
[26] Büchler M, Schiegg Y. Untersuchungen zur Potenzialfeldmessung an Stahlbetonbauten: Bundesamt für Straßenbau (ASTRA) / Office federal des routes (OFROU), 2008-3, Bern, Switzerland.
[27] Østvik JM. Thermal aspects of corrosion of steel in concrete. Trondheim: Norwegian University of Science and Technology; 2005.
[28] Jäggi S, Böhni H, Elsener B. Macrocell corrosion of steel in concrete – experiments and numerical modelling. In: Raupach M, Elsener B, Polder RB, Mietz J, editors. Corrosion of reinforcement in concrete – mechanisms, monitoring, inhibitors and rehabilitation techniques. Woodhead Publishing Limited, CRC Press; 2007. p. 75–88.
[29] Tuutti K. Corrosion of steel in concrete. Stockholm: Swedish Cement and Concrete Research Institute; 1982.
[30] Elsener B, Andrade C, Gulikers J, Polder R, Raupach M. Half-cell potential measurements – potential mapping on reinforced concrete structures. Mater Struct 2003;36(261):461–71.
[31] Millard SG, Harrison JA, Edwards AJ. Measurement of the electrical-resistivity of reinforced-concrete structures for the assessment of corrosion risk. Brit J Nondestr Test 1989;31(11):617–21.

[32] Rodriguez J, Ortega LM, Garcia AM, Johansson L, Petterson K. On site corrosion rate measurements in concrete structures using a device developed under the eureka project EU-401. Denmark: International Conference on Concrete Across Borders Odense; 1994.
[33] Angst U, Elsener B, Larsen CK, Vennesland Ø. Chloride induced reinforcement corrosion: rate limiting step of early pitting corrosion. Electrochim Acta 2011;56(17):5877–89.
[34] Angst U, Elsener B, Larsen CK, Vennesland Ø. Considerations on the effect of sample size for the critical chloride content in concrete. In: 2nd International Symposium on Service Life Design for Infrastructure, 4–6 October, Delft, The Netherlands; 2010.
[35] Andrade C, Alonso C, Gulikers J, Polder R, Cigna R, Vennesland Ø, et al. Rilem TC 154-EMC: electrochemical techniques for measuring metallic corrosion – test methods for on-site corrosion rate measurement of steel reinforcement in concrete by means of the polarization resistance method. Mater Struct 2004;37(273):623–43.
[36] Østvik JM, Larsen CK, Vennesland Ø, Sellevold EJ, Andrade MC. Electrical resistivity of concrete Part I: frequency dependence at various moisture contents and temperatures. In: 2nd International symposium on advances in concrete through science and engineering. Quebec City, Canada; 2006.
[37] Broomfield J, Millard S. Measuring concrete resistivity to assess corrosion rates. Concrete; 2002 [Current Practice Sheet No. 128:37-9].
[38] DuraCrete. Compliance Tests State-of-the-Art. The European Union – Brite EuRam III; 1997.
[39] Gowers KR, Millard SG. Measurement of concrete resistivity for assessment of corrosion severity of steel using Wenner technique. ACI Mater J 1999;9(10):536–41.
[40] Gulikers J. Theoretical considerations on the supposed linear relationship between concrete resistivity and corrosion rate of steel reinforcement. Mater Corros 2005;56(6):393–403.
[41] Stern M, Geary AL. Electrochemical polarization. I. A theoretical analysis of the shape of polarization curves. J Electrochem Soc 1957;104(1):56–63.
[42] Elsener B. Corrosion rate of steel in concrete – from laboratory to reinforced concrete structures. In: Mietz J, Elsener B, Polder R, editors. Eur Fed Corr Publ: Maney Publishing; 1998. p. 92–103.
[43] Elsener B. Corrosion rate of steel in concrete – measurements beyond the Tafel law. Corros Sci 2005;47(12):3019–33.
[44] Nygaard PV. Non-destructive electrochemical monitoring of reinforcement corrosion. Department of Civil Engineering, Technical University of Denmark; 2008.
[45] Oelssner W, Berthold F, Guth U. The iR drop – well-known but often underestimated in electrochemical polarization measurements and corrosion testing. Mater Corros 2006;57(6):455–66.
[46] Nygaard PV, Geiker MR. Measuring the corrosion rate of steel in concrete – effect of measurement technique, polarisation time and current. Mater Corros 2012;63(3):200–14.
[47] Nygaard PV, Geiker MR, Elsener B. Corrosion rate of steel in concrete: evaluation of confinement techniques for on-site corrosion rate measurements. Mater Struct 2009;42(8):1059–76.
[48] Angst U, Elsener B, Larsen CK, Vennesland Ø. Critical chloride content in reinforced concrete – a review. Cem Concr Res 2009;39:1122–38.
[49] Fiore S, Polder RB, Cigna R. Evaluation of the concrete corrosivity by means of resistivity measurements. In: Page CL, Bamforth PB, Figg JW, editors. Fourth International Symposium on Corrosion of Reinforcement in Concrete Construction. Cambridge, Great Britian: The Royal Society of Chemistry; 1996. p. 273–82.
[50] Pacheco-Farías J. Corrosion of steel reinforcement in 12 years old concrete: inspection, evaluation and electrochemical repair of corrosion. Delft University of Technology; 2010.
[51] Tondi A, Polder RB, Cigna R. TNO report – concrete resistivity and corrosion rate of reinforcement in atmospheric concrete after 1 year. TNO Building and Construction Research; 1993.
[52] Michel A, Nygaard PV, Geiker MR. Experimental investigation on the short-term impact of temperature and moisture on reinforcement corrosion. Corros Sci, 2013, http://dx.doi.org/10.1016/j.corsci.2013.02.006.
[53] Andrade C, Alonso C, Sarria J. Influence of relative humidity and temperature on-site corrosion rates. Mater Construcc 1998;48(251):5–17.
[54] Raupach M. Zur chloridinduzierten Makroelementkorrosion von Stahl in Beton (in German). Berlin: Beuth Verlag GmbH; 1992.
[55] Markeset G, Myrdal R. Modelling of reinforcement corrosion in concrete – state of the art COIN project report 7. SINTEF Building and Infrastructure; 2008.
[56] Raupach M. Models for the propagation phase of reinforcement corrosion – an overview. Mater Corros 2006;57(8):605–13.
[57] Andrade C, d'Andrea R. Electrical resistivity as microstructural parameter for the modelling of service life of reinforced concrete structures. In: Breugel Kv, Ye G, Yuan Y, editors. In: 2nd International symposium on service life design for infrastructure. Delft, The Netherlands: RILEM Publications S.A.R.L.; 2010. p. 379–88.
[58] DuraCrete – final technical report – probabilistic performance based durability design of concrete structures. The European Union – Brite EuRam III; 2000.
[59] DuraCrete – statistical quantification of the variable in the limit state functions. The European Union – Brite EuRam III; 2000.

Paper II

Application of segmented rebars for studying corrosion of steel in concrete

Proceedings Eurocorr 2013, Estoril, Portugal 2013.

Hornbostel, K.; Geiker, M. R. and Larsen, C. K.

Application of segmented rebars for studying corrosion of steel in concrete

Hornbostel, K., Norwegian University of Science and Technology, Trondheim/ Norway
Geiker, M. R., Norwegian University of Science and Technology, Trondheim/ Norway
Larsen, C., Norwegian Public Road Administration, Oslo/ Norway

Abstract

Segmented rebars consisting of one mild steel segment in between two stainless steel segments were used to study steel corrosion in concrete. In total four different mild steel segment lengths were tested: 5 mm (exposed area 157 mm^2), 10 mm (314 mm^2), 20 mm (628 mm^2) and 50 mm (1570 mm^2). The rebars were embedded in a chloride contaminated concrete (2.5 % Cl- by cement weight) which was exposed to a high relative humidity (95-98 %) and a temperature around 20 °C. The corrosion process was monitored over several months during which the segments were periodically connected. The galvanic current between the corroding mild steel segments and the passive stainless steel segments was measured. The results were compared to linear polarization resistance measurements. In the experiment, the galvanic current was just half as high as the corrosion current determined by LPR for the smallest mild steel segment length and only 5 % in case of the biggest segment.

1 Introduction

Reinforcement corrosion in concrete is seen as one of the most severe durability problems of concrete structures. It can cause considerable damage, endanger human life and lead to high maintenance costs. Thus it is necessary to assess the corrosion behaviour of concrete structures in a reliable and accurate way. Steel corrosion in concrete can either take place as general corrosion when the concrete cover carbonates or localized corrosion in the presence of chlorides. The corrosion rate for localized corrosion can be very high, up to about 1 mm/year [1]. Although investigated during more than five decades, there are still remaining many unanswered questions to the corrosion process of steel in chloride contaminated concrete. Using segmented steel bars is one of the possibilities to investigate this type of corrosion. Depending on the segment size a considerable part of the corroding segment itself might serve as cathode and the galvanic current flowing between the segments presents just a part of the actual corrosion current. The purpose of the present study was to determine a suitable segment size when galvanic current measurements are to be used for corrosion current measurements. Polarization resistance and galvanic current measurements were compared for this purpose.

2 Background

2.1 Linear polarisation resistance measurements

The linear polarisation resistance technique is the most frequently used non-destructive method to determine the corrosion rate of steel embedded in concrete, both in laboratory and on-site. The technique is executed with a three electrode setup

using the reinforcement as working electrode (WE) and employing a counter (CE) and reference electrode (RE) in addition.

The technique is based on the assumption that the polarisation curve shows a linear behaviour in the vicinity of the corrosion potential E_{corr} [V] [2]. A mathematical description for calculating the corrosion current I_{corr} [A] from R_p was suggested by Stern and Geary in 1957 [3]:

$$I_{corr} = \frac{B}{R_p} = \frac{\beta_a \cdot \beta_c}{2.3(\beta_a + \beta_c)} \cdot \frac{1}{R_p} \quad (1)$$

(β_a and β_c = tafel slopes of the anodic and cathodic reaction rate)

The factor B [V] was calibrated against gravimetric mass loss measurements and determined to be 26 mV in the active state and 52mV for passive conditions [4]. The gravimetric experiments were undertaken in solution, however the values are recommend for calculations in concrete as well [5]. The measured polarisation resistance R_p* includes always the actual polarisation resistance R_p and the ohmic resistance R_Ω between the CE and the WE. Especially for electrolytes with a high electrical resistivity, as it can be the case for concrete, the measured R_p* has to be corrected for the ohmic drop otherwise the corrosion current will be underestimated. Methods and error sources of determining R_Ω are reported amongst others in [2, 6, 7].

2.2 Galvanic current measurements

Segmented rebars are occasionally used in laboratory experiments with different purposes [8-12]. The current flowing between the segments is typically measured with a Zero-Resistance-Amperemeter (ZRA). However, the corroding segments will just in very extreme cases work as pure anodes. In the majority of the cases the anode/corroding-segment will also include cathodic acting areas. The corrosion ongoing on an actively corroding segment itself can be referred to as microcell corrosion [13] and cannot be reflected by the galvanic current. For experiments executed in solution for eight days it was found that the galvanic current measured between an actively corroding segment (exposed area 50 mm^2) and a passive segment (area ratio anode to cathode 1/10) accounts for ca 75 % of the total corrosion current [13].

3 Methods

3.1 Experimental setup

Segmented rebars consisting of one mild steel segment and two stainless steel segments, adjacent to another (Figure 1) were embedded in a chloride contaminated concrete. The mild steel “anode” segments were made of ribbed construction (carbon) steel used as received. Dependent on the size of the segment, parts of the anode segment will work cathodically as well. Different lengths of mild steel segment were used to vary the ratio between anode and cathode area in the setup. Mild steel segment lengths of 5 mm (exposed area 157 mm^2), 10 mm (314 mm^2), 20 mm (628 mm^2) and 50 mm (1570 mm^2) were produced. The two adjacent stainless steel segments were made of 316L (1.4404) steel, unribbed. They acted as cathode and are therefore also called cathode segments (exposed area 1570 cm^2 per segment). All segments were electrically disconnected from each other, but could manually be

connected through wires. Each segmented bar was, together with a reference electrode, a counter electrode and 4 resistivity sensors, placed in one individual mould.

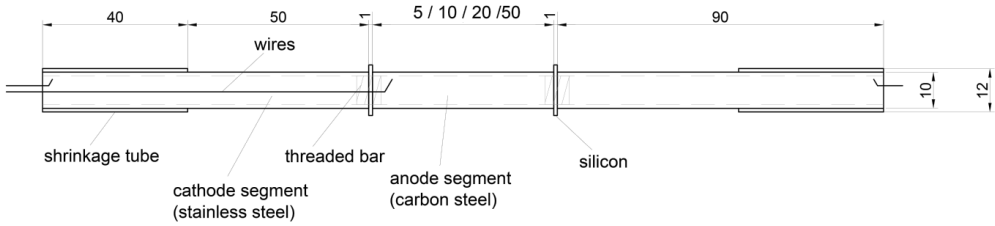

Figure 1: Segmented rebar

3.2 Concrete, curing and exposure

To shorten the initiation period (time until depassivation of the reinforcement) the segmented bars were placed in a chloride contaminated concrete (2.5 % Cl- by cement weight). The concrete was made of Norcem Anlegg cement (CEM I 52.5 N) with a water to cement ratio of 0.6 and aggregates with sizes 0-8 mm. The samples were demoulded after 1 day and stored at laboratory condition until 7 days after casting when they were sufficiently surface dry to apply an epoxy coating. All sides of the specimens were painted, except the upper and lower side. This was done to allow the penetration of water and oxygen through the sample by ensuring a one-dimensional moisture profile. Subsequently, all specimens were stored in a relative humidity of approximately 95-98 % and a temperature around 20-22 °C during the testing period.

3.3 Measurement methods

The LPR was determined by performing a potentiodynamic measurement with a Potentiostat (Princetion Parsatat 2273). The ohmic drop was separately determined by three different methods. The average value from these methods was used to correct the measurements. The ohmic drop was determined solely for the corroding segment to avoid errors due to a wrongly assumed current distribution (see discussion in [2]). The corrosion current was calculation from Equation (1), using B = 26 mV. The galvanic current flowing between the segments was measured periodically with the built-in ZRA of the Potentiostat. All measurement data discussed in this paper was recorded approximately a half year after casting, during this period the segments were periodically connected.

4 Results and Discussion

In experiments where segmented rebars are used it is common to measure the corrosion activity as the galvanic current between the segments instead of applying the LPR technique. However, dependent on the segment size a considerable amount of corrosion activity is ongoing on the corroding segment itself. By comparing the galvanic current with the corrosion current determined from LPR measurements (Equation 1), it is possible to quantify the amount of microcell corrosion, which cannot be measured by the galvanic current. It has to be kept in mind that the calculation of I_{corr} using Equation 1 is based on assumptions regarding the measurement method and the calculation as e.g. B = 26 mV [2]. These possible error sources are neglected in the further discussion and it is assumed that the corrosion current calculated from Equation 1 is the actual corrosion current.

During the testing period the segments were periodically disconnected from each other. In these periods solely microcell corrosion was ongoing on the anode segments. Dependent on the size of the segment this may lead to a limited corrosion growth due to lack of cathode area. Connecting additional cathode area might consequently lead to an increase in the corrosion rate. To evaluate the impact of connecting and disconnecting the anodic segments with the cathode segments measurements were preformed one hour and three days after connecting. It was found for all tested anodic segment lengths that the galvanic current was not increasing over time after connection (Figure 2). Based on this observation it is assumed that the galvanic current would not be higher if the segments were constantly connected.

In Figure 2 the corrosion current determined from LPR measurements and the galvanic current measured between the segments are compared. The results shown were measured a half year after casting. Corrosion rates between 4.3 and 10.9 µA/cm^2 were found for the connected segments (determined by normalizing the corrosion current measured with LPR by the anode segment area). According to [14] these numbers represent high corrosion activity. For this condition, it was observed that the galvanic current between the segments never exceeded 50% of the corrosion current (Figure 2), which indicates that a considerable amount of microcell corrosion was ongoing even on the smallest segment. Thus, galvanic current measurements could in the present investigation not be used to determine the actual corrosion current. If solely galvanic current measurements should be used for assessment of corrosion activity on segmented steel bars in concrete, it is therefore recommend using segments with smaller surface areas than 150 mm^2.

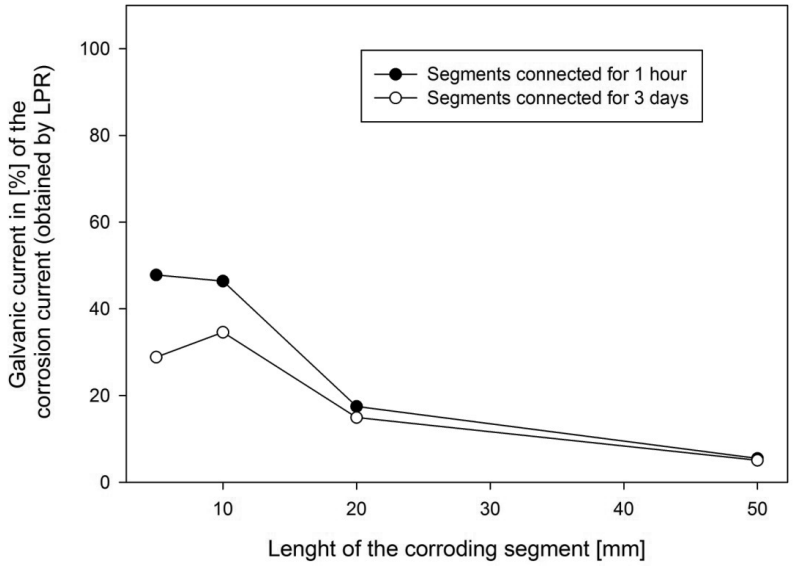

Figure 2: Comparison between the measured galvanic current between anodic and cathodic working segments and the corrosion current determined from LPR measurements, as a function of the anode segment length.

5 Conclusion

Segmented rebars can be of benefit when investigating corrosion issues experimentally. However, the galvanic current flowing between the segments cannot be assumed to be the total corrosion current as long as the segment, on which corrosion is ongoing, is not sufficiently small. For mild steel segments imbedded in chloride contaminated concrete it was found that even on a segment with a length of 5 mm (exposed area 157 mm^2) a considerable amount of corrosion was ongoing on the segment itself. The measured galvanic current did not exceeded more than 50% of the total corrosion current.

6 Acknowledgment

The paper is based on the work performed in COIN - Concrete Innovation Centre (www.coinweb.no) - which is a centre for research-based innovation, initiated by the Research Council of Norway (RCN) in 2006 - and supported by the Norwegian Public Roads Administration (www.vegvesen.no). A special thanks goes to Maria Belen Pina Fernandez for her help by the execution of the experiment.

References

[1] Bertolini L, Elsener B, Pedeferri P, Polder R. Corrosion of Steel in Concrete. Wiley-VCH Verlag GmbH & Co.; 2004.

[2] Elsener B. Corrosion rate of steel in concrete - Measurements beyond the Tafel law. Corros Sci. 2005;47(12):3019-33.

[3] Stern M, Geary AL. Electrochemical polarization. I. A theoretical analysis of the shape of polarization curves. J Electrochem Soc. 1957;104(1):56-63.

[4] Andrade C, González JA. Quantitative measurements of corrosion rate of reinforcing steels embedded in concrete using polarization resistance measurements. Materials and Corrosion. 1978;29:515-9.

[5] Andrade C, Alonso C, Gulikers J, Polder R, Cigna R, Vennesland Ø, et al. Rilem TC 154-EMC: Electrochemical techniques for measuring metallic corrosion - Test methods for on-site corrosion rate measurement of steel reinforcement in concrete by means of the polarization resistance method. Mater Struct. 2004;37(273):623-43.

[6] Nygaard PV. Non-destructive electrochemical monitoring of reinforcement corrosion, Department of Civil Engineering, Technical University of Denmark; 2008.

[7] Oelssner W, Berthold F, Guth U. The iR drop - well-known but often underestimated in electrochemical polarization measurements and corrosion testing. Mater Corros. 2006;57(6):455-66.

[8] Bertolini L, Gastaldi M, Pedeferri MP, Pedeferri P, Pstore T. Effecht of galvanic coupling between carbon steel and stainless steel reinforcement in concrete. International Conference on Corrosion and Rehabilitation of Reinforced concrete structures. Orlando, USA1998.

[9] Nygaard PV, Geiker MR, Elsener B. Corrosion rate of steel in concrete: evaluation of confinement techniques for on-site corrosion rate measurements. Mater Struct. 2009;42(8):1059-76.

[10] Raupach M. Zur chloridinduzierten Makroelementkorrosion von Stahl in Beton (in german). Berlin: Beuth Verlag GmbH; 1992.

[11] Jäggi S, Böhni H, Elsener B. Macrocell corrosion of steel in concrete - experiments and numerical modelling. In: Raupach M, Elsener B, Polder RB, Mietz J, editors. Corrosion of reinforcement in concrete - mechanisms, monitoring, inhibitors and rehabilitation techniques: Woodhead Publishing Limited / CRC Press; 2007. p. 75-88.

[12] Elsener B. Macrocell corrosion of steel in concrete - implications for corrosion monitoring. Cement Concrete Comp. 2002;24(1):65-72.

[13] Andrade C, Garces P, Martinez I. Galvanic currents and corrosion rates of reinforcements measured in cells simulating different pitting areas caused by chloride attack in sodium hydroxide. Corros Sci. 2008;50(10):2959-64.

[14] Andrade C, Alonso C. Corrosion rate monitoring in the laboratory and on-site. Constr Build Mater. 1996;10(5):315-28.

Paper III

On the limitations of predicting the ohmic resistance in a macro-cell in mortar from bulk resistivity measurements

Cement & Concrete Research, Volume 76, 147-158 (2015)

Hornbostel, K.; Angst, U.M.; Elsener B.; Larsen C.K. and Geiker M.R

Cement and Concrete Research 76 (2015) 147–158

Contents lists available at ScienceDirect

Cement and Concrete Research

journal homepage: http://ees.elsevier.com/CEMCON/default.asp

On the limitations of predicting the ohmic resistance in a macro-cell in mortar from bulk resistivity measurements

K. Hornbostel [a,*], U.M. Angst [b,c], B. Elsener [b,d], C.K. Larsen [a,e], M.R. Geiker [a]

[a] Norwegian University of Science and Technology (NTNU), Department of Structural Engineering, Richard Birkelandsvei 1a, 7491 Trondheim, Norway
[b] ETH Zurich, Institute for Building Materials (IfB), Stefano-Franscini-Platz 3, 8093 Zurich, Switzerland
[c] Swiss Society for Corrosion Protection (SGK), Technoparkstrasse 1, 8005 Zurich, Switzerland
[d] University of Cagliari, 09100 Monserrato (CA), Italy
[e] Norwegian Public Roads Administration, Brynsengfaret 6A, 0667 Oslo, Norway

ARTICLE INFO

Article history:
Received 19 January 2015
Accepted 18 May 2015
Available online xxxx

Key words:
Corrosion (C)
Electrical properties

ABSTRACT

An experimental setup was designed to simulate the conditions for chloride-induced macro-cell corrosion, in which small anodes are located in a large network of cathodes. The overall aim of the present study was to assess whether measuring the bulk resistivity of reinforced concrete/mortar can give sufficient information about the resistance between anode and cathode inside a macro-cell. Measurements were executed in mortar specimens with high and low resistivities. Both the resistance in the simulated corrosion cells and the bulk resistivity of the mortar mixtures were determined. A comparison of the results showed no direct correlation. This indicates that the common practice of comparing bulk resistivity with corrosion rate may not be sufficient to characterize the corrosion process of chloride induced macro-cell corrosion.

1. Introduction

Chloride ions penetrating the concrete cover initiate pitting corrosion when they exceed a critical content at the steel reinforcement. Chloride ions in the pore solution limit the precipitation of corrosion products which under other conditions would lead to expansion around the corroded area and the consequent cracking and spalling of the concrete cover [1]. Visual inspection of the concrete surface may therefore not give sufficient information about the stage of chloride-induced corrosion. Electrochemical and other methods must be employed to allow the detection of corrosion activity. Potential mapping has proven to be a reliable method for locating areas of corrosion within a structure [2,3]. To determine the rate of corrosion, other methods, typically polarization curves, electrochemical impedance spectroscopy or galvanostatic tests can be used [4], but most of these methods are rather difficult to apply, especially on site, and they are subject to several sources of error [5–7]. The measurement of concrete resistivity has been recommended as an alternative method for determining the corrosion rate [8,9]. However, a recent literature review showed that the scatter of the published data is high and concluded that the relationship between the corrosion rate and concrete resistivity is not yet fully understood [10]. The variations and uncertainties seem more pronounced for chloride-induced corrosion than for corrosion due to carbonation.

Chloride-induced corrosion develops as a local corrosion attack with small areas of anodic activity (pits) in contrast to a large area of passive/cathodic behaviour [3]. Because the anodic and cathodic areas are spatially separated, the corrosion process developing is associated with the formation of a macro-cell [3,11]. The macro-cell current flowing through the concrete between anode and cathode will be concentrated at the pit opening. Thus, most of the ohmic resistance occurs in the vicinity of the anode. This is known from other fields as spreading resistance, $R_{spreading}$ [12,13]. For concrete, it was suggested to use the formula of Nanis and Kesselman [14], which is valid for current flowing to a small circulate disc in an infinite plane and electrolyte volume [13]:

$$R_{spreading} = \frac{4 \cdot \rho}{3 \cdot \pi^2 \cdot r} \quad (1)$$

in which r is the radius of the disc (anode), and ρ is the resistivity of the medium which is assumed to be a homogenous electrolyte.

Concrete is an inhomogeneous material due to its composite nature consisting of cement paste, aggregates and pores with different electrical properties. Aggregates are known to have a resistivity several times higher than that of cement paste [15]. The conductivity of the pore system and voids will depend on the degree of saturation. It can be expected that saturated pores act as conductors, whereas as empty pores are insulators. The surface area of pits developing during chloride induced corrosion will be in the range of μm^2 to a few cm^2 [14,16], which is smaller or comparable in size to aggregates and pores. Thus aggregates and pores (in the following also called inhomogeneities) in front of pits are expected

* Corresponding author. Tel.: +47 73594537.
E-mail address: Karla.Hornbostel@ntnu.no (K. Hornbostel).

http://dx.doi.org/10.1016/j.cemconres.2015.05.023
0008-8846/

to influence the resistance to current flow from and to the pit. It is therefore relevant to discuss to what extend the bulk concrete resistivity can give sufficient information about the resistance between a small anode and a cathode network (in the following termed cell-resistance).

The presented investigation had the overall aim to study and characterize the cell resistance. The simulated anodes used in the experiment were intended to represent one pit located in an otherwise passive cathode network. The cathodes are located both next to and at certain distances from the simulated anodes. The setup presents the general case of localized pitting corrosion induced by chlorides in an otherwise well aerated concrete. The cell resistance was compared with the bulk resistivity with a view to explaining the observed scatter between the bulk resistivity and the corrosion rate for localized corrosion [10]. It was outside the scope of the investigation to characterize the corrosion processes and its influence on the cell resistance as well as micro-cell corrosion on the simulated anodes. This topic will be addressed in another publication [17].

2. Experimental

An experimental setup was designed to simulate a macro-cell. Anodes of similar size were located in a network of cathodes in mortars of differing quality. The anodes were arranged at different angles to the casting direction. The network of cathodes allowed for a large variation in the area ratio between cathode and anode. All the steel elements in the setup were electrically disconnected from each other, which made it possible to measure resistance between them. The simulated anodes and the cathode network were at no time connected with each other as it was outside the scope of this study to investigate the corrosion process.

The resistance which was measured between the simulated anodes and a random combination of cathodes is termed *cell resistance* and abbreviated as R_{cell} (Table 1). A similar setup was placed in a solution which was assumed to be a homogenous electrolyte with a constant conductivity. The measurements in solution were used to identify variations resulting from the production of the setup and the measurement method.

Table 1
List of symbols and abbreviations.

	Explanation
R_{cell}	Cell resistance — measured between the simulated anode and the cathode network [Ω]
ρ_{bulk}	Bulk mortar resistivity [Ω·m]
k	Geometrical cell constant [m], different indexes are explained in the text
S_a	Instrumented tube in which the anode is mounted
S_c	Centre tube (segmented in the mortar specimens)
S_d	Instrumented tube in a distance of 10 cm from the tube in which the anode is mounted
PC	Mortar with ordinary Portland cement
FA	Mortar with ordinary Portland cement and fly ash
wo/Cl	Without chlorides
w/Cl	With chlorides
A,B,C	Denotation of the simulated anodes (A = upper side, B = lower side, C = side with regard to casting direction)
C/A	Area ratio cathode to anode
EIS	Electrical impedance spectroscopy
w/b	Water/binder ratio
μ	Mean value $\mu = \frac{1}{n}\sum x_i$
σ	Standard deviation $\sigma = \sqrt{\frac{\sum (x_i-\mu)^2}{n-1}}$
c_v	Coefficient of variation $c_v = \frac{\sigma}{\mu}$
n	Number of specimens
x	Value
r	Radius

2.1. Experimental setup

2.1.1. Experimental setup — in mortar mixtures

Four instrumented mortar specimens were cast, each containing two instrumented tubes, one segmented tube, and three smaller steel tubes with which the bulk resistivity was measured (Fig. 1). With the setup the area ratio as well as the distance between cathode and simulated anode could be varied.

Each instrumented tube contained five simulated anodes. The simulated anodes were produced from a smooth mild steel bar (S235JR Ø 6 mm) cut into pieces 5–6 mm long. Each piece was sandblasted, soldered with a wire and covered with heat-shrink tubing leaving just one cut surface exposed (area 28.3 mm^2). The simulated anodes were fixed in stainless steel tubes (AISI 316 Ø 12 mm, equipped with a wire, S_a/S_d) in each of which five holes were drilled in different positions (exposed area of the tube 5780 mm^2). All simulated anodes positioned on the upper side are labelled 'A', anodes located on the lower side are labelled 'B', and anodes mounted vertically with respect to the casting direction are labelled 'C'. Dimensions and labelling can be found in Figs. 1 and 2.

In each mortar specimen, a segmented stainless steel tube (AISI 316L Ø 10 mm, S_c) was positioned in the centre between the two instrumented tubes. The segmented tube consisted of four segments, respectively 10 mm (exposed area 314 mm^2), 20 mm (exposed area 628 mm^2), 40 mm (exposed area 1257 mm^2), and 80 mm (exposed area 2513 mm^2) in length. Each piece was threaded, so that the segments could be screwed together around a plastic threaded bar. The segments were electrically isolated from each other by plastic rings on the threaded bar between the segments. Wires were soldered on to each segment.

The three resistivity sensors were made from thin stainless steel tubes (AISI 304) with a diameter of 2.5 mm and an exposed length of 15 mm (exposed area 118 mm^2), the remainder of the tube being covered with heat-shrink tubing, and wires were soldered on to each tube. The resistivity sensors were placed at the same level as the instrumented tubes with a distance of 30 mm between each other.

In addition to the instrumented mortar specimen, 4–5 mortar cubes (100 × 100 × 100 mm) were also cast for each mixture.

2.1.2. Experimental setup — in solution

An experimental setup similar to the instrumented mortar specimens was built in a water tank to establish a reference setup in a homogeneous electrolyte.

For the reference setup, two instrumented tubes were used, with the same dimensions but somewhat different anode arrangement as used for the main setup (Figs. 1 and 2). The anodes were mounted so that in total four electrodes were on the upper and lower sides (A_{ref} and B_{ref}) and two anodes positioned on the side of each tube (C_{ref}). A non-segmented stainless steel bar (AISI 316L) with diameter 10 mm was placed between the instrumented tubes. The distance between all tubes was kept as in the instrumented mortar specimens. The dimensions of the water tank were slightly different from those of the mortar specimens (200(h) × 300(w) × 150(l) mm^3), the tubes were centred in the setup. It was possible to rotate the instrumented tubes during the experiment, so that anodes could change their position.

2.2. Materials and exposure

2.2.1. The mortar mixtures

Two different mortar mixtures were prepared to make it possible to study the cell resistance at high and low bulk resistivity levels. Chlorides were added to half of each mixture, providing in total four different test mixtures. The aim was to achieve resistivity values close to 50 and 10,000 Ωm, comparable to the low and high ends of the range reported for concretes on site [18]. For low resistivity, a mortar mixture with a water/binder ratio (w/b) of 0.55 prepared with an ordinary Portland

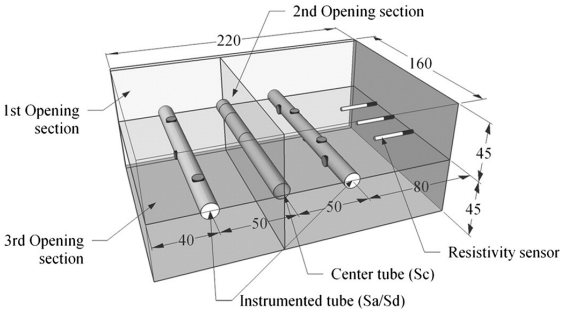

Fig. 1. Sketch of the instrumented mortar specimens, positions as cast and tested [mm]. 1st opening section — vertical 10 mm from surface, 2nd opening section — vertical at position of centre tube, 3rd opening section — horizontal at level of tubes (for abbreviations, cf. Table 1).

cement (CEM I 42.5 R) was used. High values of resistivity were achieved with a mixture with w/b of 0.4 and by replacing 30% of the Portland cement with fly ash (Table 2).

All the instrumented mortar specimens and cubes were wrapped in plastic foil after demoulding, 24 h after casting. The specimens were stored in different conditions during the testing period (Table 3). Monitoring of the specimens with different techniques was performed over 500 days. The cubes were treated in exactly the same way as the instrumented mortar specimens for the first 315 days. After 315 days, the exposure of the instrumented mortar specimens was varied (Table 3), while the cubes were kept sealed. For most of the testing period, all the specimens were kept at 20 °C, but between day 48 and day 82 after casting they were stored at 37 °C.

2.2.2. The solution experiment

For the experiment in solution, the tank was filled with tap water with a resistivity of 65 Ωm, which is comparable to a low-quality concrete. Air bubbles evolving on the steel surface were removed using a brush before each measurement.

2.3. Methods of investigation

2.3.1. Ohmic resistance

The resistivity sensors embedded in the instrumented mortar specimens were used to determine the bulk resistivity of the specimens. The sensors were calibrated against the mortar cubes 28 days after casting by determining the cell constant k_{sens}

$$k_{sens} = \frac{R_{cube.28}}{R_{sens.28}} \cdot \frac{A_{cube}}{l_{cube}}. \quad (2)$$

where $R_{cube.28}$ is the resistance measured on the cubes 28 days after casting, $R_{sens.28}$ is the resistance measured by the embedded sensors in the instrumented mortar specimens at the same time, and A_{cube} and l_{cube} are the surface area and length of the cubes respectively.

Accordingly, the resistivities of the cubes and the sensors were calculated as follows:

$$\rho_{cube} = R_{cube} \cdot \frac{A_{cube}}{l_{cube}} \quad (2.1)$$

$$\rho_{sens} = R_{sens} \cdot k_{sens}. \quad (2.2)$$

The cell resistance was measured between the simulated anodes and a given cathode configuration, the cathode configuration most used was the instrumented tube in which the anode was mounted (S_a) connected with the segmented tube (S_c = all segments connected). Where other configurations were used for measuring the cell resistance, this is explicitly noted in the results section.

In the first 96 days after casting, the measurements were carried out using a LCR meter (frequency 1 kHz, square pulse ca. 0.9 V) however it was found that the measured resistance did not in all cases correspond to the ohmic resistance. The measurement procedure was therefore changed after the first 96 days to electrical impedance spectroscopy (EIS) using a potentiostat of the type PRINCETON APPLIED RESEARCH PARSTAT 2273. The ohmic resistance was determined as the impedance with the minimum phase angle in the chosen frequency range. A frequency range between 500 kHz and 1 Hz was used. The AC amplitude was adjusted to the mortar specimen tested; in most cases 10 mV was chosen for the PC specimens and 40 mV for the FA specimens. For the experiments in solution, the amplitude chosen was 10 mV. It was found that the values measured with the LCR meter in the first 96 days of the testing period could be converted to the ohmic resistance determined with EIS by using a time independent factor.

2.3.2. Opening of instrumented mortar specimens

The four instrumented mortar specimens were opened 502 days after casting, and the condition of the anodes and the bulk mortar was examined. Each specimen was opened in three sections (Fig. 1). The 1st opening section was used to visually inspect the general condition of the mortar (segregation, distribution of air voids and other irregularities) in the vicinity of the embedded tubes. The 2nd opening section gave information about the condition of the mortar around the embedded tubes. The 3rd opening section was used to analyse the conditions around the simulated anodes in detail, including air voids, material state and corrosion products.

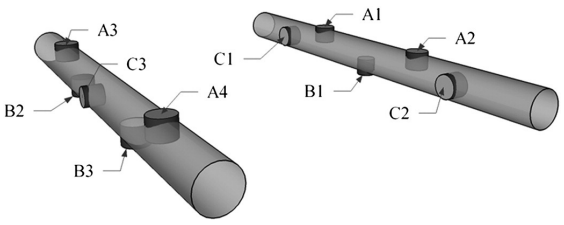

Fig. 2. Labelling of the simulated anodes on the instrumented tubes in the specimen as shown in Fig. 1: A — anodes on the top, B — anodes on the bottom, and C — anodes on the sides relative to the casting direction.

3. Results

3.1. Cell resistance in an homogenous electrolyte

Three different cathode configurations were studied in the reference setup with tap water as the homogeneous electrolyte. In addition, the position of the anodes was varied by rotating the instrumented tubes 180°, and the precision of the measurements was assessed by repeating measurements with one of the cathode configurations.

Fig. 3 illustrates the results of the test. Variations in the results for one cathode configuration (e.g. A1, A2, A3 and A4 are expected to be identical) are ascribed to the production of the setup; for example, it was not possible to mount the heat-shrink tubing in exactly the same way for all anodes. Differences between the results obtained with the same cathode configuration (grey background Fig. 3) are attributed to the measurement method (these are reparative measurements which should be identical).

The cell resistances measured in a homogenous electrolyte appear not to depend on the anode position (upper or lower side). Nor did the distance of the anode from the container walls have any influence ($A3_{ref}$, $A4_{ref}$, and $B1_{ref}$, $B2_{ref}$ are located close to the

Table 2
Mortar compositions.

Denotation		PC wo/Cl	PC w/Cl	FA wo/Cl	FA w/Cl
Cement (CEM I 42.5 R)[a]	kg/m³	503.2	503.2	378.4	378.4
Silica fume (920 D)	% cement			6	6
Fly ash	% cement			45.6	45.6
Water/binder[b]		0.55	0.55	0.4	0.4
Aggregate (0–4)	% aggregate	80	80	100	100
Aggregate (0–2)	% aggregate	20	20		
Superplasticizer (SP130)[c]	% cement			1.2	1.2
Paste	l/m³	438	438	438	438
Cl^-	% binder		3		3
	% cement		3		4.5

(%: weight percentage)
[a] Norcem
[b] Efficiency factor = 1
[c] Mapei

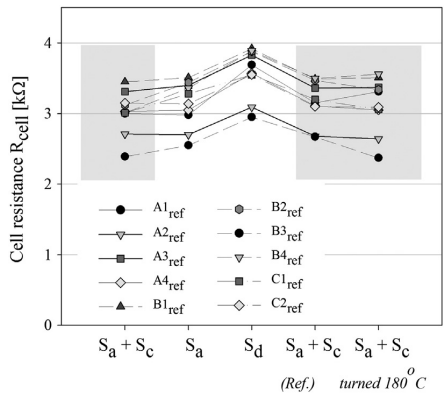

Fig. 3. Cell resistance measured in homogenous conditions and with various cathode configurations (x-axis). Anodes with the same orientation on the instrumented tube are illustrated with the same line type (cf. legend, A — top, B — bottom, C — side — beside the last measurement configuration where the instrumented tubes were turned 180 °C). Measurements on the same cathode configuration are indicated with grey background. The measurement configurations are shown in the chronology they were measured (from left to right). Further details are given in Table 1, Table 4 and Fig. 1.

walls). Consequently, the variation between the measured values in a given cathode configuration can be ascribed to the setup production (position of the heat-shrink tubing, etc.). Table 4 shows the mean value (μ), the standard deviation (σ), and the coefficient of variation (c_v) of the reference experiment for the cathode configuration Anode vs. $S_a + S_c$. Based on this, it was conclude that a coefficient of variation $c_v = 0.10$ can be attributed to the production of the setup.

No major difference was observed between the measurements that were repeated (grey background in Fig. 3). This indicates that the measurement method has a repetitious accuracy.

The difference in measured cell resistance between the cathode configuration Anode vs. S_d and the other configurations is ascribed to difference in the distance between the cathode and the anode (see Section 3.3.1).

3.2. Bulk resistivity of the mortar mixtures

The bulk resistivity of the cured and sealed mortar mixtures was determined repeatedly during the period of testing by measuring the mortar cubes and using the sensors in the instrumented mortar specimens. A good correlation was found between the two sets of data (Fig. 4). This indicates that the cell constant k_{sens} — Eq. (2) is independent of changes in material properties (at least for the conditions tested here) and that the cell constant concept is applicable for resistance measurements in a length scale above those of possible material inhomogeneities. Fig. 4 shows also that the two different methods used to measure bulk resistivity (external vs. embedded electrodes) give comparable results.

The bulk resistivity development over time is shown in Fig. 5. After 310 days, the mortar mixtures reached values between 56 and 2700 Ωm in sealed storage. This represents an adequate range of bulk resistivities. The increase in resistivity during the period of sealed storage (between ca. 100 to 300 days after casting) may be explained by prolonged cement hydration.

3.3. Cell resistance in the mortar specimens

3.3.1. Effect of cell geometry

3.3.1.1. Ratio between anode and cathode. Fig. 6 shows results from cell resistance measurements between selected simulated anodes and cathodes differing in size. The different cathode areas were achieved by varying the configuration of the centre tube, from measuring solely against the smallest segment (length = 10 mm, cathode to anode area (C/A) = 11) to measuring against all segments connected with each other (length 150 mm, C/A = 167). The figure shows that the influence of the area size vanishes for C/A > 40. The measured cell resistances do not change by more than 3% thereafter. Apart from the initial drop between C/A 10 to 20, which is most pronounced for the FA specimens, the impact of C/A on measured cell resistance was similar for all the specimens.

Table 3
Exposure conditions of the mortar specimens during the testing period.

Days after casting	Duration (days)	Temperature (°C)	Exposure	
			Instrumented mortar specimens	Cubes
0–1	1	20	Curing in the mould	Curing in the mould
1–48	48	20	Sealed	Sealed
48–82	32	37	Sealed	Sealed
82–315	233	20	Sealed	Sealed
315–384/387[a]	69/72	20	– Unwrapped, with epoxy coating on all vertical sides – exposed to tap water on lower side	Sealed
384/387–387/390[a]	3	20	– Unwrapped with epoxy coating on all vertical sides – stored in a pressure tank (72 h, 5 MPa)	Sealed
390–502	120	20	– Unwrapped, with epoxy coating on all vertical sides – Stored under laboratory conditions	Sealed
502			Opening	Sealed

[a] First value for specimens with mixed-in chloride, second value for specimens without mixed-in chlorides

Table 4
Statistical data for the experiment in solution and in mortar (for symbols, cf. Table 1).

Experiment in solution (Anode vs. $S_a + S_c$)[a]		Cell resistance μ [kΩ]			Cell resistance σ [kΩ]			Cell resistance c_v [kΩ]			ρ_{bulk} [Ωm]
		3.11			0.32			0.10			65
		A	B	C	A	B	C	A	B	C	
PC wo/Cl	Self-desiccated	4.31	14.0	10.5	0.81	6.08	6.80	0.19	0.44	0.65	70
PC w/Cl	Self-desiccated	2.66	4.03	3.45	0.18	0.59	0.47	0.07	0.15	0.13	56
FA wo/Cl	Self-desiccated	221	546	259	153	312	59	0.69	0.57	0.23	2701
FA w/Cl	Self-desiccated	53.7	116	59.0	3.24	95.3	13.2	0.06	0.82	0.22	1332
PC wo/Cl	Saturated	1.23	0.51	0.57	0.13	0.03	0.06	0.10	0.06	0.11	16
PC w/Cl	Saturated	0.81	0.48	0.46	0.11	0.00	0.04	0.14	0.01	0.10	14
FA wo/Cl	Saturated	7.41	4.25	4.58	3.53	1.10	1.18	0.48	0.26	0.26	279
FA w/Cl	Saturated	2.48	0.97	0.93	1.48	0.67	0.19	0.60	0.70	0.20	135

[a] All three measurement series with grey background cf. Fig. 3.

Most of the cell resistance values presented and discussed in this paper were measured for C/A = 370 (using cathode configuration $S_a + S_c$) and thus beyond the identified threshold of 40 (Fig. 6).

3.3.1.2. Distance between anode and cathode. The influence of the distance between anode and cathode was studied by measuring the resistance between the simulated anode and a) the instrumented tube in which it was mounted (S_a), b) the centre tube (S_c, minimum distance 50 mm) and c) the remote tube (S_d, minimum distance 100 mm). For all three configurations C/A was around 200.

Under the conditions tested here (maximum distance 100 mm and even moisture distribution in the mortar) the distance between anode and cathode was not influencing the cell resistance (Fig. 7).

3.3.2. Cell resistance

The cell resistance of each individual anode during the testing period can be seen in Fig. 8. It is clear that the cell resistance does not develop in the same way for all anodes and that there is a high variation between the results. Assuming that the data belongs to the same population, the mean value, standard deviation and coefficient of variation for the cell resistance measured in two different moisture conditions of the mortar mixtures (saturated and self-desiccated) are given in Table 4. For the statistics, the values for anode B2 in the FA specimen without chloride (FA wo/Cl) and anode B1 in FA specimen with chloride (FA w/Cl) were considered outliers (Fig. 8) and were therefore not taken into account.

3.4. Local conditions around the anodes

120 days after water pressure saturation, the instrumented mortar specimens were opened in three sections as described earlier (Fig. 1). None of the mortar mixtures showed signs of segregation. No major difference between the mortar specimens was found in the content and distribution of air voids from the visual appearance of the specimens. Major parts of the FA specimens were still wet when opened and large voids were filled with water. This was not the case when the PC specimens were opened: the mortar appeared dry and there were no signs of water in the voids. Due to the varying orientation of the anodes (Fig. 2), not all of their imprints in the mortar could be fully recovered. Information about two of the anodes was lost completely (B2 of FA wo/Cl and C1 of FA w/Cl), and from some of the anodes only half of the imprint was available for analysis. Examples of imprints are shown in Fig. 9 (the assessment criteria shown in the figure are explained in Section 4.2.1).

In general, it was found that the mortar on the upward-facing side of the tubes where the A-anodes were mounted, was dense and only a few small voids (<1 mm) were observed. The mortar on the downward-facing side (location of the B-anodes) was found to be porous with several voids of up to a few mm (Fig. 10). The latter situation indicates the presence of a bleeding zone. Bleeding zones are known to exhibit a different (coarser) microstructure than the bulk material and the material on the upper side of reinforcement [19–21]. The difference in the porosity of the mortar around the embedded tubes was more pronounced for the PC than for the FA specimens (Fig. 10). There was

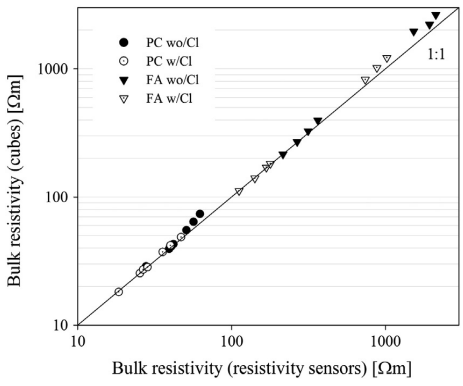

Fig. 4. Comparison between the bulk resistivity measured in the mortar cubes and the bulk resistivity measured using the sensors embedded in the instrumented mortar specimens (sealed conditions).

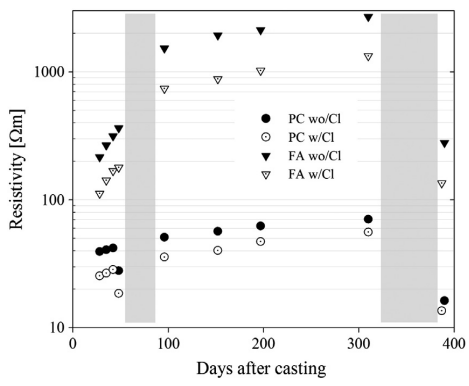

Fig. 5. Bulk mortar resistivity measured (using resistivity sensors) during the testing period until pressure saturation. Areas with a grey background are times of special exposure (cf. Table 3).

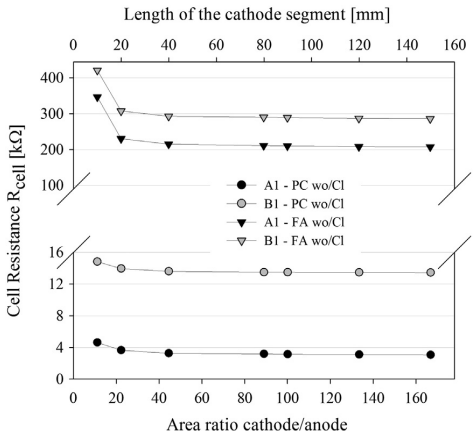

Fig. 6. Dependency of the cell resistance on the area ratio between cathode and anode, values measured 196 days after casting of the mortar specimens without mixed-in chlorides. The examples shown are for anodes mounted on the upper and lower sides with regard to the casting direction. Similar results were obtained for all other anodes.

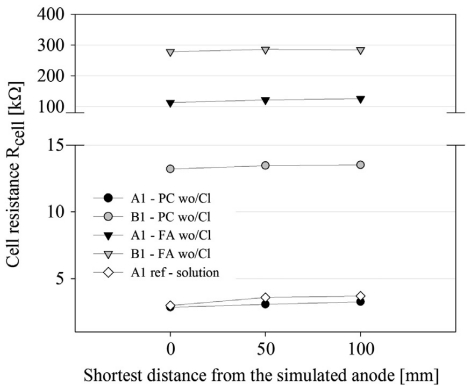

Fig. 7. Dependency of the cell resistance on the distance of the cathode from the anode, values measured 196 days after casting of the mortar specimens without mixed-in chlorides and in the solution experiment. The examples shown are for anodes mounted on the upper and lower sides with regard to the casting direction. Similar results were obtained for all other anodes.

also a difference between the PC and FA specimens in the imprints of the C-anodes. In the FA specimens, the imprints of the C-anodes were similar to the imprints of the A-anodes facing upwards, whereas in the PC specimens they were similar to the imprints of the B-anodes facing downwards, i.e. partly porous and with voids. This indicates more extensive bleeding in the PC specimens.

The corrosion products found in the specimens with mixed-in chlorides were brown-black-reddish in colour immediately after opening. The amount of corrosion products was rather low, which compares to expectations as only self-corrosion/ microcell corrosion was ongoing on the simulated anodes. The possible presence of aggregates in front of the anodes was not studied in detail, but large aggregates were sometimes found right in front anodes.

4. Discussion

4.1. Theoretical cell constant

The resistance in a macro cell is defined as the resistivity of the material divided by a geometrical constant, often referred to as the *cell constant*

$$R = \frac{\rho}{k_{geom}}. \tag{3}$$

Depending on the setup, this constant can be either estimated (cf. Eq. (1)) or determined by calibration against known values (cf. Eq. (2)). Eq. (1) was derived for estimating the resistance between a small circular disc and an infinitely large electrode in the same plane [13]. In the setup used here, the cathode can be considered as infinitely large for C/A > 40 (Fig. 6). The anode and cathode in the setup were never located in the same plane, but the results presented in Fig. 7 indicate that the distance between anode and cathode has no significant influence on cell resistance. Provided that the cathode configurations approximate relatively well the requirements of Eq. (1), a theoretical cell constant for the setup can be derived as follows:

$$k_{theo} = \frac{3 \cdot \pi^2 \cdot 0.006m}{4} = 0.022\ m. \tag{4}$$

This value is confirmed by the experiment executed in homogenous conditions (values from Table 4):

$$k_{homogen} = \frac{\rho}{R} = \frac{65\ \Omega m}{3110\ \Omega} = 0.021\ m \pm 0.002\ . \tag{5}$$

4.2. Material properties affecting the cell resistance

The statistical evaluation of the data (Table 4) shows that a much higher coefficient of variation for cell resistance was obtained in the mortar specimens than in the homogenous electrolyte. Neither differences in setup production nor inaccuracies of the measurement method can explain the increase in scatter observed when using mortar instead of solution.

Concrete/mortar is a composite material of non-conductive inclusions (aggregates and empty voids) and conductive phases (cement paste and voids varying in porosity and moisture content) and is thus not homogenous. However, depending on the length scale, the material may appear quasi-homogenous. This can be confirmed by the applicability of the cell constant concept for bulk resistivity measurements where equally sized electrodes cover a mortar volume several times larger than the aggregate and void sizes (Fig. 4). This is not the case for cell resistance. Fig. 11 shows the actual cell constants for selected anodes calculated in accordance with Eq. (3) by dividing the bulk resistivity (determined with the embedded sensors) by the measured cell resistance. The actual cell constants for the anodes in the mortar specimens differ from the theoretical value derived from Eq. (1) and given in Eq. (4). It can be seen that actual cell constants are anode-dependent and that they vary during the period of testing and are especially affected by changes in the moisture content of the specimens. Note also the differences concerning the standard deviation and coefficient of variance between the different anode positions (Table 4).

The dimensions of the anodes used were comparable to the maximum aggregate and void sizes. It is therefore to be expected that aggregates and voids located in close proximity to the anodes will have a strong influence on the current flow between anode and cathode and thus on the cell resistance. Fig. 12 a) shows the equipotential and current lines for a circular anode disc located in a cathodic plane and surrounded by homogenous material. Interfacial inhomogeneities near the anode will disturb the potential field and thus have a direct influence on the cell resistance (Fig. 12 b)–d)). In contrast, the resistivity of the bulk material will have

less influence. This can explain why the actual cell constants differ from the theoretical cell constant and varies between anodes.

4.2.1. Interfacial inhomogeneities

The actual cell constants for the individual anodes were compared to identify the impact of variations in material composition in front of the anodes (Figs. 13 and 14).

4.2.1.1. PC specimens. In the PC specimens, a pronounced difference can be observed between the anodes located on the upper side of the tube and the others. The difference is most pronounced in the saturated conditions (Fig. 14 a)). The cell constants of the anodes facing upwards (A-anodes) were lower than the theoretical value, indicating a higher resistivity in the material in front of the anode than the bulk resistivity. This may be explained by an accumulation of aggregates in front of these anodes. In contrast, the cell constants for the other anodes (B- and C-anodes) were higher than the theoretical value (Fig. 14), which indicates a lower resistivity in the material adjacent to the anode than in the bulk material. In self-desiccated conditions (Fig. 13), the situation (as a trend) is reversed, the cell constants of the A-anodes being higher than those of the B-anodes. These observations are what should be expected if bleeding and accumulation of voids have taken place. Note that specific anodes have very high cell resistance (low cell constant) in self-desiccated condition and low cell resistance (high cell constant) in saturated conditions (see e.g. PC wo/Cl anode B1, B2, C3 in Figs. 13 and 14). This indicates that saturated pores act as conductors, whereas as empty pores are insulators (cf. Fig. 12).

4.2.1.2. FA specimens. In the FA specimens, the variation in actual cell constants between the anodes was greater, but there was no pronounced difference between anodes in different locations, which indicates less bleeding. In self-desiccated conditions (Fig. 13), the actual cell constants of the anodes in the FA specimen with mixed-in chlorides were quite similar or higher than the theoretical value, whereas the cell constants from anodes in the specimen without chlorides were lower than the theoretical value. For the saturated conditions (Fig. 14), all of the anodes in the FA specimens had actual cell constants higher than the theoretical values, suggesting that the resistivity of the local material was lower than the bulk resistivity.

The actual cell constants in the saturated conditions are markedly higher for the anodes in the FA specimens than for the anodes in the PC specimens (Fig. 14). The same cannot be observed for the

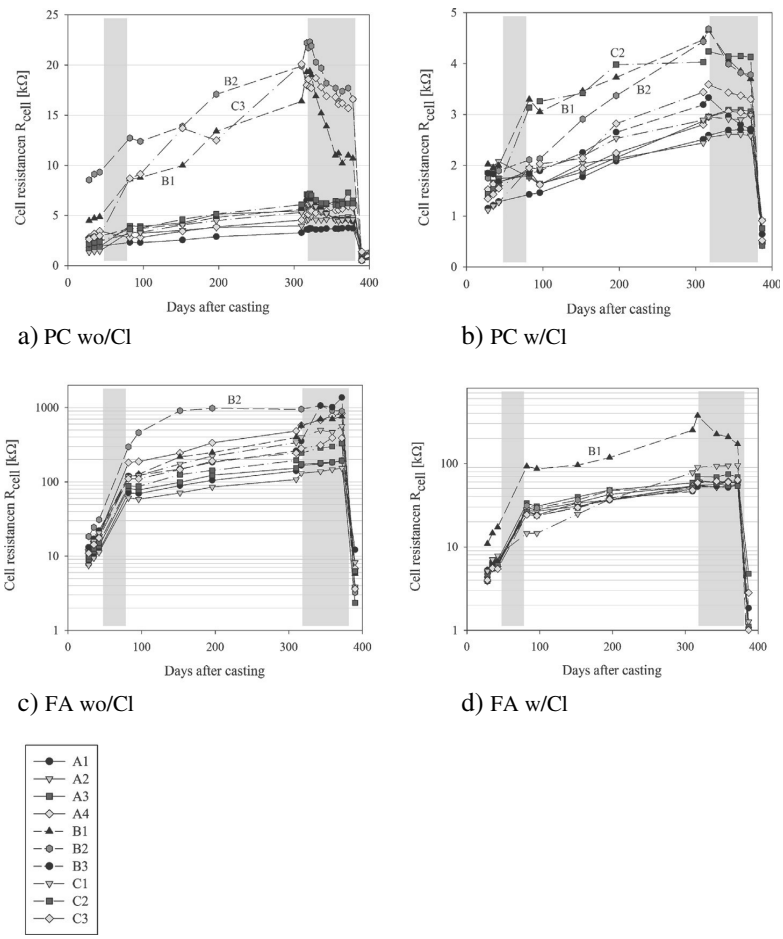

Fig. 8. Development of the cell resistance over the testing period in the mortar specimens. Anodes with the same orientation on the instrumented tube are illustrated with the same line type. Areas with a grey background are times of special exposure (cf. Table 3). Note different y-axes.

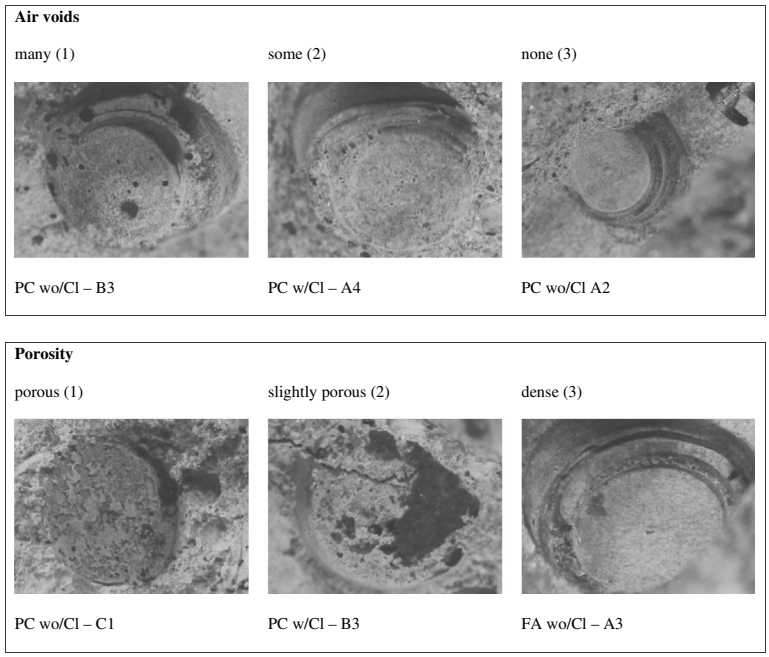

Fig. 9. Assessment of the imprints of the simulated anodes in the mortar with respect to voids and porosity. The number in brackets indicates their influence on the cell resistance in the saturated state: (1) = very low, (2) = low cell resistance, compared to reference (3).

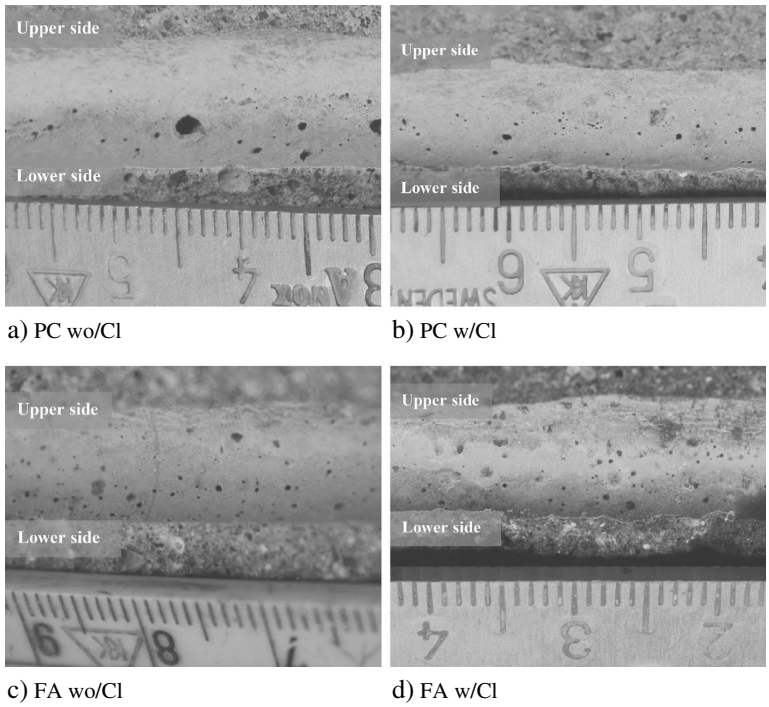

Fig. 10. Vertical cross section of the mortar specimens along the segmented tube (2nd Opening section, Fig. 1) [cm].

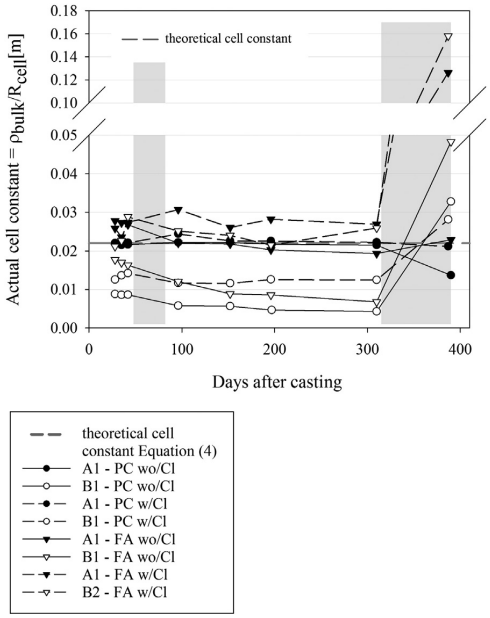

Fig. 11. Actual cell constants for selected anodes over the testing period. The examples shown are for anodes mounted on the upper and lower sides with regard to the casting direction. Similar results were obtained for other anodes. Areas with a grey background are times of special exposure (cf. Table 3). The grey dashed line at 0.022 indicates the theoretical cell constant derived from Eq. (1) and given in Eq. (4).

self-desiccated condition (Fig. 13) or during the rest of the testing period (cf. Fig. 11). The actual cell constants for the FA and PC specimens determined during these periods are in good agreement.

4.2.1.3. PC and FA specimens. No systematic difference was observed between the specimens containing chlorides and the specimens without. This indicates that the presence of corrosion products adjacent to the anode (in the amount observed) has no significant effect on the cell resistance, at least not in the conditions tested here.

The four instrumented mortar specimens were opened 502 days after casting and the condition of the anodes and the surrounding mortar was examined (Fig. 1, 3rd opening section), see Section 3.4. To quantify the condition, assessment criteria were established for the categories 'voids' and 'porosity' (Fig. 9). Each category was assigned a value from one to three relating to its presumed influence on the cell resistance in the pressure-saturated state. In this state, the voids/pores were filled with water and therefore assumed to decrease the cell resistance. The values determined for the two categories were added and resulted in an assessment value which was compared with the cell resistance measured in pressure-saturated conditions, 387/390 days after casting (Fig. 15). A general trend between the assessment value and the cell resistance can be observed. As expected, a void-free dense material increases the cell resistance. It should be noted that the classification carried out here is relatively coarse because it is a simple 2D visual assessment.

The results presented in Figs. 11–15 indicate differences in the material composition adjacent to the anodes. In the PC specimens, it was observed that the interfacial zone between the anodes and the bulk material has different electrical properties on the upper and the lower sides of the tubes with regard to the casting direction. The condition adjacent to the anodes located on the side seems similar to that of the anodes on the lower side (Fig. 13). This is in agreement with observations of porous zones in imprints of anodes, see Section 3.4. In the FA specimens, no pronounced differences in measured cell resistance pertaining to the orientation of the anodes were observed. The visual assessment showed a correlation between local defects and the cell resistance also for the FA specimens, indicating a more even distribution of inhomogeneities around the tubes. No explanation could be found for the large difference in the actual cell constants between FA and PC specimens for the saturated state.

4.2.2. Exposure conditions

The variation of the cell constant for a particular anode during the testing period (Fig. 11) may be explained by the influence of exposure which can influence the bulk resistivity differently than local inhomogeneities (especially pores/voids). A saturated void, containing a highly conductive pore solution at the anode will permit the flow of current and thus lead to a low voltage drop across it. However, if the void is empty, it will act as an insulator against the flow of current from the anode into the mortar (see for example PC wo/Cl anodes B1, B2 and C3). In this case, the potential drop near the anode will be high (Fig. 12 b)). Of course, the bulk resistivity will also be influenced by moisture changes in the material. However, since a much larger volume is covered, the current flow will not be restricted to the same extent. This is reflected very well by the development of the actual cell constants for the anodes mounted on the lower side of the tube (B-anodes, especially in the PC specimens) where several voids were found (Fig. 10). The actual cell constants decrease during the testing period, being lower than the theoretical k-facture (higher local resistivity) until pressure saturation of the specimens. Thereafter, the trend reverses, indicating a much lower resistance against current flow near the anodes than in the bulk material. On the upper side this effect cannot be seen, which correlates well with the dense material observed in the imprints.

4.3. Perspectives

4.3.1. Influence of anode size and position

The size and the location of the simulated anodes had to be decided before casting the mortar specimens and thus also before corrosion initiation. It is currently not known whether corrosion would spontaneously initiate on all of the presently defined locations. Moreover, pits will increase in area and depth over the corrosion process, which would continuously change the geometrical conditions for the cell. Testing just one constant anode size restricts the amount of information that can be obtained from the measurements. From Eq. (1), it is clear that the cell resistance will increase exponentially with decreasing anode radius.

The ratio between the maximum aggregate/void size and the anode size is approximately 1:1 in the setup and mortar mixtures tested here. In practice, larger aggregates are used and, as a consequence, the anodes will be smaller than the biggest aggregates in most cases. It is to be expected that the larger the aggregates (and the air voids) are, compared to the pits, the greater will be their influence on the cell resistance. This means that in practice it can be expected that the variation in cell resistance between anodes and the degree to which it differs from the bulk resistivity will be higher than has been reported in this investigation.

When it comes to the geometrical arrangement between anode and cathode, it was found that it was not influencing the cell resistance as long as the C/A ratio was higher than 40 (which it will be in most practice related cases). This means that even when the anode is located at a certain distance from the cathode (e.g. due to the lack of oxygen in the near vicinity of the anode) the cell resistance is dominated by local inhomogeneities. In the experiment this was tested for distances up to approximately 100 mm and for limited moisture variation.

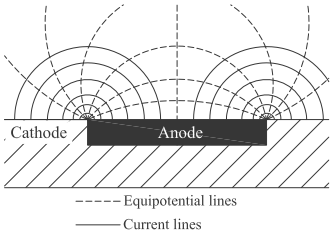

a) Current and equipotential lines in homogenous conditions.

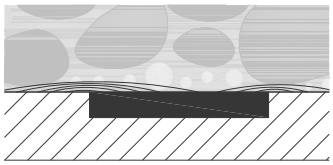

b) Current lines in inhomogeneous conditions (mortar) with nonconductive aggregates (dark grey) and conductive water-filled voids (light grey).

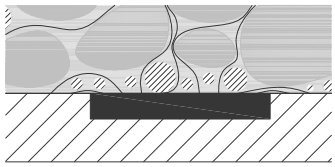

c) Current lines in inhomogeneous conditions (mortar) with nonconductive aggregates (dark grey) and nonconductive empty voids (shaded areas).

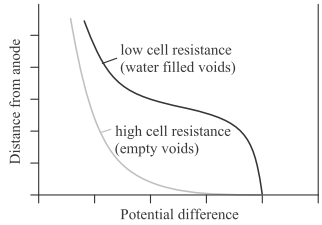

d) Sketch of the potential distribution dependent on the moisture state of voids near the anode

Fig. 12. Schematic view of the electrical field and current flow around a small circular disc in a large cathode plane affected by material conditions around the disc. Also illustrated is the change in potential created by the resistance of local inhomogeneities.

4.3.2. Impact of cell resistance on the relationship corrosion rate and concrete resistivity

The fact that bulk resistivity is not directly correlated to the cell resistance may explain the scatter in the relationship between bulk resistivity and the corrosion rate [10]. To assess the difference in terms of absolute numbers, the theoretical cell constant (Eq. (4)) was compared to the actual cell constants of the anodes (the second y-axis in Figs. 13 and 14). In this work, the maximum deviation was ten, while on average a deviation of around two can be expected. The variation reported in the literature review exceeds two but seldom ten. It must be remembered that the growth of the anode was not considered in this investigation, so the variation can differ depending on anode size, and can be expected to be higher for smaller anodes. Assuming that the ohmic resistance between anode and cathode has a major impact on the corrosion process for chloride-induced corrosion, the results of this investigation indicate that measuring the bulk resistivity may not be sufficient to characterize the corrosion rate for this corrosion morphology (macro-cell). Nevertheless, it could be claimed that the growth of the pit is linked not only to the ohmic resistance between anode and cathode, but also to bulk material conditions, such as the diffusion of chloride ions and the availability of oxygen and water. This means that it may be an oversimplification to ascribe the scatter in the relationship obtained between corrosion rate and concrete resistivity solely to the difference between bulk resistivity and cell resistance.

5. Summary and conclusions

An experimental setup was designed to simulate conditions for chloride-induced pitting corrosion (macro-cell corrosion), in which small anodes are located in a large network of cathodes. The resistance between the simulated anodes and the cathode network ('cell resistance') was measured for different anode locations and compared with the bulk resistivity. Measurements were carried out in mortar specimens differing in bulk resistivity. A reference experiment was carried out in solution to assess the influence of the setup and the measurement method. The following conclusions were drawn:

- The cell resistance between small anodes and a large cathode network was independent of the cathode size when the cathode to anode area ratio exceeded 40. The distance between anode and cathode did not affect the cell resistance.
- The cell resistance measured between the simulated anodes and the cathode network showed considerable scatter. For the mortar

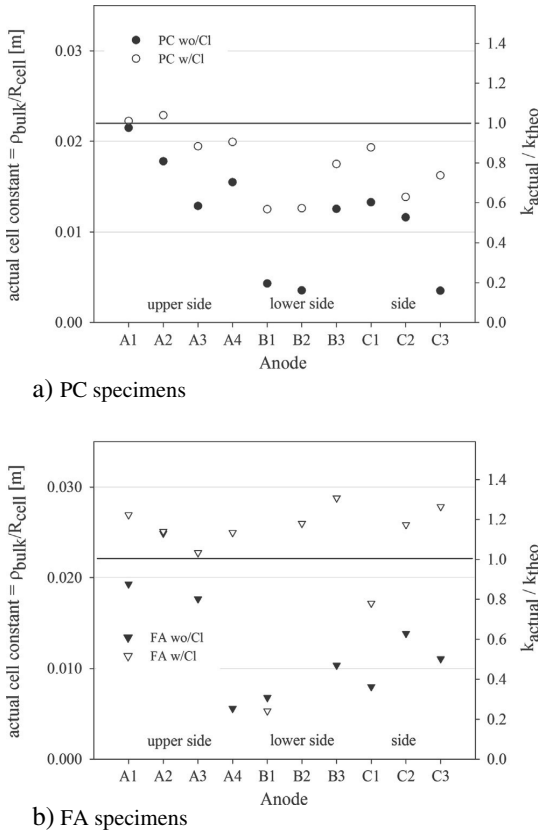

Fig. 13. Actual cell constants for self-desiccated conditions (310 days after casting) in the mortar specimens (theoretical cell constant, cf. Eq. (4), indicated as grey line in the figure).

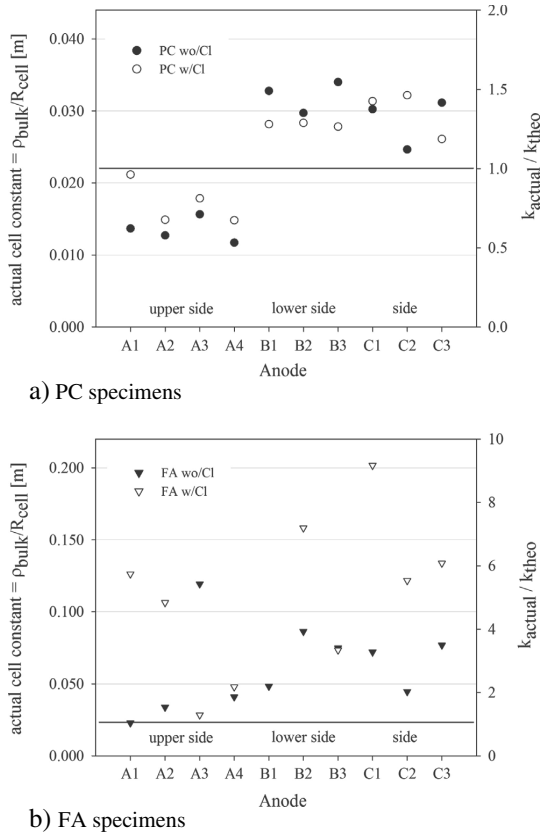

Fig. 14. Actual cell constants for pressure-saturated conditions (390 days after casting) in the mortar specimens (theoretical cell constant, cf. Eq. (4), indicated as grey line in the figure) — Note different y-scales.

specimens with a low bulk resistivity, the location of the anode in relation to the casting direction influenced the cell resistance. This was not the case for the high-quality mortar specimens. For all the mortar specimens, it was shown that local inhomogeneities affected the cell resistance.

- The actual cell constants (ratio between bulk resistivity and cell resistance) for the simulated anodes were not stable over time and varied between anodes. This suggests that the cell resistance cannot be directly derived from the bulk resistivity.
- The variations observed for the cell constant over time and between samples may explain the scatter observed in the literature for the relationship between bulk resistivity and the corrosion rate for chloride-induced corrosion (macro-cell corrosion). This suggests that the common practice of comparing bulk resistivity with corrosion rate may be inadequate for this corrosion morphology.

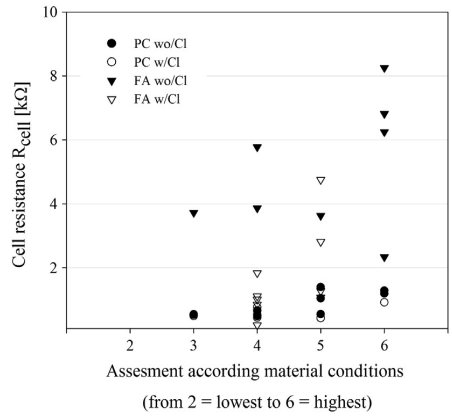

Fig. 15. Comparison between the assessment of the imprints (cf. criteria in Fig. 9, values of both categories added) and the cell resistance (measured 387/390 days after casting).

Acknowledgements

The paper is based on work carried out at the NTNU Trondheim and COIN — the Concrete Innovation Centre (www.coinweb.no) – which is a centre for research-based innovation, initiated by the Research Council of Norway (RCN) in 2006 – and supported by the Norwegian Public Roads Administration (www.vegvesen.no). Special thanks to Kristine Andersen and Kristian Sætre for their help with the experimental work.

References

[1] U. Angst, B. Elsener, A. Jamali, B. Adey, Concrete cover cracking owing to reinforcement corrosion — theoretical considerations and practical experience, Mater. Corros. 63 (2012) 1069–1077.

[2] B. Elsener, C. Andrade, J. Gulikers, R.B. Polder, M. Raupach, Half-cell potential measurements — potential mapping on reinforced concrete structures, Mater. Struct. 36 (2003) 461–471.

[3] L. Bertolini, B. Elsener, P. Pedeferri, R.B. Polder, Corrosion of Steel in Concrete: Prevention, Diagosis, Repair, Wiley-VCH Verlag GmbH & Co, 2004.

[4] C. Andrade, C. Alonso, Corrosion rate monitoring in the laboratory and on-site, Constr. Build. Mater. 10 (1996) 315–328.

[5] U. Angst, M. Büchler, On the applicability of the Stern-Geary relationship to determine instantaneous corrosion rates in macro-cell corrosion, Mater. Corros. (2014) http://dx.doi.org/10.1002/maco.201407997.

[6] P.V. Nygaard, M.R. Geiker, Measuring the corrosion rate of steel in concrete — effect of measurement technique, polarisation time and current, Mater. Corros. 63 (2012) 200–214.

[7] P.V. Nygaard, M.R. Geiker, B. Elsener, Corrosion rate of steel in concrete: evaluation of confinement techniques for on-site corrosion rate measurements, Mater. Struct. 42 (2009) 1059–1076.

[8] J. Broomfield, S. Millard, Measuring concrete resistivity to assess corrosion rates, Concrete, Current Practice Sheet No.1282002. 37–39.

[9] C. Andrade, R. d'Andrea, Electrical resistivity as microstructural parameter for the calculation of reinforcement service life, in: W. Sun, K.V. Breugel, C. Miao, G. Ye, H. Chen (Eds.), First International Conference on Microstructure Related Durability of Cementitious Composites, RILEM Publications, Nanjing, China, 2008.

[10] K. Hornbostel, C.K. Larsen, M.R. Geiker, Relationship between concrete resistivity and corrosion rate — a literature review, Cem. Concr. Compos. 39 (2013) 60–72.

[11] M. Raupach, Zur chloridinduzierten Makroelementkorrosion von Stahl in Beton (in German), Beuth Verlag GmbH, Berlin, 1992.

[12] M.W. Denhoff, An accurate calculation of spreading resistance, J. Phys. D. Appl. Phys. 39 (2006) 1761–1765.

[13] L. Nanis, W. Kesselman, Engineering applications of current and potential distributions in disk electrode systems, J. Electrochem. Soc. 118 (1971) 454.

[14] U. Angst, B. Elsener, C.K. Larsen, Ø. Vennesland, Chloride induced reinforcement corrosion: rate limiting step of early pitting corrosion, Electrochim. Acta 56 (2011) 5877–5889.

[15] M. Nagi, D. Whiting, Electrical Resisitivity of Concrete — A Literatur Review, Portland Cement Association PCA R&D Serial No. 2457, Illinois, 2003.

[16] C.A. Apostolopoulos, S. Demis, V.G. Papadakis, Chloride-induced corrosion of steel reinforcement — mechanical performance and pit depth analysis, Constr. Build. Mater. 38 (2013) 139–146.

[17] K. Hornbostel, Macro-cell corrosion of steel in concrete — role of concrete resistivity (in preparation)(Doctoral thesis) Department of Structural Engineering, Norwegian University of Science and Technology (NTNU), Trondheim, Norway, 2015. (expected).

[18] R.B. Polder, Test methods for on site measurement of resistivity of concrete — a RILEM TC-154 technical recommendation, Constr. Build. Mater. 15 (2001) 125–131.

[19] M.N. Al Khalaf, C.L. Page, Steel/mortar interfaces: microstructural features and mode of failure, Cem. Concr. Res. 9 (1979) 197–207.

[20] U. Angst, Chloride induced reinforcement corrosion in concrete — concept of critical chloride content — methods and mechanisms(Doctoral thesis) Department of Structural Engineering, Norwegian University of Science and Technology, Trondheim, 2011.

[21] J. Bensted, P. Barnes, Structure and Performance of Cements, 2 ed. Taylor & Francis, Oxon, 2009.

Paper IV

Influence of mortar resistivity on the rate-limiting step of chloride-induced macro-cell corrosion of reinforcing steel

Submitted to Corrosion Science (2015)

Hornbostel, K.; Angst, U.M.; Elsener B.; Larsen C.K. and Geiker M.R.

Is not included due to copyright

Paper V

Limitations of the use of concrete resistivity as an indicator for the rate of chloride-induced macro-cell corrosion

Submitted to Structural Concrete (2015)

Hornbostel, K.; Elsener, B.; Larsen, C. K.; Angst, U. M. and Geiker, M. R.

Is not included due to copyright

NTNU – Trondheim
Norwegian University of
Science and Technology

Volume analyses of corroded cylindrical steel pieces using GOM inspect.

Trine-Lise Lorentsen, M.Sc.

Friday 8th May, 2015

Contents

1 Introduction

The following report was requested by Karla Hornbostel, PhD student at the Norwegian University of Science and Technology. It contains volume analyses of corroded cylindrical steel pieces comprising of the volumes after the extensive testing phase and estimations of the original volumes.

3D scanned models of the steel pieces were received as STL files describing their surface. A total of 17 models have been analysed where the steel pieces are labeled into two groups, seven are labeled FA and ten PC. In Figure 1, a typical steel piece and the corresponding STL model is shown.

Four of the samples analysed are special cases where the steel pieces are still embedded in the installation they were attached to during the testing phase. Because of this, the only part available for estimations are the top parts, see Figure 2. The special cases are part of the PC series, and the rest of the series can be found in Figure 3. In Figure 4 the FA series is presented. Steel pieces marked with a star (*) were connected in the macro cell arrangement, see Hornbostel (to be submitted in 2015).

Some of the samples contained unwanted masses such as mortar rests or remains of the soldered wire connection. These masses were repaired or removed in the model meshes to get accurate values for the volumes. Repairs, reconstructions and estimations were performed using GOM inspect, a 3D inspection and mesh processing software.

1.1 Scope of analysis

The scope of this analysis is to determine the actual volume for each steel piece, and to give an estimation of the original volume before the onset of corrosion. From the difference in these volumes the loss in volume due to corrosion can be calculated. Thus, the estimations done in this report includes the following three items:

- Exact volume of the STL model (after testing phase and removal of excessive masses).

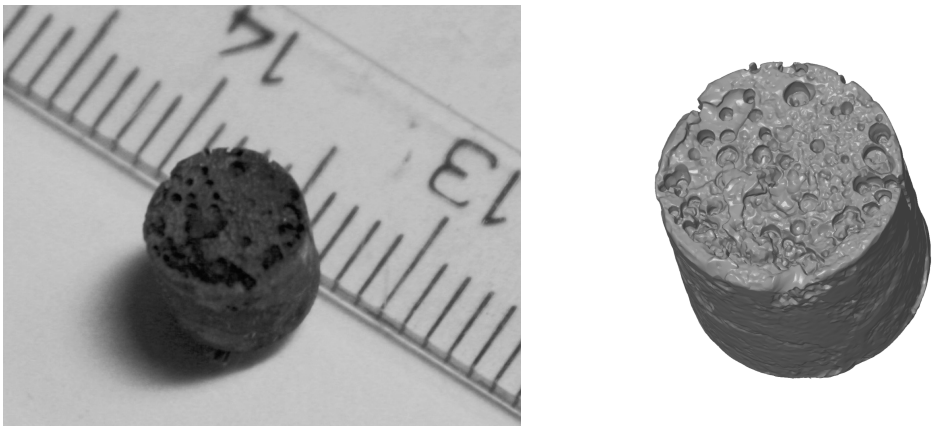

Figure 1: *The left picture shows sample PC5D2 steel piece 3 with a regular ruler, i.e. [cm]. The corresponding STL model is shown in the right image.*

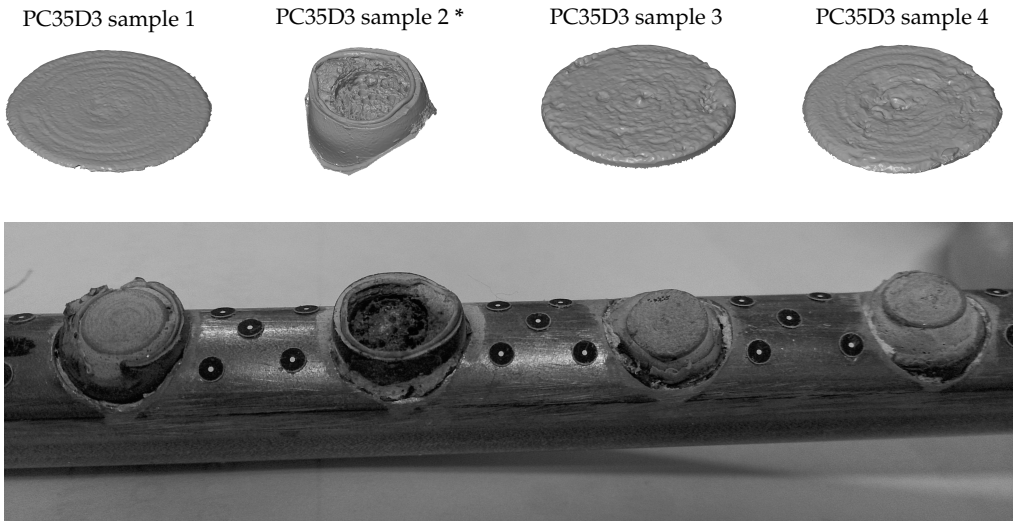

Figure 2: *Special cases from the* PC *series. Here only the top part of the steel piece samples are available for calculations.*

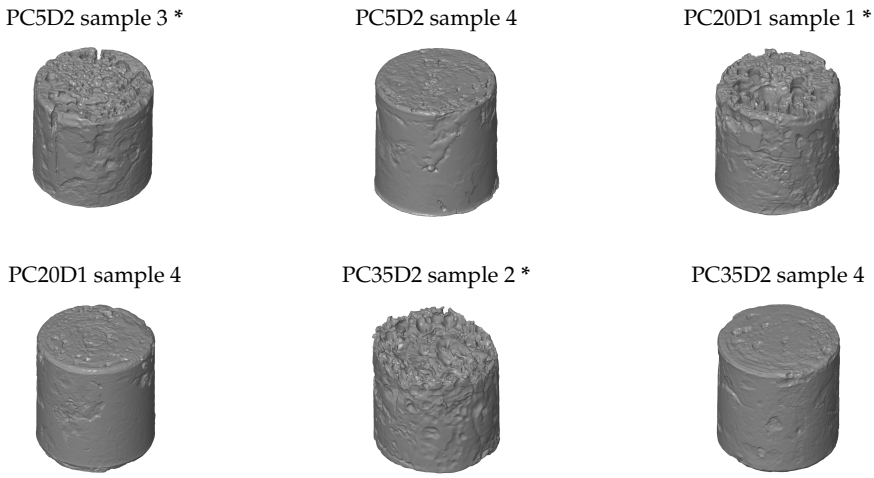

Figure 3: *Full sized samples labeled* PC*. Samples labeled with a star (*) were connected in the macro cell arrangement.*

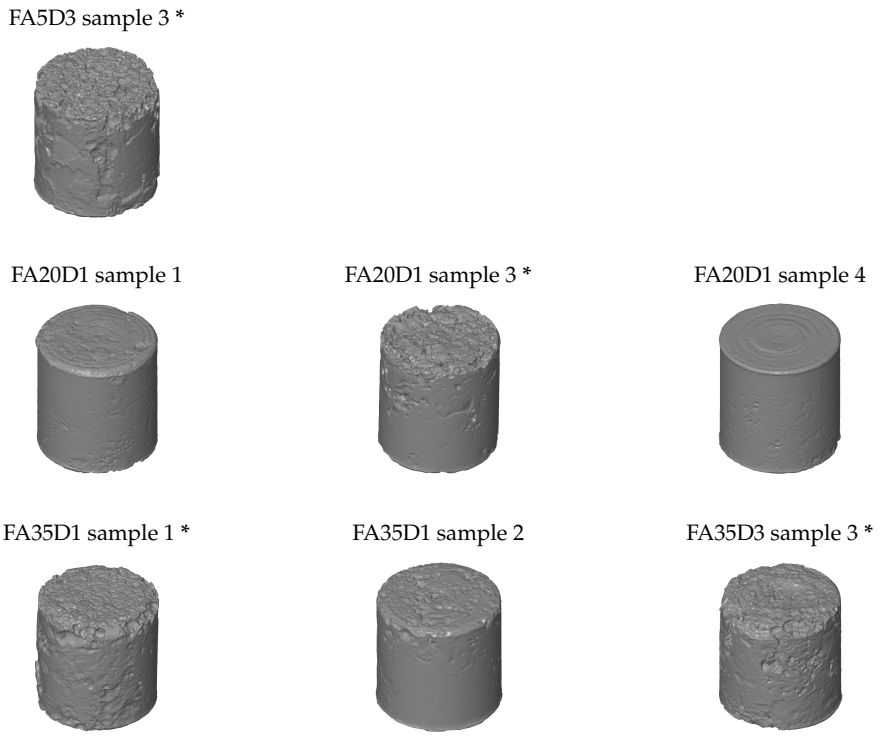

Figure 4: *All steel pieces labeled* FA. *Again the samples connected to the macro cell arrangement have been marked with a star (*).*

- Diameter and height of the cylinder before corrosion.
- Original volume - i.e. calculated volume from estimated diameter and height.

2 Method

GOM inspect 3D inspection and mesh processing software offers a variety of built in functions. In this section the methods used and examples of the preparations made to the steel pieces are presented.

2.1 Preparations

In order to estimate the volume of the STL bodies, some of the steel pieces needed adjustments. Among GOM inspects built in tools, mesh repair is an option. The software will take a user marked area and adapt it to resemble the surrounding surface. Another option is deleting the marked areas of the mesh.

Many steel pieces had smaller masses attached to the STL body. These were left by the abrasion-resistant mortar around the lateral surfaces, and were handled using mesh repair. The masses did

not have a large impact on the volume of the STL model, but were removed for accuracy in the calculations. Figure 5 shows an example of one such mass that was removed from FA35D1 sample 1.

In some cases, larger areas of the mesh needed to be entirely removed. A few of the steel piece cylinders had a large mass attached to the STL model due to the soldered wire connection, and in Figure 6 FA20D1 sample 4 is shown with this kind of problem. The excessive mass that is attached to the model has been marked in red, see Figure 6a, and is then removed all together as is shown in Figure 6b. After deleting this part of the mesh, the model is left with a hole in the surface. This was sealed of using a fitted plane to the bottom of the cylinder.

2.2 Volume

The volume of the STL models are provided by the software. In this section the approach for estimating the original volume of the cylindrical steel pieces is presented, i.e. estimation of the volume before the onset of corrosion.

GOM inspect allows automatic selection of the mesh based on geometrical bodies such as cylinders. The mesh points are then used to create a best fitted cylinder using built in algorithms. For the analyses done in this report the steel pieces are fitted with cylinders using the Gaussian best-fit algorithm, which is based on minimizing the sum of squares in the deviations. In Figure 7 the fitting of a Gaussian cylinder is shown for PC5D2 sample 4. The cylindrical mesh selection is shown in Figure 7a and the corresponding fitted cylinder in Figure 7b.

2.3 Special cases

The four samples of PC35D3, see Figure 2, are all special cases where only the top of the steel pieces are available for calculations. Preparations for these cases where slightly different than for the other 13, and fitting elements were done in a different manner. For sample 1, 3 and 4 the same procedures were used, but for sample 2 several steps needed to be taken to gain estimations for the variables.

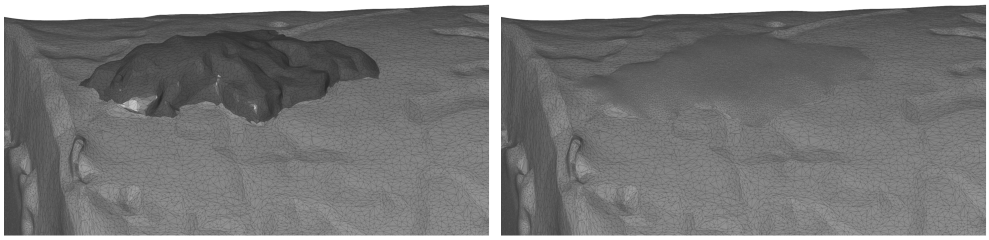

(a) (b)

Figure 5: *Excessive mass on the surface of FA35D1 sample 1. Figure a) shows the markup of mortar rest, and in b) the area has been repaired using GOM inspect.*

(a) (b)

Figure 6: *Large excessive mass located at the bottom of FA20D1 sample 4. Figure a) shows the excessive mass marked, and in b) the mass is removed and the hole sealed.*

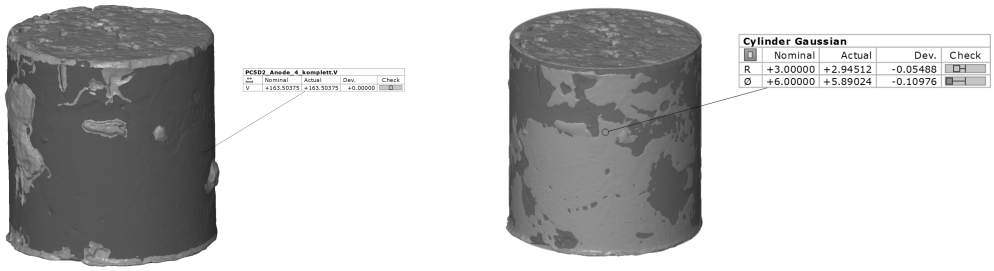

(a) (b)

Figure 7: *Case PC5D2 sample 4, where a) shows the cylindrical mesh point selection and b) the corresponding Gaussian best-fit cylinder. For this particular case a total of 162826 points were used in the fitting.*

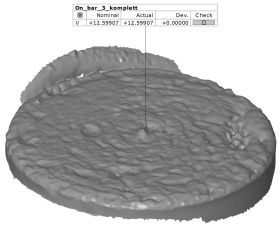

(a) *Starting point.*

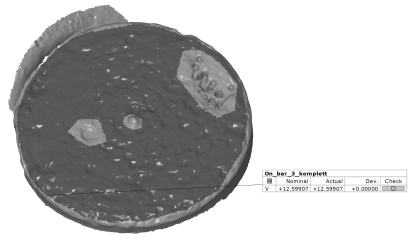

(b) *Mesh markup used to fit plane.*

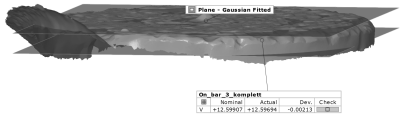

(c) *The fitted- and parallel plane.*

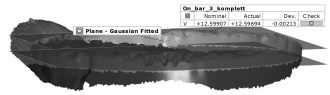

(d) *Markup for deleting mesh.*

Figure 8: *Fitting a plane to the top of the steel piece and creating a parallel plane. Here for FA35D3 sample 3. Parallel planes are for this case* $0.35\ mm$ *apart.*

Samples 1, 3 and 4:

The STL models for these cases were initially open underneath, and thus needed to be sealed of. First a plane was fitted to the top of the sample. This allowed the possibility of generating a parallel plane beneath it, resulting in an exact height to a preconceived cylinder. The mesh below the second parallel plane was then marked and removed. As an example, the described procedure is shown in Figure 8 for sample 3.

After the excessive mesh beneath the parallel plane was removed in Figure 8, the STL model still had a mass on one of the sides creating problems for sealing of the model. Removing this mass left a gap between the two parallel planes which needs to be closed of. To close such holes, mesh bridges were used and then the repair option was enabled. This was done to some extent to all three samples. When the holes and gaps were mended, the bottom of the models were sealed of using the parallel plane. GOM inspect then provided the volume of the STL bodies.

Finally a circle was fitted to the bottom of the STL body, this to estimate the diameter of the preconceived cylinders. Then, using the exact height and the diameter of the circle, an original volume was estimated.

Sample 2:

This particular case needed a special approach and it is by far the case with the highest uncertainty in its calculations. As Figure 2 shows, sample 2 has no geometrical body to work with, but on the inside

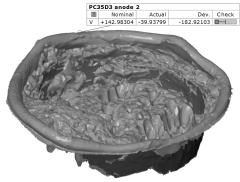

(a) *Cylindrical markup.*

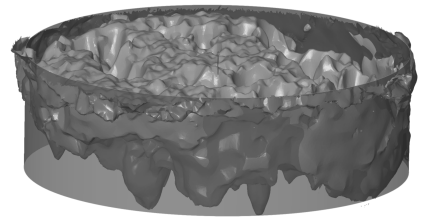

(b) *Final crater measurements.*

Figure 9: *Case FA35D3 sample 2. (a) Cylindrical markup. (b) Final crater which gave a negative volume for the STL model.*

of the crater a tendency of the original steel pieces cylindrical curves can be seen. Using a markup of this area generated with the cylindrical mesh markup, a starting point was gained, see Figure 9. Using the cylinder and the highest point of the "top" of the crater, a circle is fitted. The initial height of the cylinder is denoted and the area of the STL body above this circle is marked and deleted. This also removed the upper part of this samples preconceived cylinder.

Some mending of holes in the crater was done, and the final variant of the steel piece is shown in Figure 9b. The absolute value of the volume provided for the STL body, plus the volume of the cylinder that was removed above the fitted circle, is taken as the estimated loss of volume to FA35D3 sample 2.

3 Results

All estimated variables of the 17 steel pieces can be found in Table 1. The table contains estimated diameters and heights, providing calculations for the original volume of all received models. It also includes the actual volume of the steel pieces as provided by the STL models, and then finally the loss of volume.

		Estiamtions Original			STL Model	Estimated
		Height $[mm]$	Diameter $[mm]$	Volume *before corrosion* $[mm^3]$	Volume *after corrosion* $[mm^3]$	Volume *loss* $[mm^3]$
FA5D3	Sample 3 *	5.83	5.89	158.80	150.83	8.0
FA20D1	Sample 1	6.12	5.90	167.18	165.99	1.2
	Sample 3 *	6.23	5.89	169.94	163.97	6.0
	Sample 4	6.21	5.90	169.77	169.31	0.5
FA35D1	Sample 1 *	6.02	5.88	163.45	158.58	4.9
	Sample 2	5.81	5.88	158.06	156.50	1.6
FA35D3	Sample 3 *	6.08	5.88	165.21	158.76	6.5
PC 5D2	Sample 3 *	5.81	5.87	157.13	145.08	12.0
	Sample 4	6.02	5.89	164.15	163.05	1.1
PC20D1	Sample 1 *	5.87	5.82	156.22	136.16	20.1
	Sample 4	6.20	5.89	168.92	167.68	1.2
PC35D2	Sample 2 *	5.83	5.88	158.52	135.31	23.2
	Sample 4	5.97	5.88	162.29	162.02	0.3
PC35D3	Sample 1	0.15	5.91	4.11	3.87	0.2
	Sample 2 *	2.71	5.97	75.78		40.6
	Sample 3	0.35	5.93	9.66	9.27	0.4
	Sample 4	0.25	5.92	6.88	5.26	1.6

Table 1: *Estimations and resulting calculations for the cylindrical steel pieces. Samples that were connected in the macro arrangement are labeled with a star (*).*

References

HORNBOSTEL, K. (to be submitted in 2015). *The role of concrete resistivity in chloride-induced macro-cell corrosion of reinforcement.* Ph.D. thesis, Department of Structural Engineering - Norwegian University of Science and Technology (NTNU), Trondheim, Norway.

Doctoral Theses at the Department of Structural Engineering, Norwegian University of Science and Technology

DEPARTMENT OF STRUCTURAL ENGINEERING
NORWEGIAN UNIVERSITY OF SCIENCE AND TECHNOLOGY

N–7491 TRONDHEIM, NORWAY
Telephone: +47 73 59 47 00 Telefax: +47 73 59 47 01

"Reliability Analysis of Structural Systems using Nonlinear Finite Element Methods",
C. A. Holm, 1990:23, ISBN 82-7119-178-0.

"Uniform Stratified Flow Interaction with a Submerged Horizontal Cylinder",
Ø. Arntsen, 1990:32, ISBN 82-7119-188-8.

"Large Displacement Analysis of Flexible and Rigid Systems Considering Displacement-Dependent Loads and Nonlinear Constraints",
K. M. Mathisen, 1990:33, ISBN 82-7119-189-6.

"Solid Mechanics and Material Models including Large Deformations",
E. Levold, 1990:56, ISBN 82-7119-214-0, ISSN 0802-3271.

"Inelastic Deformation Capacity of Flexurally-Loaded Aluminium Alloy Structures",
T. Welo, 1990:62, ISBN 82-7119-220-5, ISSN 0802-3271.

"Visualization of Results from Mechanical Engineering Analysis",
K. Aamnes, 1990:63, ISBN 82-7119-221-3, ISSN 0802-3271.

"Object-Oriented Product Modeling for Structural Design",
S. I. Dale, 1991:6, ISBN 82-7119-258-2, ISSN 0802-3271.

"Parallel Techniques for Solving Finite Element Problems on Transputer Networks",
T. H. Hansen, 1991:19, ISBN 82-7119-273-6, ISSN 0802-3271.

"Statistical Description and Estimation of Ocean Drift Ice Environments",
R. Korsnes, 1991:24, ISBN 82-7119-278-7, ISSN 0802-3271.

“Properties of concrete related to fatigue damage: with emphasis on high strength concrete”,
G. Petkovic, 1991:35, ISBN 82-7119-290-6, ISSN 0802-3271.

"Turbidity Current Modelling",
B. Brørs, 1991:38, ISBN 82-7119-293-0, ISSN 0802-3271.

"Zero-Slump Concrete: Rheology, Degree of Compaction and Strength. Effects of Fillers as Part Cement-Replacement",
C. Sørensen, 1992:8, ISBN 82-7119-357-0, ISSN 0802-3271.

"Nonlinear Analysis of Reinforced Concrete Structures Exposed to Transient Loading",
K. V. Høiseth, 1992:15, ISBN 82-7119-364-3, ISSN 0802-3271.

"Finite Element Formulations and Solution Algorithms for Buckling and Collapse Analysis of Thin Shells",
R. O. Bjærum, 1992:30, ISBN 82-7119-380-5, ISSN 0802-3271.

"Response Statistics of Nonlinear Dynamic Systems",
J. M. Johnsen, 1992:42, ISBN 82-7119-393-7, ISSN 0802-3271.

"Digital Models in Engineering. A Study on why and how engineers build and operate digital models for decisison support",
J. Høyte, 1992:75, ISBN 82-7119-429-1, ISSN 0802-3271.

"Sparse Solution of Finite Element Equations",
A. C. Damhaug, 1992:76, ISBN 82-7119-430-5, ISSN 0802-3271.

"Some Aspects of Floating Ice Related to Sea Surface Operations in the Barents Sea",
S. Løset, 1992:95, ISBN 82-7119-452-6, ISSN 0802-3271.

"Modelling of Cyclic Plasticity with Application to Steel and Aluminium Structures",
O. S. Hopperstad, 1993:7, ISBN 82-7119-461-5, ISSN 0802-3271.

"The Free Formulation: Linear Theory and Extensions with Applications to Tetrahedral Elements
with Rotational Freedoms",
G. Skeie, 1993:17, ISBN 82-7119-472-0, ISSN 0802-3271.

"Høyfast betongs motstand mot piggdekkslitasje. Analyse av resultater fra prøving i Veisliter'n",
T. Tveter, 1993:62, ISBN 82-7119-522-0, ISSN 0802-3271.

"A Nonlinear Finite Element Based on Free Formulation Theory for Analysis of Sandwich Structures",
O. Aamlid, 1993:72, ISBN 82-7119-534-4, ISSN 0802-3271.

"The Effect of Curing Temperature and Silica Fume on Chloride Migration and Pore Structure of High Strength Concrete",
C. J. Hauck, 1993:90, ISBN 82-7119-553-0, ISSN 0802-3271.

"Failure of Concrete under Compressive Strain Gradients",
G. Markeset, 1993:110, ISBN 82-7119-575-1, ISSN 0802-3271.

"An experimental study of internal tidal amphidromes in Vestfjorden",
J. H. Nilsen, 1994:39, ISBN 82-7119-640-5, ISSN 0802-3271.

"Structural analysis of oil wells with emphasis on conductor design",
H. Larsen, 1994:46, ISBN 82-7119-648-0, ISSN 0802-3271.

"Adaptive methods for non-linear finite element analysis of shell structures",
K. M. Okstad, 1994:66, ISBN 82-7119-670-7, ISSN 0802-3271.

"On constitutive modelling in nonlinear analysis of concrete structures",
O. Fyrileiv, 1994:115, ISBN 82-7119-725-8, ISSN 0802-3271.

"Fluctuating wind load and response of a line-like engineering structure with emphasis on motion-induced wind forces",
J. Bogunovic Jakobsen, 1995:62, ISBN 82-7119-809-2, ISSN 0802-3271.

"An experimental study of beam-columns subjected to combined torsion, bending and axial actions",
A. Aalberg, 1995:66, ISBN 82-7119-813-0, ISSN 0802-3271.

"Scaling and cracking in unsealed freeze/thaw testing of Portland cement and silica fume concretes",
S. Jacobsen, 1995:101, ISBN 82-7119-851-3, ISSN 0802-3271.

"Damping of water waves by submerged vegetation. A case study of laminaria hyperborea",
A. M. Dubi, 1995:108, ISBN 82-7119-859-9, ISSN 0802-3271.

"The dynamics of a slope current in the Barents Sea",
Sheng Li, 1995:109, ISBN 82-7119-860-2, ISSN 0802-3271.

"Modellering av delmaterialenes betydning for betongens konsistens",
Ernst Mørtsell, 1996:12, ISBN 82-7119-894-7, ISSN 0802-3271.

"Bending of thin-walled aluminium extrusions",
Birgit Søvik Opheim, 1996:60, ISBN 82-7119-947-1, ISSN 0802-3271.

"Material modelling of aluminium for crashworthiness analysis",
Torodd Berstad, 1996:89, ISBN 82-7119-980-3, ISSN 0802-3271.

"Estimation of structural parameters from response measurements on submerged floating tunnels",
Rolf Magne Larssen, 1996:119, ISBN 82-471-0014-2, ISSN 0802-3271.

“Numerical modelling of plain and reinforced concrete by damage mechanics”,
Mario A. Polanco-Loria, 1997:20, ISBN 82-471-0049-5, ISSN 0802-3271.

“Nonlinear random vibrations - numerical analysis by path integration methods”,
Vibeke Moe, 1997:26, ISBN 82-471-0056-8, ISSN 0802-3271.

"Numerical prediction of vortex-induced vibration by the finite element method",
Joar Martin Dalheim, 1997:63, ISBN 82-471-0096-7, ISSN 0802-3271.

"Time domain calculations of buffeting response for wind sensitive structures",
Ketil Aas-Jakobsen, 1997:148, ISBN 82-471-0189-0, ISSN 0802-3271.

"A numerical study of flow about fixed and flexibly mounted circular cylinders",
Trond Stokka Meling, 1998:48, ISBN 82-471-0244-7, ISSN 0802-3271.

"Estimation of chloride penetration into concrete bridges in coastal areas",
Per Egil Steen, 1998:89, ISBN 82-471-0290-0, ISSN 0802-3271.

"Stress-resultant material models for reinforced concrete plates and shells",
Jan Arve Øverli, 1998:95, ISBN 82-471-0297-8, ISSN 0802-3271.

"Chloride binding in concrete. Effect of surrounding environment and concrete composition",
Claus Kenneth Larsen, 1998:101, ISBN 82-471-0337-0, ISSN 0802-3271.

"Rotational capacity of aluminium alloy beams",
Lars A. Moen, 1999:1, ISBN 82-471-0365-6, ISSN 0802-3271.

"Stretch Bending of Aluminium Extrusions",
Arild H. Clausen, 1999:29, ISBN 82-471-0396-6, ISSN 0802-3271.

"Aluminium and Steel Beams under Concentrated Loading",
Tore Tryland, 1999:30, ISBN 82-471-0397-4, ISSN 0802-3271.

"Engineering Models of Elastoplasticity and Fracture for Aluminium Alloys",
Odd-Geir Lademo, 1999:39, ISBN 82-471-0406-7, ISSN 0802-3271.

"Kapasitet og duktilitet av dybelforbindelser i trekonstruksjoner",
Jan Siem, 1999:46, ISBN 82-471-0414-8, ISSN 0802-3271.

"Etablering av distribuert ingeniørarbeid; Teknologiske og organisatoriske erfaringer fra en norsk ingeniørbedrift",
Lars Line, 1999:52, ISBN 82-471-0420-2, ISSN 0802-3271.

"Estimation of Earthquake-Induced Response",
Símon Ólafsson, 1999:73, ISBN 82-471-0443-1, ISSN 0802-3271.

"Coastal Concrete Bridges: Moisture State, Chloride Permeability and Aging Effects"
Ragnhild Holen Relling, 1999:74, ISBN 82-471-0445-8, ISSN 0802-3271.

"Capacity Assessment of Titanium Pipes Subjected to Bending and External Pressure",
Arve Bjørset, 1999:100, ISBN 82-471-0473-3, ISSN 0802-3271.

“Validation of Numerical Collapse Behaviour of Thin-Walled Corrugated Panels”,
Håvar Ilstad, 1999:101, ISBN 82-471-0474-1, ISSN 0802-3271.

“Strength and Ductility of Welded Structures in Aluminium Alloys”,
Miroslaw Matusiak, 1999:113, ISBN 82-471-0487-3, ISSN 0802-3271.

“Thermal Dilation and Autogenous Deformation as Driving Forces to Self-Induced Stresses in High Performance Concrete”,
Øyvind Bjøntegaard, 1999:121, ISBN 82-7984-002-8, ISSN 0802-3271.

“Some Aspects of Ski Base Sliding Friction and Ski Base Structure”,
Dag Anders Moldestad, 1999:137, ISBN 82-7984-019-2, ISSN 0802-3271.

"Electrode reactions and corrosion resistance for steel in mortar and concrete",
Roy Antonsen, 2000:10, ISBN 82-7984-030-3, ISSN 0802-3271.

"Hydro-Physical Conditions in Kelp Forests and the Effect on Wave Damping and Dune Erosion. A case study on Laminaria Hyperborea",
Stig Magnar Løvås, 2000:28, ISBN 82-7984-050-8, ISSN 0802-3271.

"Random Vibration and the Path Integral Method",
Christian Skaug, 2000:39, ISBN 82-7984-061-3, ISSN 0802-3271.

"Buckling and geometrical nonlinear beam-type analyses of timber structures",
Trond Even Eggen, 2000:56, ISBN 82-7984-081-8, ISSN 0802-3271.

”Structural Crashworthiness of Aluminium Foam-Based Components”,
Arve Grønsund Hanssen, 2000:76, ISBN 82-7984-102-4, ISSN 0809-103X.

“Measurements and simulations of the consolidation in first-year sea ice ridges, and some aspects of mechanical behaviour”,
Knut V. Høyland, 2000:94, ISBN 82-7984-121-0, ISSN 0809-103X.

”Kinematics in Regular and Irregular Waves based on a Lagrangian Formulation”,
Svein Helge Gjøsund, 2000-86, ISBN 82-7984-112-1, ISSN 0809-103X.

”Self-Induced Cracking Problems in Hardening Concrete Structures”,
Daniela Bosnjak, 2000-121, ISBN 82-7984-151-2, ISSN 0809-103X.

"Ballistic Penetration and Perforation of Steel Plates",
Tore Børvik, 2000:124, ISBN 82-7984-154-7, ISSN 0809-103X.

"Freeze-Thaw resistance of Concrete. Effect of: Curing Conditions, Moisture Exchange and Materials",
Terje Finnerup Rønning, 2001:14, ISBN 82-7984-165-2, ISSN 0809-103X

"Structural behaviour of post tensioned concrete structures. Flat slab. Slabs on ground",
Steinar Trygstad, 2001:52, ISBN 82-471-5314-9, ISSN 0809-103X.

"Slipforming of Vertical Concrete Structures. Friction between concrete and slipform panel",
Kjell Tore Fosså, 2001:61, ISBN 82-471-5325-4, ISSN 0809-103X.

"Some numerical methods for the simulation of laminar and turbulent incompressible flows",
Jens Holmen, 2002:6, ISBN 82-471-5396-3, ISSN 0809-103X.

“Improved Fatigue Performance of Threaded Drillstring Connections by Cold Rolling”,
Steinar Kristoffersen, 2002:11, ISBN: 82-421-5402-1, ISSN 0809-103X.

"Deformations in Concrete Cantilever Bridges: Observations and Theoretical Modelling",
Peter F. Takâcs, 2002:23, ISBN 82-471-5415-3, ISSN 0809-103X.

"Stiffened aluminium plates subjected to impact loading",
Hilde Giæver Hildrum, 2002:69, ISBN 82-471-5467-6, ISSN 0809-103X.

"Full- and model scale study of wind effects on a medium-rise building in a built up area",
Jónas Thór Snæbjørnsson, 2002:95, ISBN82-471-5495-1, ISSN 0809-103X.

“Evaluation of Concepts for Loading of Hydrocarbons in Ice-infested water”,
Arnor Jensen, 2002:114, ISBN 82-417-5506-0, ISSN 0809-103X.

”Numerical and Physical Modelling of Oil Spreading in Broken Ice”,
Janne K. Økland Gjøsteen, 2002:130, ISBN 82-471-5523-0, ISSN 0809-103X.

”Diagnosis and protection of corroding steel in concrete”,
Franz Pruckner, 20002:140, ISBN 82-471-5555-4, ISSN 0809-103X.

“Tensile and Compressive Creep of Young Concrete: Testing and Modelling”,
Dawood Atrushi, 2003:17, ISBN 82-471-5565-6, ISSN 0809-103X.

“Rheology of Particle Suspensions. Fresh Concrete, Mortar and Cement Paste with Various Types of Lignosulfonates”,
Jon Elvar Wallevik, 2003:18, ISBN 82-471-5566-4, ISSN 0809-103X.

“Oblique Loading of Aluminium Crash Components”,
Aase Reyes, 2003:15, ISBN 82-471-5562-1, ISSN 0809-103X.

“Utilization of Ethiopian Natural Pozzolans”,
Surafel Ketema Desta, 2003:26, ISSN 82-471-5574-5, ISSN:0809-103X.

“Behaviour and strength prediction of reinforced concrete structures with discontinuity regions”, Helge Brå, 2004:11, ISBN 82-471-6222-9, ISSN 1503-8181.

“High-strength steel plates subjected to projectile impact. An experimental and numerical study”, Sumita Dey, 2004:38, ISBN 82-471-6282-2 (printed version), ISBN 82-471-6281-4 (electronic version), ISSN 1503-8181.

“Alkali-reactive and inert fillers in concrete. Rheology of fresh mixtures and expansive reactions.”
Bård M. Pedersen, 2004:92, ISBN 82-471-6401-9 (printed version), ISBN 82-471-6400-0 (electronic version), ISSN 1503-8181.

“On the Shear Capacity of Steel Girders with Large Web Openings”.
Nils Christian Hagen, 2005:9 ISBN 82-471-6878-2 (printed version), ISBN 82-471-6877-4 (electronic version), ISSN 1503-8181.

”Behaviour of aluminium extrusions subjected to axial loading”.
Østen Jensen, 2005:7, ISBN 82-471-6873-1 (printed version), ISBN 82-471-6872-3 (electronic version), ISSN 1503-8181.

”Thermal Aspects of corrosion of Steel in Concrete”.
Jan-Magnus Østvik, 2005:5, ISBN 82-471-6869-3 (printed version), ISBN 82-471-6868 (electronic version), ISSN 1503-8181.

”Mechanical and adaptive behaviour of bone in relation to hip replacement.” A study of bone remodelling and bone grafting.
Sébastien Muller, 2005:34, ISBN 82-471-6933-9 (printed version), ISBN 82-471-6932-0 (electronic version), ISSN 1503-8181.

“Analysis of geometrical nonlinearities with applications to timber structures”.
Lars Wollebæk, 2005:74, ISBN 82-471-7050-5 (printed version), ISBN 82-471-7019-1 (electronic version), ISSN 1503-8181.

“Pedestrian induced lateral vibrations of slender footbridges”,
Anders Rönnquist, 2005:102, ISBN 82-471-7082-5 (printed version), ISBN 82-471-7081-7 (electronic version), ISSN 1503-8181.

“Initial Strength Development of Fly Ash and Limestone Blended Cements at Various Temperatures Predicted by Ultrasonic Pulse Velocity”,
Tom Ivar Fredvik, 2005:112, ISBN 82-471-7105-8 (printed version), ISBN 82-471-7103-1 (electronic version), ISSN 1503-8181.

“Behaviour and modelling of thin-walled cast components”,
Cato Dørum, 2005:128, ISBN 82-471-7140-6 (printed version), ISBN 82-471-7139-2 (electronic version), ISSN 1503-8181.

“Behaviour and modelling of selfpiercing riveted connections”,
Raffaele Porcaro, 2005:165, ISBN 82-471-7219-4 (printed version), ISBN 82-471-7218-6 (electronic version), ISSN 1503-8181.

”Behaviour and Modelling og Aluminium Plates subjected to Compressive Load”,
Lars Rønning, 2005:154, ISBN 82-471-7169-1 (printed version), ISBN 82-471-7195-3 (electronic version), ISSN 1503-8181.

”Bumper beam-longitudinal system subjected to offset impact loading”,
Satyanarayana Kokkula, 2005:193, ISBN 82-471-7280-1 (printed version), ISBN 82-471-7279-8 (electronic version), ISSN 1503-8181.

“Control of Chloride Penetration into Concrete Structures at Early Age”,
Guofei Liu, 2006:46, ISBN 82-471-7838-9 (printed version), ISBN 82-471-7837-0 (electronic version), ISSN 1503-8181.

“Modelling of Welded Thin-Walled Aluminium Structures”,
Ting Wang, 2006:78, ISBN 82-471-7907-5 (printed version), ISBN 82-471-7906-7 (electronic version), ISSN 1503-8181.

”Time-variant reliability of dynamic systems by importance sampling and probabilistic analysis of ice loads”,
Anna Ivanova Olsen, 2006:139, ISBN 82-471-8041-3 (printed version), ISBN 82-471-8040-5 (electronic version), ISSN 1503-8181.

“Fatigue life prediction of an aluminium alloy automotive component using finite element analysis of surface topography”.
Sigmund Kyrre Ås, 2006:25, ISBN 82-471-7791-9 (printed version), ISBN 82-471-7791-9 (electronic version), ISSN 1503-8181.

”Constitutive models of elastoplasticity and fracture for aluminium alloys under strain path change”,
Dasharatha Achani, 2006:76, ISBN 82-471-7903-2 (printed version), ISBN 82-471-7902-4 (electronic version), ISSN 1503-8181.

“Simulations of 2D dynamic brittle fracture by the Element-free Galerkin method and linear fracture mechanics”,
Tommy Karlsson, 2006:125, ISBN 82-471-8011-1 (printed version), ISBN 82-471-8010-3 (electronic version), ISSN 1503-8181.

“Penetration and Perforation of Granite Targets by Hard Projectiles”,
Chong Chiang Seah, 2006:188, ISBN 82-471-8150-9 (printed version), ISBN 82-471-8149-5 (electronic version), ISSN 1503-8181.

"Deformations, strain capacity and cracking of concrete in plastic and early hardening phases",
Tor Arne Hammer, 2007:234, ISBN 978-82-471-5191-4 (printed version), ISBN 978-82-471-5207-2 (electronic version), ISSN 1503-8181.

"Crashworthiness of dual-phase high-strength steel: Material and Component behaviour", Venkatapathi Tarigopula, 2007:230, ISBN 82-471-5076-4 (printed version), ISBN 82-471-5093-1 (electronic version), ISSN 1503-8181.

"Fibre reinforcement in load carrying concrete structures",
Åse Lyslo Døssland, 2008:50, ISBN 978-82-471-6910-0 (printed version), ISBN 978-82-471-6924-7 (electronic version), ISSN 1503-8181.

"Low-velocity penetration of aluminium plates",
Frode Grytten, 2008:46, ISBN 978-82-471-6826-4 (printed version), ISBN 978-82-471-6843-1 (electronic version), ISSN 1503-8181.

"Robustness studies of structures subjected to large deformations",
Ørjan Fyllingen, 2008:24, ISBN 978-82-471-6339-9 (printed version), ISBN 978-82-471-6342-9 (electronic version), ISSN 1503-8181.

"Constitutive modelling of morsellised bone",
Knut Birger Lunde, 2008:92, ISBN 978-82-471-7829-4 (printed version), ISBN 978-82-471-7832-4 (electronic version), ISSN 1503-8181.

"Experimental Investigations of Wind Loading on a Suspension Bridge Girder",
Bjørn Isaksen, 2008:131, ISBN 978-82-471-8656-5 (printed version), ISBN 978-82-471-8673-2 (electronic version), ISSN 1503-8181.

"Cracking Risk of Concrete Structures in The Hardening Phase",
Guomin Ji, 2008:198, ISBN 978-82-471-1079-9 (printed version), ISBN 978-82-471-1080-5 (electronic version), ISSN 1503-8181.

"Modelling and numerical analysis of the porcine and human mitral apparatus",
Victorien Emile Prot, 2008:249, ISBN 978-82-471-1192-5 (printed version), ISBN 978-82-471-1193-2 (electronic version), ISSN 1503-8181.

"Strength analysis of net structures",
Heidi Moe, 2009:48, ISBN 978-82-471-1468-1 (printed version), ISBN 978-82-471-1469-8 (electronic version), ISSN1503-8181.

"Numerical analysis of ductile fracture in surface cracked shells",
Espen Berg, 2009:80, ISBN 978-82-471-1537-4 (printed version), ISBN 978-82-471-1538-1 (electronic version), ISSN 1503-8181.

"Subject specific finite element analysis of bone – for evaluation of the healing of a leg lengthening and evaluation of femoral stem design",
Sune Hansborg Pettersen, 2009:99, ISBN 978-82-471-1579-4 (printed version), ISBN 978-82-471-1580-0 (electronic version), ISSN 1503-8181.

"Evaluation of fracture parameters for notched multi-layered structures",
Lingyun Shang, 2009:137, ISBN 978-82-471-1662-3 (printed version), ISBN 978-82-471-1663-0 (electronic version), ISSN 1503-8181.

"Modelling of Dynamic Material Behaviour and Fracture of Aluminium Alloys for Structural Applications"
Yan Chen, 2009:69, ISBN 978-82-471-1515-2 (printed version), ISBN 978-82 471-1516-9 (electronic version), ISSN 1503-8181.

"Nanomechanics of polymer and composite particles"
Jianying He 2009:213, ISBN 978-82-471-1828-3 (printed version), ISBN 978-82-471-1829-0 (electronic version), ISSN 1503-8181.

"Mechanical properties of clear wood from Norway spruce"
Kristian Berbom Dahl 2009:250, ISBN 978-82-471-1911-2 (printed version) ISBN 978-82-471-1912-9 (electronic version), ISSN 1503-8181.

"Modeling of the degradation of TiB_2 mechanical properties by residual stresses and liquid Al penetration along grain boundaries"
Micol Pezzotta 2009:254, ISBN 978-82-471-1923-5 (printed version) ISBN 978-82-471-1924-2 (electronic version) ISSN 1503-8181.

"Effect of welding residual stress on fracture"
Xiabo Ren 2010:77, ISBN 978-82-471-2115-3 (printed version) ISBN 978-82-471-2116-0 (electronic version), ISSN 1503-8181.

"Pan-based carbon fiber as anode material in cathodic protection system for concrete structures"
Mahdi Chini 2010:122, ISBN 978-82-471-2210-5 (printed version) ISBN 978-82-471-2213-6 (electronic version), ISSN 1503-8181.

"Structural Behaviour of deteriorated and retrofitted concrete structures"
Irina Vasililjeva Sæther 2010:171, ISBN 978-82-471-2315-7 (printed version) ISBN 978-82-471-2316-4 (electronic version) ISSN 1503-8181.

"Prediction of local snow loads on roofs"
Vivian Meløysund 2010:247, ISBN 978-82-471-2490-1 (printed version) ISBN 978-82-471-2491-8 (electronic version) ISSN 1503-8181.

"Behaviour and modelling of polymers for crash applications"
Virgile Delhaye 2010:251, ISBN 978-82-471-2501-4 (printed version) ISBN 978-82-471-2502-1 (electronic version) ISSN 1503-8181.

"Blended cement with reducted CO_2 emission – Utilizing the Fly Ash-Limestone Synergy",
Klaartje De Weerdt 2011:32, ISBN 978-82-471-2584-7 (printed version) ISBN 978-82-471-2584-4 (electronic version) ISSN 1503-8181.

"Chloride induced reinforcement corrosion in concrete" Concept of critical chloride content – methods and mechanisms.
Ueli Angst 2011:113, ISBN 978-82-471-2769-9 (printed version) ISBN 978-82-471-2763-6 (electronic version) ISSN 1503-8181.

"A thermo-electric-Mechanical study of the carbon anode and contact interface for Energy savings in the production of aluminium".
Dag Herman Andersen 2011:157, ISBN 978-82-471-2859-6 (printed version) ISBN 978-82-471-2860-2 (electronic version) ISSN 1503-8181.

"Structural Capacity of Anchorage Ties in Masonry Veneer Walls Subjected to Earthquake". The implications of Eurocode 8 and Eurocode 6 on a typical Norwegain veneer wall.
Ahmed Mohamed Yousry Hamed 2011:181, ISBN 978-82-471-2911-1 (printed version) ISBN 978-82-471-2912-8 (electronic ver.) ISSN 1503-8181.

"Work-hardening behaviour in age-hardenable Al-Zn-Mg(-Cu) alloys".
Ida Westermann , 2011:247, ISBN 978-82-471-3056-8 (printed ver.) ISBN 978-82-471-3057-5 (electronic ver.) ISSN 1503-8181.

"Behaviour and modelling of selfpiercing riveted connections using aluminium rivets".
Nguyen-Hieu Hoang, 2011:266, ISBN 978-82-471-3097-1 (printed ver.) ISBN 978-82-471-3099-5 (electronic ver.) ISSN 1503-8181.

"Fibre reinforced concrete".
Sindre Sandbakk, 2011:297, ISBN 978-82-471-3167-1 (printed ver.) ISBN 978-82-471-3168-8 (electronic ver) ISSN 1503:8181.

"Dynamic behaviour of cablesupported bridges subjected to strong natural wind".
Ole Andre Øiseth, 2011:315, ISBN 978-82-471-3209-8 (printed ver.) ISBN 978-82-471-3210-4 (electronic ver.) ISSN 1503-8181.

"Constitutive modeling of solargrade silicon materials"
Julien Cochard, 2011:307, ISBN 978-82-471-3189-3 (printed ver). ISBN 978-82-471-3190-9 (electronic ver.) ISSN 1503-8181.

"Constitutive behavior and fracture of shape memory alloys"
Jim Stian Olsen, 2012:57, ISBN 978-82-471-3382-8 (printed ver.) ISBN 978-82-471-3383-5 (electronic ver.) ISSN 1503-8181.

“Field measurements in mechanical testing using close-range photogrammetry and digital image analysis”
Egil Fagerholt, 2012:95, ISBN 978-82-471-3466-5 (printed ver.) ISBN 978-82-471-3467-2 (electronic ver.) ISSN 1503-8181.

“Towards a better under standing of the ultimate behaviour of lightweight aggregate concrete in compression and bending”,
Håvard Nedrelid, 2012:123, ISBN 978-82-471-3527-3 (printed ver.) ISBN 978-82-471-3528-0 (electronic ver.) ISSN 1503-8181.

“Numerical simulations of blood flow in the left side of the heart”
Sigrid Kaarstad Dahl, 2012:135, ISBN 978-82-471-3553-2 (printed ver.) ISBN 978-82-471-3555-6 (electronic ver.) ISSN 1503-8181.

“Moisture induced stresses in glulam”
Vanessa Angst-Nicollier, 2012:139, ISBN 978-82-471-3562-4 (printed ver.) ISBN 978-82-471-3563-1 (electronic ver.) ISSN 1503-8181.

“Biomechanical aspects of distraction osteogensis”
Valentina La Russa, 2012:250, ISBN 978-82-471-3807-6 (printed ver.) ISBN 978-82-471-3808-3 (electronic ver.) ISSN 1503-8181.

“Ductile fracture in dual-phase steel. Theoretical, experimental and numerical study”
Gaute Gruben, 2012:257, ISBN 978-82-471-3822-9 (printed ver.) ISBN 978-82-471-3823-6 (electronic ver.) ISSN 1503-8181.

“Damping in Timber Structures”
Nathalie Labonnote, 2012:263, ISBN 978-82-471-3836-6 (printed ver.) ISBN 978-82-471-3837-3 (electronic ver.) ISSN 1503-8181.

“Biomechanical modeling of fetal veins: The umbilical vein and ductus venosus bifurcation”
Paul Roger Leinan, 2012:299, ISBN 978-82-471-3915-8 (printed ver.) ISBN 978-82-471-3916-5 (electronic ver.) ISSN 1503-8181.

“Large-Deformation behaviour of thermoplastics at various stress states”
Anne Serine Ognedal, 2012:298, ISBN 978-82-471-3913-4 (printed ver.) ISBN 978-82-471-3914-1 (electronic ver.) ISSN 1503-8181.

“Hardening accelerator for fly ash blended cement”
Kien Dinh Hoang, 2012:366, ISBN 978-82-471-4063-5 (printed ver.) ISBN 978-82-471-4064-2 (electronic ver.) ISSN 1503-8181.

“From molecular structure to mechanical properties”
Jianyang Wu, 2013:186, ISBN 978-82-471-4485-5 (printed ver.) ISBN 978-82-471-4486-2 (electronic ver.) ISSN 1503-8181.

"Experimental and numerical study of hybrid concrete structures"
Linn Grepstad Nes, 2013:259, ISBN 978-82-471-4644-6 (printed ver.) ISBN 978-82-471-4645-3 (electronic ver.) ISSN 1503-8181.

"Mechanics of ultra-thin multi crystalline silicon wafers"
Saber Saffar, 2013:199, ISBN 978-82-471-4511-1 (printed ver.) ISBN 978-82-471-4513-5 (electronic ver). ISSN 1503-8181.

"Through process modelling of welded aluminium structures"
Anizahyati Alisibramulisi, 2013:325, ISBN 978-82-471-4788-7 (printed ver.) ISBN 978-82-471-4789-4 (electronic ver.) ISSN 1503-8181.

"Combined blast and fragment loading on steel plates"
Knut Gaarder Rakvåg, 2013:361, ISBN978-82-471-4872-3 (printed ver.) ISBN 978-82-4873-0 (electronic ver.). ISSN 1503-8181.

"Characterization and modelling of the anisotropic behaviour of high-strength aluminium alloy"
Marion Fourmeau, 2014:37, ISBN 978-82-326-0008-3 (printed ver.) ISBN 978-82-326-0009-0 (electronic ver.) ISSN 1503-8181.

"Behaviour of threated steel fasteners at elevated deformation rates"
Henning Fransplass, 2014:65, ISBN 978-82-326-0054-0 (printed ver.) ISBN 978-82-326-0055-7 (electronic ver.) ISSN 1503-8181.

"Sedimentation and Bleeding"
Ya Peng, 2014:89, ISBN 978-82-326-0102-8 (printed ver.) ISBN 978-82-326-0103-5 (electric ver.) ISSN 1503-8181.

"Impact against X65 offshore pipelines"
Martin Kristoffersen, 2014:362, ISBN 978-82-326-0636-8 (printed ver.) ISBN 978-82-326-0637-5 (electronic ver.) ISSN 1503-8181.

"Formability of aluminium alloy subjected to prestrain by rolling"
Dmitry Vysochinskiy, 2014:363,, ISBN 978-82-326-0638-2 (printed ver.) ISBN 978-82-326-0639-9 (electronic ver.) ISSN 1503-8181.

"Experimental and numerical study of Yielding, Work-Hardening and anisotropy in textured AA6xxx alloys using crystal plasticity models"
Mikhail Khadyko, 2015:28, ISBN 978-82-326-0724-2 (printed ver.) ISBN 978-82-326-0725-9 (electronic ver.) ISSN 1503-8181.

"Behaviour and Modelling of AA6xxx Aluminium Alloys Under a Wide Range of Temperatures and Strain Rates"
Vincent Vilamosa, 2015:63, ISBN 978-82-326-0786-0 (printed ver.) ISBN 978-82-326-0787-7 (electronic ver.) ISSN 1503-8181.

“A Probabilistic Approach in Failure Modelling of Aluminium High Pressure Die-Castings”
Octavian Knoll, 2015:137, ISBN 978-82-326-0930-7 (printed ver.) ISBN 978-82-326-0931-4 (electronic ver.) ISSN 1503-8181.

“Ice Abrasion on Marine Concrete Structures”
Egil Møen, 2015:189, ISBN 978-82-326-1034-1 (printed ver.) ISBN 978-82-326-1035-8 (electronic ver.) ISSN 1503-8181.

“Fibre Orientation in Steel-Fibre-Reinforced Concrete”
Giedrius Zirgulis, 2015:229, ISBN 978-82-326-1114-0 (printed ver.) ISBN 978-82-326-1115-7 (electronic ver.) ISSN 1503-8181.

“Effect of spatial variation and possible interference of localised corrosion on the residual capacity of a reinforced concrete beam”
Mohammad Mahdi Kioumarsi, 2015:282, ISBN 978-82-326-1220-8 (printed ver.) ISBN 978-82-1221-5 (electronic ver.) ISSN 1503-8181.